**RECICLAJE DEL FÓSFORO REMOVIDO DESDE SOLUCIONES
ACUOSAS USANDO UN ADSORBENTE OBTENIDO A PARTIR DE JACINTO DE
AGUA (*Eichhornia Crassipes*)**

ANYI PAOLA RAMIREZ MUÑOZ

UNIVERSIDAD DE MEDELLIN

FACULTAD DE CIENCIAS BÁSICAS

MAESTRÍA EN MODELACIÓN Y CIENCIA COMPUTACIONAL

MEDELLIN

JUNIO, 2021

RECICLAJE DEL FÓSFORO REMOVIDO DESDE SOLUCIONES ACUOSAS USANDO UN ADSORBENTE OBTENIDO A PARTIR DE JACINTO DE AGUA (*Eichhornia Crassipes*)

ANYI PAOLA RAMIREZ MUÑOZ

Tesis para optar al título de Magíster en Modelación y Ciencia computacional

Asesoras:

Dra. NANCY ACELAS SOTO

Dra. ELIZABETH FLÓREZ YEPES

Co-asesor:

Dr. CARLOS JIMÉNEZ OROZCO

UNIVERSIDAD DE MEDELLIN

FACULTAD DE CIENCIAS BÁSICAS

MAESTRÍA EN MODELACIÓN Y CIENCIA COMPUTACIONAL

MEDELLIN

JUNIO, 2021

A mi madre Asalis, hermanos Roiby, Rafael y Adriana y a Víctor por

su amor, confianza y apoyo constante e incondicional.

Agradecimientos

Resumen

El fósforo (P) es un elemento no renovable, esencial para el desarrollo de las plantas. La principal fuente de P es la roca fosfórica, la cual ha disminuido notablemente en décadas recientes, ya que durante los últimos 20 años entre un 80 - 90% se ha consumido para la producción de fertilizantes. A su vez, el P es el principal responsable de la eutrofización de ecosistemas acuáticos, que se genera por la lixiviación del P presente en el suelo luego de su aplicación como fertilizante y por la descarga de aguas residuales industriales, ganaderas y domésticas con alta concentración de P [1,2]. Por lo tanto, es necesario buscar procesos sostenibles y eficientes, que permitan remover el P presente en medios acuosos, recuperarlo y reciclarlo después de ser removido [1].

En este trabajo, se evaluó la producción de materiales y su capacidad como adsorbentes para remover P desde soluciones acuosas, mediante una transformación térmica sencilla del jacinto de agua (*Eichhornia Crassipes*), el cual es una maleza nociva que crece y se propaga rápidamente en la superficie del agua generando serios problemas ambientales. La extensa red de enraizamiento le permite absorber nutrientes (P, N, K, S) del medio acuoso, lo cual, junto con su reproducción excesiva impiden el paso de la luz a través del agua disminuyendo los niveles de oxígeno. La conversión de *Eichhornia Crassipes* en un material adsorbente para la descontaminación de agua, representa un método atractivo para mejorar la gestión de esta especie invasiva tan problemática.

Éste trabajo se desarrolló en tres grandes bloques, los cuales son presentados a continuación:

1. Debido a que el jacinto de agua es una especie que contiene 8.1% de P_2O_5 y 32.4% de CaO, inicialmente se estudió el efecto de la temperatura de calcinación en la transformación del P y Ca presente en esta biomasa, a compuestos inorgánicos asimilables por las plantas como la apatita. Los resultados mostraron que a temperaturas de calcinación de 450 y 550 °C se obtuvo 5.5 y 6.3% de apatita $[Ca_5(PO_4)_3(OH)]$, respectivamente, y que esta cantidad aumentó con el incremento de la temperatura de calcinación hasta alcanzar un 36.6% a 800 °C, valores que se verificaron mediante el uso de técnicas de análisis como difracción de rayos X (XRD)

y espectroscopía infrarroja (FTIR). La apatita es un compuesto rico en P y Ca con baja solubilidad en el agua, y se caracteriza por ser biocompatible con el suelo ya que mejora el crecimiento de las plantas. Por lo tanto, una vez se logró obtener la mayor cantidad de apatita se realizaron pruebas de biodisponibilidad, las cuales mostraron liberación lenta de P (entre 27.9 y 45.1%) y baja lixiviación de P (entre 0.9 y 14.7%) por escorrentía de aguas, las cuales son dos características fundamentales en un fertilizante, mostrando que este material constituye un recurso adecuado para este fin [3].

2. La caracterización química realizada al material obtenido mostró que además de la apatita, los materiales contienen óxidos e hidróxidos metálicos como $Ca(OH)_2$, Al_2O_3, MgO y Fe_3O_4. Con lo anterior y teniendo en cuenta que los óxidos/hidróxidos metálicos han sido reportados como fases activas en la eliminación de P, se estudió la capacidad de adsorción de P usando los materiales obtenidos por calcinación del jacinto de agua. Adicionalmente, se evaluó si mediante un tratamiento térmico adicional es posible transformar el P adsorbido a apatita, y así enriquecer el material, incrementando la cantidad formada inicialmente. Durante el proceso de adsorción de P usando materiales obtenidos a 650 °C y mediante el uso de modelos cinéticos y de isotermas en combinación con técnicas de caracterización química (FTIR y XRD), se encontró una capacidad máxima de adsorción de 21.2 mg P/g, donde la quimisorción es el paso limitante del proceso de adsorción, y el intercambio de ligandos seguido de la precipitación son los mecanismos dominantes en el proceso de adsorción. En este estudio se demostró que después de calcinar el material adsorbido con P, la cantidad de apatita incrementó de 25.1 a 41.0%. Las pruebas de solubilidad mostraron el potencial uso del material obtenido como fertilizante fosfatado, ya que presentó baja solubilidad en el agua, lo que garantiza liberación lenta del nutriente al suelo [4].

3. Teniendo en cuenta el potencial del material obtenido para la remediación de aguas, y la presencia de apatita y otras fases de Ca generadas en el proceso térmico, en este trabajo se buscó evaluar una aplicación alternativa relacionada con la inmovilización de metales pesados como Cd^{2+} y Cu^{2+}. Los resultados mostraron que la eficiencia de remoción de estos metales desde soluciones acuosas incrementó con el aumento de la

temperatura de calcinación desde 550 °C (24.9% Cd^{2+} y 12.7% Cu^{2+}) hasta 700 °C (51,5% Cd^{2+} y 31,8% Cu^{2+}). Se demostró que los compuestos producidos durante la calcinación del jacinto de agua promueven la adsorción de Cd^{2+} y Cu^{2+} a través de la precipitación de $CdCO_3$, $Cd_2P_2O_7$ y $Cu_{0.05}Mg_{0.95}O$, $Cu_2P_2O_7$, los cuales tienen baja solubilidad y reducen la movilidad de estos metales [5].

En general, esta investigación demuestra que es posible realizar de manera sostenible la eliminación y recuperación de P utilizando biomasas residuales, lo que contribuye con la recirculación de este elemento vital y finito. Del mismo modo, se logra valorizar el jacinto de agua, biomasa residual con alto impacto negativo en el medio ambiente.

Palabras claves: reciclaje de fosfato, jacinto de agua, apatita, adsorción, metales pesados, inmovilización de metales

Abstract

Phosphorus (P) is a non-renewable and essential element for plants development. The main source of P is the phosphate rock which is in depletion due to the high fertilizer consumption and production. Besides, P is the main responsible for the eutrophication of aquatic ecosystems, which is generated by the discharge of industrial, livestock, and domestic wastewater with high P concentration [1,2]. Therefore, it is necessary to search for sustainable and efficient processes for the removal of P from aqueous media, its recovery, and recycling [1].

In this work, water hyacinth (*Eichhornia Crassipes*), a noxious weed that grows and spreads on water surface generating environmental problems, is treated with simple thermal transformations to produce adsorbent materials for the removal of P from aqueous solutions. The extensive rooting network in water hyacinth allows it to absorb nutrients (P, N, K, S) from the aqueous systems, which, together with its excessive reproduction, impedes the passage of light through the water and decreases oxygen levels. The conversion of *Eichhornia Crassipes* into an adsorbent material for water decontamination represents an attractive method to improve the management of this problematic invasive species.

This work was developed in three large blocks, which are presented below:

1. Water hyacinth contains 8.1% of P_2O_5 and 32.4% of CaO, therefore, in this work effect of calcination temperature on P and Ca transformation to inorganic compounds assimilable by plants such as apatite was initially studied. Results showed that at calcination temperatures of 450 and 550 °C, it was obtained 5.5 and 6.3% of apatite [$Ca_5(PO_4)_3(OH)$], respectively. These values increased with calcination temperature until reaching 36.6% at 800 °C, which were verified using analysis techniques such as X-ray diffraction (XRD) and infrared spectroscopy (FTIR). Apatite is a compound rich in P and Ca with low water solubility, and it is characterized by being biocompatible with soil as it improves plant growth. Therefore, once it was possible to obtain the material with the largest amount of apatite, solubility tests were performed. It was shown slow P release (between 27.9 and 45.1%) and low P leaching (between 0.9 and 14.7%) by water runoff, which are two fundamental

characteristics in a fertilizer, showing that this material constitutes a suitable resource for this purpose [3].

2. Chemical characterization performed on the material produced from the calcination of water hyacinth showed that in addition to apatite, materials contain metal oxides and hydroxides such as $Ca(OH)_2$, Al_2O_3, MgO, and Fe_3O_4. Therefore, considering that metal oxides/hydroxides have been reported as active phases in P removal P adsorption capacity was studied. Additionally, the effect of the thermal treatments in materials after P adsorption and the transformation to apatite was studied. Results indicated that it is possible to transform the adsorbed P to apatite, increasing the amount initially formed. Adsorption of P on materials obtained at 650 °C was studied by modelling the experimental data to kinetic and isotherm models. A maximum adsorption capacity of 21.3 mg P/g was found. The characterization with FTIR and XRD for the materials before and after P adsorption in combination with the kinetics and isotherms models allowed us to identify the chemisorption as the limiting step of P adsorption and, ligand exchange followed by precipitation as the dominant mechanisms in the adsorption process. In this study, it was also shown that the calcination of these materials after P adsorption induced the transformation to apatite which increased from 25.1 to 41.0%. Solubility tests showed the potential use of these materials as phosphate fertilizer since it presented low solubility in water that guarantees the slow nutrient release in soils [4].

3. This work considered an alternative application in water remediation for the obtained material. Due to the presence of apatite and other Ca phases generated during the thermal process, this work sought to evaluate the immobilization of heavy metals such as Cd^{2+} y Cu^{2+}. Results showed that the removal efficiency of these metals from aqueous solutions increased with increasing calcination temperature from 550 °C (24.9% Cd^{2+} and 12.7% Cu^{2+}) to 700 °C (51,5% Cd^{2+} and 31,8% Cu^{2+}). It was shown that the compounds produced during water hyacinth calcination promote adsorption of Cd^{2+} and Cu^{2+} through precipitation of $CdCO_3$, $Cd_2P_2O_7$, and $Cu_{0.05}Mg_{0.95}O$, $Cu_2P_2O_7$, which have low solubility reducing the mobility of these metals [5].

In general, this research demonstrates that the sustainably perform of P removal and recovery by using waste biomasses is possible, which contributes to the recirculation of this vital and finite element. Likewise, water hyacinth, waste biomass with a high negative impact on the environment, can be valorized.

Keywords: phosphate recycling, water hyacinth, apatite, adsorption, heavy metals, immobilization metals

Organización de la tesis

La tesis se presenta como una colección de capítulos individuales que contribuyen a la obtención de los objetivos de esta investigación. La mayoría de estos capítulos corresponden a artículos que han sido publicados o sometidos en revistas científicas, especializadas en el área de investigación de este trabajo de maestría.

El capítulo 1 corresponde al estado de arte, donde se muestra la importancia del fósforo y la necesidad de buscar fuentes alternativas para el reciclaje de este elemento. Se resalta la eutrofización como uno de los principales problemas en sistemas acuosos, debido al alto contenido de fósforo en aguas residuales descargadas sin un tratamiento adecuado. Se identifican los principales métodos usados para la eliminación de fósforo, tales como remoción biológica, química y física, los cuales no son eficientes al momento de reducir la concentración de fósforo a niveles tan bajos (entre 0.02 - 0.05 mg/L) para evitar que se presente eutrofización de ecosistemas acuáticos. Por lo tanto, se exploran otras alternativas como la adsorción, usando materiales de bajo costo obtenidos a partir de biomasas (como el jacinto de agua), que además permitan recuperar el fósforo adsorbido. De igual manera, se muestran los principales mecanismos que gobiernan el proceso de adsorción de fósforo y los métodos existentes para la recuperación del fósforo adsorbido.

El capítulo 2 presenta la hipótesis planteada para el desarrollo de la investigación y los objetivos de este trabajo.

En el capítulo 3 se muestra el efecto de la temperatura de calcinación en la transformación del fósforo presente naturalmente en el jacinto de agua a un fosfato de calcio biocompatible con el suelo y asimilable por las plantas como la apatita. La caracterización química mediante difracción de rayos X (XRD) y espectroscopía infrarroja (FTIR) indica que el contenido de apatita en los materiales obtenidos depende de la temperatura de calcinación, el cual incrementa con el aumento de la temperatura. Adicionalmente, se evidenció el potencial uso de los materiales como fertilizante fosfatado, debido a la liberación lenta y bajo porcentaje de lixiviación en agua; además, que no contiene trazas de metales que causen efectos negativos en el suelo. En este capítulo se le da valor agregado al jacinto de agua, el cual se caracteriza por ser una maleza acuática con problemas de disposición final.

(Artículo publicado: Anyi Ramirez; Sebastián Pérez; Elizabeth Flórez y Nancy Acelas. *Utilization of water hyacinth (Eichhornia crassipes) rejects as phosphate-rich fertilizer.* **Journal of Environmental Chemical Engineering (2021)** 9(1) 104776).

El capítulo 4 proporciona un enfoque circular para reciclar el jacinto de agua como un material multifuncional para diversas aplicaciones ambientales; por ejemplo, remoción del fósforo desde soluciones acuosas, la recuperación y el reciclaje de este mediante el potencial uso como enmienda para el suelo. El jacinto de agua calcinado a 650 °C proporciona un material heterogéneo que contiene principalmente, en mayor proporción $Ca(OH)_2$, MgO, Al_2O_3 y $Ca_5(PO_4)_3OH$, las cuales son especies que se caracterizan por favorecer la adsorción de fósforo desde soluciones acuosas. Se presenta el ajuste a modelos cinéticos y de isotermas, los mecanismos que gobiernan el proceso de adsorción de fósforo, al igual que la posterior transformación del fósforo adsorbido a apatita y su biodisponibilidad para las plantas. (Artículo sometido: Anyi Ramirez-Muñoz; Sebastián Pérez; Elizabeth Flórez y Nancy Acelas. *Phosphorus recovery from aqueous solution using water hyacinth (Eichhornia Crassipes) toward sustainability through transformation to apatite*. **Journal of Environmental Chemical Engineering**).

En el capítulo 5 se presenta una aplicación alternativa para los materiales obtenidos a partir de jacinto de agua. Teniendo en cuenta que la presencia de apatita y otras fases de Ca se han estudiado en procesos de inmovilización de metales pesados como cadmio (Cd) y cobre (Cu), los cuales se encuentran como iones Cd^{2+} y Cu^{2+} en sistemas acuosos. En este estudio se detalla el proceso de adsorción y la caracterización de la superficie de los materiales antes y después de adsorber Cd^{2+} y Cu^{2+}, usando técnicas de análisis como espectroscopía Infrarroja por Transformada de Fourier (FTIR), difracción de rayos x (XRD) y espectroscopia de fotoelectrones emitidos por rayos X (XPS). Igualmente se muestran experimentos que corroboran la inmovilización del cadmio y cobre en la estructura del material. (Artículo sometido: Anyi Ramirez-Muñoz; Sebastián Pérez; Juan Muñoz-Saldaña; Elizabeth Flórez y Nancy Acelas. *The role of inorganic compounds obtained from the calcination treatments of water hyacinth (Eichhornia Crassipes) on the Cd^{2+} and Cu^{2+} heavy metals uptake (removal and immobilization) from contaminated water*. **Environmental Nanotechnology, Monitoring & Management**).

El capítulo 6 muestra los aspectos relevantes de este trabajo de maestría y adicionalmente, se plantean algunas recomendaciones y perspectivas de futuras investigaciones.

Contenido

Lista de tablas

Lista de figuras

Capítulo 4

Capítulo 5

Capítulo 6

Capítulo 1

1. Estado del arte

1.1. Importancia del fósforo

El fósforo (P) es uno de los elementos fundamentales para la vida y es esencial para la producción de alimentos [6]. La principal fuente de obtención de P es la roca fosfórica, con un 35% de fosfatos (P_2O_5), la cual no es renovable, sus reservas cada día son más limitadas y su precio incrementa de forma continua, debido al aumento de fertilizantes a base de fosfato para la producción agrícola [7,8]. La demanda de fertilizantes fosfatados aumenta anualmente entre 1 y 2% y se espera que para el año 2023 sea aproximadamente 50 millones de toneladas, ocasionando una notable disminución de la fuente de fosfato, que solo podrá satisfacer la demanda de fertilizantes fosfatados durante sólo unos años más [1]. Actualmente, con el objetivo de usar eficientemente los recursos, evitar la fertilización excesiva y reciclar el P, algunos agricultores han optado por aplicar el estiércol de animal en las tierras de cultivo [8]. Sin embargo, estas medidas por sí solas no son suficientes para lograr la sostenibilidad y optimización respecto al uso de P [8]. Por lo tanto, es necesario realizar una mejor gestión del ciclo del P, con un enfoque que aborde la futura escasez de P y explore los métodos de recuperación y reutilización de este.

El P además de ser un nutriente importante para las plantas, es un elemento con movilidad baja en el suelo y a su vez el principal responsable de la eutrofización de ecosistemas acuáticos [7,9,10], debido a la lixiviación [2] por el agua de escorrentía del P presente en el suelo luego de su aplicación como fertilizante [7,9,11]. Adicionalmente, aguas residuales industriales, ganaderas y domésticas con un alto contenido de P y sin un adecuado tratamiento en plantas de tratamiento de aguas residuales (PTAR's), impactan negativamente la biodiversidad de los ecosistemas acuáticos [1,12].

1.2. Métodos de eliminación de fósforo desde soluciones acuosas

En aguas superficiales se ha reportado que concentraciones de P entre 0.02 - 0.05 mg/L, pueden conducir a un crecimiento descontrolado de algas (eutrofización), lo que causa reducción del oxígeno disuelto en el agua y producción de toxinas, llevando a la muerte de peces y pérdida de la vida acuática [7,10]. Por lo tanto, es necesario eliminar el P de aguas superficiales y para ello se han estudiado una variedad de técnicas que involucran métodos biológicos, químicos y físicos.

Los métodos biológicos están basados en la degradación que se presenta en el tratamiento convencional de lodos activados, el cual necesita un estricto control de parámetros operativos para eliminar la gran mayoría de P [13] y genera grandes cantidades de lodos que requieren una adecuada disposición final [14]. En este proceso (lodos activados) las bacterias con capacidad de absorción biológica prolongada de fósforo se multiplican y el P se deposita en la pared celular. La eliminación de P ocurre en el tanque de activación de las PTAR's, por donde circula la corriente principal de las aguas residuales, a través del enriquecimiento biológico y la descarga posterior por medio del lodo excedente [15]. La degradación biológica generada en este tratamiento está sujeta a la necesidad que tienen las bacterias de usar el P para satisfacer sus requerimientos metabólicos básicos, lo cual solo resulta en remociones entre el 20% y el 40% del P presente en el agua residual [16]. Sin embargo, es importante mencionar que existe una clase de bacterias, conocidas como organismos acumuladores de polifosfatos (Polyphosphate Acumulating Organisms, PAOs) [17], los cuales bajo condiciones óptimas pueden tomar P en exceso; es decir, más del que necesitan para el metabolismo normal, fenómeno denominado "luxury uptake". A esto se le conoce como: eliminación biológica mejorada de fósforo (Enhanced Biological Phosphorus Removal, EBPR). Sin embargo, este proceso requiere una configuración más compleja en la PTAR junto con un proceso anaerobio antes del proceso aerobio [16]. En este caso las remociones del P pueden ser mayores al 40%, con la respectiva alta producción de lodos que requieren una disposición final y un incremento en el costo del tratamiento, lo cual constituye una desventaja de los métodos biológicos.

Los métodos químicos están basados principalmente en la precipitación química mediante el uso de calcio, hierro y aluminio. Este proceso es susceptible a condiciones

ambientales como el pH y presenta problemas tanto en la neutralización del efluente como en la disposición final de la alta cantidad de lodos que quedan después del tratamiento [13,14]. En este proceso, el anión fosfato reacciona con los cationes del precipitante (sales) [9,15] y de esta manera se desestabilizan los coloides contenidos en las aguas residuales y cohesionan en microflóculos, que dan paso a la formación de macroflóculos o flóculos [9]. Finalmente, los macroflóculos se separan de las aguas residuales por medio de sedimentación, filtración o la combinación de estos procedimientos. Este proceso de precipitación de fosfatos afecta la degradación biológica de la materia orgánica y la oxido-reducción bacteriana del nitrógeno, ya que se producen cambios en la relación N/DBO (relación Nitrógeno/Demanda Bioquímica de Oxígeno) [15]. El porcentaje de remoción de fósforo con este método es del 80% aproximadamente [15].

Respecto a los métodos físicos, se destacan tres procesos: i) la ósmosis inversa, ii) la electrodiálisis y iii) la adsorción. No obstante, se ha reportado que los dos primeros son ineficientes y costosos [13]. Sin embargo, la adsorción ha demostrado ser prometedora, ya que los contaminantes se pueden eliminar en un amplio rango de pH, a bajas concentraciones de P, algo que no es posible con los métodos biológicos y químicos, pues en estos no es posible eliminar el P hasta una concentración cercana a cero [13]. Esto lleva a una ruta viable para la recuperación y reutilización del P removido. Autores como Cordell et al. [8] han reportado que las aguas residuales tienen un alto contenido de P y que la demanda de fósforo se puede satisfacer mediante la recuperación del P presente en estos medios acuosos. Por lo tanto, los métodos de adsorción de P desde aguas residuales pueden contribuir a satisfacer la demanda futura de P y a ayudar a mitigar los impactos ambientales que conlleva el alto contenido de P en los ecosistemas acuáticos.

Adicionalmente, los métodos de adsorción han demostrado ser atractivos debido a la simplicidad, alta eficiencia y bajo costo de operación. Sin embargo, la baja selectividad hacia el fosfato (en presencia de aniones competitivos, tales como sulfato, cloruro o carbonato) hace que los adsorbentes convencionales no sean útiles para la adsorción y recuperación de P desde soluciones acuosas [18]. Debido a estas dificultades se han desarrollado adsorbentes que son considerados útiles y eficientes, en términos de capacidad y reversibilidad en el

proceso de adsorción [18]. Con este método el porcentaje de remoción de fósforo es del 98% aproximadamente [12,18].

1.3. Adsorción de fósforo desde soluciones acuosas

1.3.1. Cinética e isotermas de adsorción - modelos

La cinética del proceso de adsorción es importante durante los estudios de adsorción, ya que puede predecir la velocidad a la que un contaminante es removido desde soluciones acuosas y proporcionar datos valiosos para el entendimiento del mecanismo de adsorción [19]. Los modelos cinéticos (Tabla 1-1) de pseudo primer orden (ecuación 1-1) [20] y pseudo segundo orden (ecuación 1-2), permiten determinar si el paso que limita el proceso de adsorción es la fisisorción o la quimisorción. En la Tabla 1-2 se presentan los parámetros cinéticos y de isotermas para la adsorción de fósforo desde soluciones acuosas, usando biomasas modificadas y sin modificar. Como se puede observar, la mayoría de los estudios de adsorción de P desde soluciones acuosas usando materiales obtenidos a partir de biomasas (biochars), han reportado que el paso que limita el proceso de adsorción es la quimisorción, el cual por lo general es determinado por el buen ajuste de los datos experimentales a la forma lineal del modelo de pseudo segundo orden. Es importante mencionar que la forma lineal sólo es ideal para explicar los datos de los primeros tiempos de contacto (< 30 minutos) mientras que la forma no lineal proporciona valores más confiables de velocidad y capacidad de adsorción, ya que disminuye el sesgo entre los datos experimentales y los calculados por el modelo [21]. Por lo tanto, es importante evaluar el ajuste de los datos experimentales usando las formas no lineales de los modelos cinéticos de pseudo segundo orden y pseudo primer orden, tal y como se presenta en la Tabla 1-2, donde la mayoría de los estudios han reportado el uso de los modelos cinéticos no lineales.

Por otra parte, la retención de una sustancia en un sólido a diversas concentraciones se mide a través de una isoterma de adsorción [22]. Los modelos de isotermas (Tabla 1-1) de Langmuir (ecuación 1-3), Freundlich (ecuación 1-4) [23], Temkin (ecuación 1-5) [24] y Langmuir-Freundlich (ecuación 1-6) [25,26] son muy usados para los estudios de equilibrio en los procesos de adsorción de P. Estos modelos permiten determinar características como: a) la capacidad máxima de adsorción; b) la favorabilidad o no favorabilidad del proceso de adsorción; c) el tipo de interacción; y d) la heterogeneidad del adsorbente.

De los datos presentados en la Tabla 1-2 se tiene que los datos experimentales se ajustan a cualquiera de los modelos de isotermas mencionados. Por lo tanto, de cada ajuste es posible obtener datos importantes que ayudan a entender el proceso de adsorción de P. Cuando los datos se ajustan al modelo de Langmuir, significa que en el equilibrio la adsorción ocurre en monocapa, con una superficie homogénea que presenta número fijo de sitios activos que tienen la misma afinidad por P. En cambio, si los datos se ajustan al modelo de Freundlich, se puede interpretar que existen interacciones en superficies heterogéneas en multicapas, las cuales presentan diferentes afinidades y energías de interacción entre los sitios activos de la superficie del adsorbente y el P, lo que indica diferentes sitios activos para remover P. Ahora bien, como se observa en la Tabla 1-2 los datos pueden ajustarse a más de un modelo de isoterma, de lo que se puede inferir que en ese caso no existe una única forma de interacción entre el material adsorbente (Biochar)–P y que además hay mezcla de mecanismos de adsorción. Por otro lado, cuando los datos se ajustan al modelo de Langmuir-Freundlich, se puede encontrar comportamiento tanto de Langmuir como de Freundlich, lo que corresponde a una isoterma versátil que adicionalmente aporta un dato importante que permite determinar la homogeneidad o heterogeneidad del material adsorbente [10]. Con el ajuste al modelo de Temkin, se asume que el calor de adsorción del adsorbato en una capa disminuye linealmente con el cubrimiento de la superficie del adsorbente debido a las interacciones adsorbente–P [27].

Tabla 1-1. Ecuaciones de los modelos cinéticos y de isotermas.

Modelo	Ecuación	
Pseudo primer orden	$q_t = q_e(1-e^{-k_1 t})$	(1-1)
Pseudo segundo orden	$q_t = \dfrac{q_e{}^2 k_2 t}{1 + q_e k_2 t}$	(1-2)
Langmuir	$q_e = \dfrac{C_e Q_m K_L}{C_e K_L + 1}$	(1-3)
Freundlich	$q_e = K_F C_e^{\frac{1}{n}}$	(1-4)

Temkin		$q_e = \dfrac{RT}{b} Ln(K_T C_e)$			(1-5)
Langmuir-Freundlich		$q_e = \dfrac{Q_m (K_a C_{eq})^{n_{LF}}}{(K_a C_{eq})^{n_{LF}} + 1}$			(1-6)

En la Tabla 1-1, q_e: cantidad de contaminante adsorbido en el equilibrio (mg/g); q_t: es la cantidad de contaminante adsorbido en tiempo (mg/g); t: tiempo (min); k_1: constante de velocidad de pseudo primer orden (1/min); k_2: constante de velocidad de pseudo segundo orden (g/mg.min); Q_m: capacidad máxima de adsorción (mg/g); C_e: concentración en el equilibrio (mg/L); K_L: constante de Langmuir (L/g); K_F: capacidad de adsorción en multicapa (mg/g); $\frac{1}{n}$: constante ligada a la intensidad de adsorción; K_a: constante de afinidad de adsorción (L/mg); n_{LF}: índice de heterogeneidad; R: constante universal de los gases (kJ/mol.K); T: temperatura (K); K_T: constante de Temkin (L/g); b: constante relacionada con el calor de la adsorción (kJ/mol).

Tabla 1-2. Parámetros cinéticos y de isotermas para la adsorción de fósforo desde soluciones acuosas usando biomasas modificadas y sin modificar.

Adsorbente	Método de modificación	Modelo cinético	Modelo de isoterma	Capacidad máxima de adsorción, Q_m (mg/g)	Referencia
Residuos de concha de mejillón	Impregnación con Fe	Pseudo segundo orden - lineal	Freundlich	0.30	[28]
Residuo de lodos activados	Impregnación con Fe	Pseudo segundo	Freundlich	111.0	[29]

		orden - lineal			
Lodos de depuradora	Sin modificar	Pseudo segundo orden - lineal	Langmuir y Temkin	3.8	[30]
Paja de trigo	Sin modificar	Pseudo primer orden y pseudo segundo orden -no lineal	Langmuir	1.64	[31]
Paja de trigo	Impregnación con Al	Pseudo segundo orden -no lineal	Langmuir	82.78	[31]
Paja de trigo	Impregnación con Mg	Pseudo primer orden y pseudo segundo orden -no lineal	Langmuir	153.40	[31]
Paja de trigo	Impregnación con Mg y Al	Pseudo segundo orden -no lineal	Langmuir	153.40	[31]

Paja de caña de azúcar	Impregnación con Mg	-	Langmuir	17.60	[32]
Bambú	Sin modificar	-	-	1.33	[33]
Bambú	Impregnación con Mg	Pseudo segundo orden -no lineal	Langmuir y Freundlich	344	[33]
Cáscara de huevo / fibra de palma	Sin modificar	Pseudo segundo orden -no lineal	Langmuir	72.0	[34]
Cáscara de huevo / paja de arroz	Sin modificar	Pseudo segundo orden - lineal	Langmuir	231	[35]
Jacinto de agua	Co-precipitación con Fe	Pseudo segundo orden -no lineal	Langmuir - Freundlich	5.07	[10]
Jacinto de agua	Enriquecimiento con Fe, Mn, Zn y Cu	Pseudo segundo orden -no lineal	Freundlich	entre 12.15 y 31.55	[37]
Microalga marina marrón	Sin modificar	-	Langmuir y Langmuir - Freundlich	8.23	[36]

Microalga marina marrón	Electroquímica	-	Langmuir - Freundlich	31.28	[36]

1.3.2. Materiales usados para adsorber fósforo

En los procesos de adsorción de P se ha reportado el uso de materiales adsorbentes como carbón activado, zeolita, quitosano, hidróxidos metálicos, entre otros [12,38–41]. Estos materiales, en especial los carbones activados, se pueden impregnar o modificar con diferentes iones metálicos para mejorar la capacidad de adsorción de P [1]. Sin embargo, la búsqueda de adsorbentes más económicos y con alta capacidad de adsorción de P, sigue representando un desafío para las investigaciones futuras.

La búsqueda de adsorbentes económicos ha tenido especial atención en aquellos que son obtenidos a partir de diferentes biomasas generadas en los procesos agroindustriales por su bajo costo, amplia variedad de materia prima y facilidad de modificación, y como valor agregado, reducción de carga ambiental producida por dichos residuos [1]. Como se observa en la Tabla 1-2, en la adsorción de P se puede usar biomasa modificada o sin modificar. La biomasa sin modificar generalmente tiene mucha materia orgánica y una fuerte capacidad de adsorción de cationes, pero una adsorción limitada de contaminantes aniónicos (como fosfatos), debido al bajo contenido de cationes metálicos; además, dado que la estructura de la biomasa tiene compuestos orgánicos ricos en P, durante los procesos de adsorción se evidencia liberación de P [35]. Por lo tanto, para mejorar la capacidad de adsorción de P de los residuos de biomasa, se ha planteado introducir minerales y especies catiónicas en su estructura. Para tal fin, diversas metodologías han sido reportadas: a) impregnación (antes y después de pirólisis), b) modificación electroquímica, c) enriquecimiento de la biomasa con metales usando soluciones de adición (bioacumulación), d) co-pirólisis de la biomasa y fuentes naturales de iones metálicos, entre otras metodologías [1]. Por otra parte, características fisicoquímicas como composición elemental, área de superficie y porosidad de los adsorbentes, son otros factores que afectan la capacidad de adsorción, los cuales varían dependiendo el tipo de biomasa y la temperatura del tratamiento. Específicamente, cuando

se habla de materiales eficientes para remover P, se ha reportado que la presencia de elementos metálicos tales como Mg, Al, Ca, La y Fe, son los que influyen en la adsorción de P [1,35,42]. Por lo tanto, biomasas ricas en estos minerales tales como cáscara de huevo, thalia dealbata, cáscara de maní, lodos de depuradora y jacinto de agua, se convierten en una alternativa para producir materiales adsorbentes para remover P desde sistemas acuosos [34,37,43–45].

Diversos autores han evaluado el uso de jacinto de agua (*Eichhornia Crassipes*) para la adsorción de P. Por ejemplo, Cai et al. [10] estudiaron la adsorción de P de un biochar preparado a partir de la pirólisis de jacinto de agua, modificado con óxido de hierro, encontrando una capacidad máxima de adsorción (Q_m) de 5.07 mg/g. Los autores determinaron que los principales mecanismos responsables de la elimnación de P eran la atracción electrostática entre la superficie del adsorbente cargada positivamente y los aniones de P presentes en solución, y el intercambio de ligandos entre los grupos –OH de la superficie enlazados a los átomos de Fe y los aniones de P en la solución para formar los enlaces Fe–O–P. Por otro lado, Mosa et al. [37] estudiaron la adsorción de P usando biochars, generados en la pirólisis de jacinto de agua ricos en metales (Fe, Mn, Zn y Cu). Ellos encontraron Q_m entre 12.15 y 31.55 mg/g, sugiriendo la precipitación como el mecanismo predominante en el proceso de adsorción, con contribución parcial de intercambio iónico, atracción electrostática y formación de complejos con los grupos funcionales activos. Para nuestro conocimiento, aún no se conocen reportes donde los residuos de Jacinto de agua sean transformados térmicamente y que sus minerales presentes naturalmente se usen como fases activas para la eliminación selectiva de P desde sistemas acuosos, y su posterior recuperación desde el material adsorbido.

1.3.3. *Mecanismo de adsorción de fósforo*

Los análisis de modelos cinéticos y de isotermas permiten tener una idea de la manera como se da el proceso de adsorción. Sin embargo, para entender el mecanismo de adsorción que involucra interacciones físicas y químicas entre el P en forma del anión fosfato ($H_2PO_4^-$) y el adsorbente, es necesario usar técnicas químicas de caracterización. El mecanismo varía dependiendo del material adsorbente utilizado e incluye interacciones electrostáticas,

interacción con hidrógenos, intercambio iónico, intercambio de ligandos, complejación y precipitación [1,18,46,47] (Fig. 1-1).
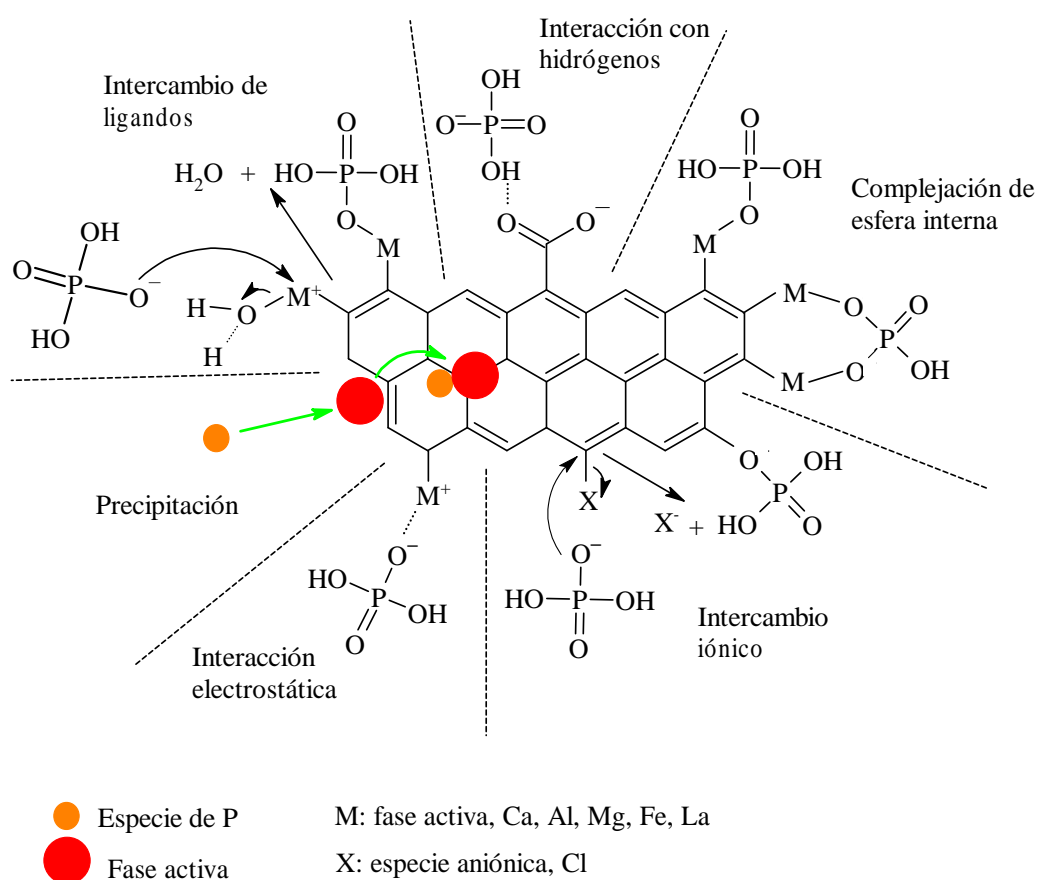
Fig. 1-1. Mecanismos que pueden intervenir en el proceso de adsorción de fosfato.

La interacción electrostática es afectada por el pH de la solución y del punto de carga cero (pH_{PZC}) del adsorbente, lo cual se presenta en procesos químicos y físicos, y se considera como un proceso de adsorción fácil y reversible [1,48]. En este mecanismo hay atracción entre las cargas negativas del fosfato y las positivas presentes en la superficie del adsorbente.

En la interacción con hidrógeno los aniones de fosfato ($H_2PO_4^-$ y HPO_4^{2-}) pueden interactuar con los aceptores de hidrógeno del material, formando enlaces de hidrógeno [47,49].

El intercambio de iones se da cuando un anión de fosfato reemplaza a un anión de la estructura del adsorbente, y se considera un proceso reversible cuando los iones de fosfato se pueden recuperar de la superficie del material adsorbente [1,29].

11

En el intercambio de ligandos, el anión fosfato forma un enlace con un catión metálico en la superficie del adsorbente, dando como resultado la liberación de iones OH^- que se encontraban unidos al catión metálico [18,48,49], ocasionando un incremento del pH final de la solución. La adsorción de fosfato mediante este mecanismo, está relacionada con la complejación de esfera interna, la cual da como resultado una unión más fuerte de los aniones de P con el adsorbente en comparación con el intercambio iónico [48].

La complejación (interna o externa) tiene lugar en soluciones acuosas donde la superficie de los óxidos/hidróxidos metálicos está generalmente cubierta con grupos hidroxilo. En la complejación de esfera interna, una molécula de fosfato se une a uno o dos átomos de metal (mono o binuclear, respectivamente), mediante uno o dos enlaces de oxígeno (mono o bidentado, respectivamente) [18,47,49]. Mientras que en la complejación de esfera externa, una molécula de agua está presente entre los iones y la superficie del óxido metálico [49].

La precipitación de sales de fosfato poco solubles ocurre cuando la concentración del fosfato excede su solubilidad. La precipitación de las especies de fosfato sobre la superficie del adsorbente se ha reportado ampliamente para materiales modificados con Ca, Mg, Al y Fe [37,50,51]. Con materiales que contienen grandes cantidades de Ca soluble y un pH alto, la eliminación puede ocurrir directamente a través de la formación de precipitados de fosfato de Ca. Este proceso es rápido y los fosfatos precipitados no se recuperan fácilmente [1].

1.4. Métodos de recuperación del fósforo adsorbido

Generalmente, se han usado dos métodos para recuperar el P desde el material adsorbido, uno está enfocado a la desorción del fosfato adsorbido en el material y en el otro se trata de utilizar directamente el material adsorbido con P en aplicaciones agrícolas, como un tipo de fertilizante fosfatado.

La desorción de P desde los materiales adsorbidos está pensada para adsorbentes cuyo costo de producción es elevado, por lo que es necesario encontrar soluciones eluyentes de fosfato para dejar el material adsorbente en óptimas condiciones y que pueda ser utilizado en un nuevo ciclo de adsorción; esto implica que dicho adsorbente se someta a varios ciclos de adsorción-regeneración [12]. Se han usado soluciones eluyentes basadas en ácidos (HCl,

H$_2$SO$_4$ y C$_6$H$_8$O$_7$), bases (NaOH) y sales (NaCl), donde su eficiencia de desorción depende de la fortaleza de la interacción P-adsorbente, del número de ciclos de regeneración y del efecto de la solución sobre los elementos con los que fue dopado el biochar [1]. Una vez el P es retirado del adsorbente se obtiene una solución concentrada de P con la cual es posible sintetizar materiales ricos en fosfato; por ejemplo, la estruvita, que puede ser utilizada como fertilizante [52–54]. Ramirez et al. [12] estudiaron la desorción de P usando NaOH, NaCl y NaOH/NaCl desde una resina sintética impregnada con óxidos de Fe hidratados, la cual previamente había adsorbido P. Encontraron que el NaCl tenía la capacidad de desorber hasta el 97% del P adsorbido; adicionalmente, el material adsorbente quedaba en óptimas condiciones para adsorber P nuevamente, soportando hasta 3 ciclos de adsorción-regeneración y reduciendo solo un 26% de su capacidad de adsorción inicial. Por su parte, Shiba y Ntuli [55] obtuvieron una tasa de extracción de P de lodos de depuradora de 82% en 2 horas, y con el fin de eliminar metales (Fe) de la solución rica en P, esta fue sometida a un proceso de adsorción usando una resina catiónica; la solución libre de Fe fue usada en la precipitación de P en forma de estruvita.

Para materiales adsorbentes producidos a partir de biomasa como el biochar, que es un material rico en carbono y otros nutrientes, una vez se logra una adsorción eficiente de P, la mejor manera de usarlo es aplicándolo directamente como enmienda para suelos; así, además de mejorar la capacidad de retención de agua, aumenta la capacidad de unión de nutrientes y mejora la fertilidad del suelo [56,57]. Esta es la mejor manera de utilizar el P adsorbido, dado que para estos materiales la regeneración después de la adsorción suele ser difícil [31,58,59]. Las aplicaciones de los materiales cargados con fosfato están sujetas tanto a la biodisponibilidad del P como a la posibilidad de desorción de iones metálicos (Cu, Cd, Pb, Cr, entre otros) presentes en el material que pueden tener un efecto negativo para el suelo. Por lo que es necesario garantizar que el adsorbente no posea esos metales en su estructura.

La biodisponibilidad de P, luego de ser adsorbido en el material y el suministro de fosfato a las plantas cultivadas, depende de factores como la cantidad de fosfato que ya se encuentra en la estructura del material, la cantidad de fosfato adsorbido en el material, la interacción entre el fosfato adsorbido y otros nutrientes presentes en el biochar que podrían agregarse de otras fuentes, y de la interacción entre el fosfato y los elementos disponibles en

los materiales [37]. Algunos autores han investigado la biodisponibilidad del fosfato en los materiales adsorbidos y el suministro de fosfato a las plantas, mediante el estudio de liberación de fosfato por medio de su lixiviación de los materiales en el tiempo. Por ejemplo, Yao et al. [60] obtuvieron una tasa de liberación de P de 4.5 mg/g en 144 horas, para un biochar preparado a partir de tejidos de tomate enriquecidos con Mg que contenían 116.6 mg/g de fosfato; Liu et al. [61] estudiaron la transformación del P presente en lodos de depuradora adicionando CaO para obtener un material rico en fases de fosfato de calcio (apatita) que mejoraba la disponibilidad de P para las plantas; adicionalmente, ellos estudiaron la lixiviación de metales peligrosos (Zn, Mn, Cu, Cr y Pb) y encontraron que la adición de CaO ayudaba a disminuir la liberación de dichos metales, debido a la posible formación de fases cristalizadas en las que quedaban inmovilizados. Sin embargo, a pesar del progreso que se ha logrado utilizando los materiales cargados de fosfato como fertilizantes de liberación lenta, se requieren más investigaciones que tengan en cuenta el problema de inmovilización de iones metálicos, ya que su alto contenido en el material conlleva a riesgos para el medio ambiente y la salud humana y, por lo tanto, limita su aplicación como enmienda o fertilizante del suelo.

1.5. Justificación de la investigación

Para la eliminación de P desde soluciones acuosas, minerales compuestos de Ca, Al, Mg, Si y Fe se han reportado como activos para la adsorción selectiva de este elemento, a través de formación de complejos de esfera interna, precipitación química, intercambio iónico e intercambio de ligandos [18,47,49,62,63]. Por lo tanto, biomasas ricas en estos minerales tal como el jacinto de agua, se convierten en una alternativa para producir materiales adsorbentes con gran potencial. Los tratamientos térmicos al Jacinto de agua, permiten transformar los minerales presentes en las principales fases activas para el proceso de adsorción de P. Sin embargo, a la fecha no se conocen estudios donde se reporte que a través de una transformación térmica simple y económica del Jacinto de agua, pueda obtenerse un material adsorbente aprovechando los minerales presentes naturalmente, actuando estos como fases activas en la eliminación de P, lo cual permita alcanzar alta capacidad de adsorción de P y su posterior recuperación desde el material adsorbido. Del mismo modo, dichos estudios no incluyen análisis cinéticos detallados para entender

procesos de adsorción de P y una caracterización minuciosa que permita elucidar el mecanismo que da lugar al proceso de adsorción.

Por consiguiente, este estudio está basado en la hipótesis de que la transformación térmica simple y económica del Jacinto de agua (*Eichhornia Crassipes*), permite generar un material adsorbente para remover fósforo desde soluciones acuosas, con el que adicionalmente se pueda obtener un producto de alto valor agregado y biodisponible en el suelo.

1.6. Referencias

[1]   I.W. Almanassra, G. Mckay, V. Kochkodan, M. Ali Atieh, T. Al-Ansari, A state of the art review on phosphate removal from water by biochars, Chem. Eng. J. 409 (2021) 128211. https://doi.org/10.1016/j.cej.2020.128211.

[2]   Q.-F. Bi, K.-J. Li, B.-X. Zheng, X.-P. Liu, H.-Z. Li, B.-J. Jin, K. Ding, X.-R. Yang, X.-Y. Lin, Y.-G. Zhu, Partial replacement of inorganic phosphorus (P) by organic manure reshapes phosphate mobilizing bacterial community and promotes P bioavailability in a paddy soil, Sci. Total Environ. 703 (2020) 134977. https://doi.org/https://doi.org/10.1016/j.scitotenv.2019.134977.

[3]   A. Ramirez, S. Pérez, N. Acelas, E. Flórez, Utilization of water hyacinth (Eichhornia crassipes) rejects as phosphate-rich fertilizer, J. Environ. Chem. Eng. 9 (2021) 104776. https://doi.org/10.1016/j.jece.2020.104776.

[4]   A. Ramirez-Muñoz, S. Pérez, E. Flórez, N.Y. Acelas, Phosphorus removal and hydroxyapatite formation from aqueous solution using water hyacinth (Eichhornia Crassipes), Sometido. (2021).

[5]   A. Ramirez-Muñoz, S. Pérez, J. Muñoz-Saldaña, E. Flórez, N.Y. Acelas, The role of inorganic compounds obtained from the calcination treatments of water hyacinth (Eichhornia Crassipes) on the Cd^{2+} and Cu^{2+} heavy metals uptake (removal and immobilization) from contaminated water, Sometido. (2021).

[6]   D. Cordell, S. White, Peak phosphorus: Clarifying the key issues of a vigorous debate

about long-term phosphorus security, Sustainability. 3 (2011) 2027–2049. https://doi.org/10.3390/su3102027.

[7]   R. Li, J.J. Wang, B. Zhou, M.K. Awasthi, A. Ali, Z. Zhang, A.H. Lahori, A. Mahar, Recovery of phosphate from aqueous solution by magnesium oxide decorated magnetic biochar and its potential as phosphate-based fertilizer substitute, Bioresour. Technol. 215 (2016) 209–214. https://doi.org/10.1016/j.biortech.2016.02.125.

[8]   D. Cordell, A. Rosemarin, J.J. Schröder, A.L. Smit, Towards global phosphorus security: A systems framework for phosphorus recovery and reuse options, Chemosphere.   84   (2011)   747–758. https://doi.org/10.1016/j.chemosphere.2011.02.032.

[9]   N. Tran, P. Drogui, J.F. Blais, G. Mercier, Phosphorus removal from spiked municipal wastewater using either electrochemical coagulation or chemical coagulation as tertiary   treatment,   Sep.   Purif.   Technol.   95   (2012)   16–25. https://doi.org/10.1016/j.seppur.2012.04.014.

[10]   R. Cai, X. Wang, X. Ji, B. Peng, C. Tan, X. Huang, Phosphate reclaim from simulated and real eutrophic water by magnetic biochar derived from water hyacinth, J. Environ. Manage. 187 (2017) 212–219. https://doi.org/10.1016/j.jenvman.2016.11.047.

[11]   G. Rodriguez-Garcia, M. Molinos-Senante, A. Hospido, F. Hernández-Sancho, M.T. Moreira, G. Feijoo, Environmental and economic profile of six typologies of wastewater   treatment   plants,   Water   Res.   45   (2011)   5997–6010. https://doi.org/10.1016/j.watres.2011.08.053.

[12]   A. Ramirez, S. Giraldo, J. García-Nunez, E. Flórez, N. Acelas, Phosphate removal from water using a hybrid material in a fixed-bed column, J. Water Process Eng. 26 (2018) 131–137. https://doi.org/10.1016/j.jwpe.2018.10.008.

[13]   R. Liu, L. Chi, X. Wang, Y. Sui, Y. Wang, H. Arandiyan, Review of metal (hydr)oxide and other adsorptive materials for phosphate removal from water, J. Environ. Chem. Eng. 6 (2018) 5269–5286. https://doi.org/10.1016/j.jece.2018.08.008.

[14]   J.A. Marshall, B.J. Morton, R. Muhlack, D. Chittleborough, C.W. Kwong, Recovery

of phosphate from calcium-containing aqueous solution resulting from biochar-induced calcium phosphate precipitation, J. Clean. Prod. 165 (2017) 27–35. https://doi.org/10.1016/j.jclepro.2017.07.042.

[15] L.E. de-Bashan, Y. Bashan, Recent advances in removing phosphorus from wastewater and its future use as fertilizer (1997–2003), Water Res. 38 (2004) 4222–4246. https://doi.org/https://doi.org/10.1016/j.watres.2004.07.014.

[16] G.K. Morse, S.W. Brett, J.A. Guy, J.N. Lester, Review: Phosphorus removal and recovery technologies, Sci. Total Environ. 212 (1998) 69–81. https://doi.org/10.1016/S0048-9697(97)00332-X.

[17] H. Ge, D.J. Batstone, J. Keller, Biological phosphorus removal from abattoir wastewater at very short sludge ages mediated by novel PAO clade Comamonadaceae, Water Res. 69 (2015) 173–182. https://doi.org/https://doi.org/10.1016/j.watres.2014.11.026.

[18] N.Y. Acelas, B.D. Martin, D. López, B. Jefferson, Selective removal of phosphate from wastewater using hydrated metal oxides dispersed within anionic exchange media, Chemosphere. 119 (2015) 1353–1360. https://doi.org/10.1016/j.chemosphere.2014.02.024.

[19] A. Ramirez, S. Giraldo, E. Flórez Yepes, N.Y. Acelas Soto, Preparación de carbón activado a partir de residuos de palma de aceite y su aplicación para la remoción de colorantes, Rev. Colomb. Química. 46 (2017) 33–41. https://doi.org/10.15446/rev.colomb.quim.v46n1.62851.

[20] S. Lagergren, Zur theorie der sogenannten adsorption geloster stoffe, K. Sven. Vetenskapsakademiens. Handl. 24 (1898) 1–39.

[21] H. Nguyen, S. You, A. Hosseini-bandegharaei, Mistakes and inconsistencies regarding adsorption of contaminants from aqueous solutions : A critical review, Water Res. 120 (2017) 88–116. https://doi.org/10.1016/j.watres.2017.04.014.

[22] G. Limousin, J.P. Gaudet, L. Charlet, S. Szenknect, V. Barthès, M. Krimissa, Sorption isotherms: A review on physical bases, modeling and measurement, Appl.

Geochemistry. 22 (2007) 249–275. https://doi.org/10.1016/j.apgeochem.2006.09.010.

[23]   H. Freundlich, Über die adsorption in lösungen, Zeitschrift Für Phys. Chemie. 57 (1907) 385–470.

[24]   M.J. Temkin, V. Pyzhev, Recent modifications to Langmuir isotherms, Acta Physicochim. USSR. 12 (1940) 217–222.

[25]   R. Sips, On the structure of a catalyst surface, J. Chem. Phys. 16 (1948) 490–495.

[26]   R. Sips, On the structure of a catalyst surface. II, J. Chem. Phys. 18 (1950) 1024–1026.

[27]   A. Ramirez, R. Ocampo, S. Giraldo, E. Padilla, E. Flórez, N. Acelas, Removal of Cr(VI) from an aqueous solution using an activated carbon obtained from teakwood sawdust: Kinetics, equilibrium, and density functional theory calculations, J. Environ. Chem. Eng. 8 (2020) 103702. https://doi.org/10.1016/j.jece.2020.103702.

[28]   N.A.A. Salim, M.A. Fulazzaky, M.H. Puteh, M.H. Khamidun, A.R.M. Yusoff, N.H. Abdullah, N. Ahmad, Z.M. Lazim, M. Nuid, Adsorption of phosphate from aqueous solution onto iron-coated waste mussel shell: Physicochemical characteristics, kinetic, and isotherm studies, Biointerface Res. Appl. Chem. 11 (2021) 12831–12842. https://doi.org/10.33263/BRIAC115.1283112842.

[29]   Q. Yang, X. Wang, W. Luo, J. Sun, Q. Xu, F. Chen, J. Zhao, S. Wang, F. Yao, D. Wang, X. Li, G. Zeng, Effectiveness and mechanisms of phosphate adsorption on iron-modified biochars derived from waste activated sludge, Bioresour. Technol. 247 (2018) 537–544. https://doi.org/10.1016/j.biortech.2017.09.136.

[30]   L. Zhang, J. Liu, X. Guo, Investigation on mechanism of phosphate removal on carbonized sludge adsorbent, J. Environ. Sci. (China). 64 (2018) 335–344. https://doi.org/10.1016/j.jes.2017.06.034.

[31]   Q. Zheng, L. Yang, D. Song, S. Zhang, H. Wu, S. Li, X. Wang, High adsorption capacity of Mg–Al-modified biochar for phosphate and its potential for phosphate interception in soil, Chemosphere. 259 (2020) 127469. https://doi.org/https://doi.org/10.1016/j.chemosphere.2020.127469.

[32]   S.V. Novais, M.D.O. Zenero, J. Tronto, R.F. Conz, C.E.P. Cerri, Poultry manure and sugarcane straw biochars modified with MgCl2 for phosphorus adsorption, J. Environ. Manage. 214 (2018) 36–44. https://doi.org/10.1016/j.jenvman.2018.02.088.

[33]   D. Jiang, B. Chu, Y. Amano, M. Machida, Removal and recovery of phosphate from water by Mg-laden biochar: Batch and column studies, Colloids Surfaces A. 558 (2018) 429–437. https://doi.org/10.1016/j.colsurfa.2018.09.016.

[34]   S. Pérez, J. Muñoz-Sadaña, N. Acelas, E. Flórez, Phosphate removal from aqueous solutions by heat treatment of eggshell and palm fiber, J. Environ. Chem. Eng. (2020) 104684. https://doi.org/10.1016/j.jece.2020.104684.

[35]   X. Liu, F. Shen, X. Qi, Adsorption recovery of phosphate from aqueous solution by CaO-biochar composites prepared from eggshell and rice straw, Sci. Total Environ. 666 (2019) 694–702. https://doi.org/10.1016/j.scitotenv.2019.02.227.

[36]   K.W. Jung, M.J. Hwang, T.U. Jeong, K.H. Ahn, A novel approach for preparation of modified-biochar derived from marine macroalgae: Dual purpose electro-modification for improvement of surface area and metal impregnation, Bioresour. Technol. 191 (2015) 342–345. https://doi.org/10.1016/j.biortech.2015.05.052.

[37]   A. Mosa, A. El-ghamry, M. Tolba, Functionalized biochar derived from heavy metal rich feedstock: Phosphate recovery and reusing the exhausted biochar as an enriched soil amendment, Chemosphere. 198 (2018) 351–363. https://doi.org/10.1016/j.chemosphere.2018.01.113.

[38]   J. Lalley, C. Han, X. Li, D.D. Dionysiou, M.N. Nadagouda, Phosphate adsorption using modified iron oxide-based sorbents in lake water: Kinetics, equilibrium, and column tests, Chem. Eng. J. 284 (2016) 1386–1396. https://doi.org/10.1016/j.cej.2015.08.114.

[39]   S. Egemose, M.J. Sønderup, M. V Beinthin, K. Reitzel, C.C. Hoffmann, M.R. Flindt, Crushed Concrete as a Phosphate Binding Material: A Potential New Management Tool, J. Environ. Qual. 41 (2012) 647–653. https://doi.org/10.2134/jeq2011.0134.

[40]   X. Liu, L. Zhang, Removal of phosphate anions using the modified chitosan beads:

Adsorption kinetic, isotherm and mechanism studies, Powder Technol. 277 (2015) 112–119. https://doi.org/10.1016/j.powtec.2015.02.055.

[41] A.S. Tofik, A.M. Taddesse, K.T. Tesfahun, G.G. Girma, Fe-Al binary oxide nanosorbent: Synthesis, characterization and phosphate sorption property, J. Environ. Chem. Eng. 4 (2016) 2458–2468. https://doi.org/10.1016/j.jece.2016.04.023.

[42] C.A. Takaya, L.A. Fletcher, S. Singh, K.U. Anyikude, A.B. Ross, Phosphate and ammonium sorption capacity of biochar and hydrochar from different wastes, Chemosphere. 145 (2016) 518–527. https://doi.org/10.1016/j.chemosphere.2015.11.052.

[43] Z. Zeng, S. Da Zhang, T.Q. Li, F.L. Zhao, Z.L. He, H.P. Zhao, X.E. Yang, H.L. Wang, J. Zhao, M.T. Rafiq, Sorption of ammonium and phosphate from aqueous solution by biochar derived from phytoremediation plants, J. Zhejiang Univ. Sci. B. 14 (2013) 1152–1161. https://doi.org/10.1631/jzus.B1300102.

[44] X. Zheng, Y. Ye, Z. Jiang, Z. Ying, S. Ji, W. Chen, B. Wang, B. Dou, Enhanced transformation of phosphorus (P) in sewage sludge to hydroxyapatite via hydrothermal carbonization and calcium-based additive, Sci. Total Environ. 738 (2020) 139786. https://doi.org/10.1016/j.scitotenv.2020.139786.

[45] K.W. Jung, M.J. Hwang, K.H. Ahn, Y.S. Ok, Kinetic study on phosphate removal from aqueous solution by biochar derived from peanut shell as renewable adsorptive media, Int. J. Environ. Sci. Technol. 12 (2015) 3363–3372. https://doi.org/10.1007/s13762-015-0766-5.

[46] I.W. Almanassra, V. Kochkodan, M. Subeh, G. Mckay, M. Atieh, T. Al-Ansari, Phosphate removal from synthetic and treated sewage effluent by carbide derive carbon, J. Water Process Eng. 36 (2020) 101323. https://doi.org/10.1016/j.jwpe.2020.101323.

[47] N.Y. Acelas, S.M. Mejia, F. Mondragón, E. Flórez, Density functional theory characterization of phosphate and sulfate adsorption on Fe-(hydr)oxide: Reactivity, pH effect, estimation of Gibbs free energies, and topological analysis of hydrogen bonds, Comput. Theor. Chem. 1005 (2013) 16–24.

https://doi.org/10.1016/j.comptc.2012.11.002.

[48] P. Loganathan, S. Vigneswaran, J. Kandasamy, N.S. Bolan, Removal and recovery of phosphate from water using sorption, Crit. Rev. Environ. Sci. Technol. 44 (2014) 847–907. https://doi.org/10.1080/10643389.2012.741311.

[49] B. Wu, J. Wan, Y. Zhang, B. Pan, I.M.C. Lo, Selective phosphate removal from water and wastewater using sorption: process fundamentals and removal mechanisms, Environ. Sci. Technol. 54 (2020) 50–66. https://doi.org/10.1021/acs.est.9b05569.

[50] R. Li, J.J. Wang, Z. Zhang, M. Kumar, D. Du, P. Dang, Q. Huang, Y. Zhang, L. Wang, Recovery of phosphate and dissolved organic matter from aqueous solution using a novel CaO-MgO hybrid carbon composite and its feasibility in phosphorus recycling, Sci. Total Environ. 642 (2018) 526–536. https://doi.org/10.1016/j.scitotenv.2018.06.092.

[51] S. Liu, X. Tan, Y. Liu, Y. Gu, G. Zeng, X. Hu, H. Wang, L. Zhou, L. Jiang, B. Zhao, Production of biochars from Ca impregnated ramie biomass (Boehmeria nivea (L.) Gaud.) and their phosphate removal potential, RSC Adv. 6 (2016) 5871–5880. https://doi.org/10.1039/C5RA22142K.

[52] N. Acelas, E. Flórez, D. López, Phosphorus recovery through struvite precipitation from wastewater: effect of the competitive ions, Desalin. Water Treat. 54 (2015) 2468–2479. https://doi.org/10.1080/19443994.2014.902337.

[53] M.M. Thant Zin, D.J. Kim, Simultaneous recovery of phosphorus and nitrogen from sewage sludge ash and food wastewater as struvite by Mg-biochar, J. Hazard. Mater. 403 (2021) 123704. https://doi.org/10.1016/j.jhazmat.2020.123704.

[54] M. Li, H. Sun, H. Zhang, A. Mohammed, Y. Liu, Q. Lu, Phosphorus recovery from synthetic biosolid digestion supernatant through lignin-induced struvite precipitation, J. Clean. Prod. 276 (2020) 124235. https://doi.org/10.1016/j.jclepro.2020.124235.

[55] N.C. Shiba, F. Ntuli, Extraction and precipitation of phosphorus from sewage sludge, Waste Manag. 60 (2017) 191–200. https://doi.org/10.1016/j.wasman.2016.07.031.

[56] W. Wu, M. Yang, Q. Feng, K. McGrouther, H. Wang, H. Lu, Y. Chen, Chemical

characterization of rice straw-derived biochar for soil amendment, Biomass and Bioenergy. 47 (2012) 268–276. https://doi.org/https://doi.org/10.1016/j.biombioe.2012.09.034.

[57] A. Placek, A. Grobelak, M. Kacprzak, Improving the phytoremediation of heavy metals contaminated soil by use of sewage sludge, Int. J. Phytoremediation. 18 (2016) 605–618. https://doi.org/10.1080/15226514.2015.1086308.

[58] K.W. Jung, K. Kim, T.U. Jeong, K.H. Ahn, Influence of pyrolysis temperature on characteristics and phosphate adsorption capability of biochar derived from waste-marine macroalgae (Undaria pinnatifida roots), Bioresour. Technol. 200 (2016) 1024–1028. https://doi.org/10.1016/j.biortech.2015.10.016.

[59] Y. Yao, B. Gao, M. Inyang, A.R. Zimmerman, X. Cao, P. Pullammanappallil, L. Yang, Removal of phosphate from aqueous solution by biochar derived from anaerobically digested sugar beet tailings, J. Hazard. Mater. 190 (2011) 501–507. https://doi.org/10.1016/j.jhazmat.2011.03.083.

[60] Y. Yao, B. Gao, J. Chen, L. Yang, Engineered Biochar Reclaiming Phosphate from Aqueous Solutions: Mechanisms and Potential Application as a Slow-Release Fertilizer, Environ. Sci. Technol. 47 (2013) 8700–8708. https://doi.org/10.1021/es4012977.

[61] Q. Liu, Z. Fang, Y. Liu, Y. Liu, Y. Xu, X. Ruan, X. Zhang, W. Cao, Phosphorus speciation and bioavailability of sewage sludge derived biochar amended with CaO, Waste Manag. 87 (2019) 71–77. https://doi.org/10.1016/j.wasman.2019.01.045.

[62] Lena Johansson Westholm, Substrates for phosphorus removal — Potential benefits for on-site wastewater treatment?, Water Res. 40 (2006) 23–36. https://doi.org/10.1016/j.watres.2005.11.006.

[63] K.W. Jung, M.J. Hwang, K.H. Ahn, Y.S. Ok, Kinetic study on phosphate removal from aqueous solution by biochar derived from peanut shell as renewable adsorptive media, Int. J. Environ. Sci. Technol. 12 (2015) 3363–3372. https://doi.org/10.1007/s13762-015-0766-5.

Capítulo 2

2.   Objetivos

2.1. General

Evaluar la remoción y recuperación del fósforo adsorbido desde aguas residuales sintéticas usando un material adsorbente obtenido a partir de Jacinto de agua (*Eichhornia Crassipes*).

2.2. Específicos

o   Evaluar el efecto de la temperatura de calcinación en la transformación del fósforo presente naturalmente en el jacinto de agua a un producto biocompatible con el suelo y asimilable por las plantas.

o   Evaluar la eliminación de fósforo desde soluciones acuosas usando el material obtenido y su potencial aplicación como fertilizante.

o   Evaluar el uso potencial del material obtenido a partir de residuos de jacinto de agua (*Eichhornia Crassipes*) para la remoción de metales pesados (Cd^{2+} y Cu^{2+}) desde soluciones acuosas y la posterior inmovilización en la estructura del material.

Capítulo 3

3. Utilization of water hyacinth (*Eichhornia crassipes*) rejects as phosphate-rich fertilizer

Abstract

Phosphorus (P) recovery from water hyacinth is one of the promising sources to recovery and recycle P to alleviate P supply shortage in the future. The result of calcination temperature during the thermal treatment of calcium (Ca) and P-rich water hyacinth is presented here. Results showed a Ca/P molar ratio of 5.07 in water hyacinth ashes and, that with the increase in calcination temperature, P and Ca are transformed into hydroxyapatite. The amount of hydroxyapatite increased until 34.0%, while other Ca phases such as CaO, $CaCO_3$, and $Ca(OH)_2$ were obtained in 6.1%, 3.9%, and 18.0%, respectively. The bioavailability test showed that the material produced at 700 °C (hydroxyapatite and other Ca-rich phases) could be used as a fertilizer, with P slow release in aqueous solutions, giving up 3.7% and 29.3% of P release in deionized water and formic acid, respectively. Besides, CaO and $Ca(OH)_2$ are used for soil neutralization as their disposition can help the crops.

3.1. Introduction

Water hyacinth (*Eichhornia crassipes*) is a weed native to the lakes and swamps of the Amazon basin in western Brazil and is one of the most complex invasive species in aquatic ecosystems with high growth rates [1–3]. It excessively reproduces on the aquatic surface and negatively impacts the native biodiversity and lake hydrology by increasing the evapotranspiration rate of water [3]. The extensive rooting scheme of water hyacinth allows it to absorb hazardous elements and nutrients from aqueous mediums [4,5], which together with excessive reproduction prevents light from passing through the water. Consequently, this results in decreased amount of dissolved oxygen, increased CO_2 levels in the water, and

ultimately eutrophication [2,3,6]. The physical extraction of water hyacinth from water bodies is an adequate method to clean up [7,8]. However, because of the high volume of water and pollutants, a challenge is posed for sustainable waste management [1,6,9]. Notably, water hyacinth contains nutrients and thus is a potential fertilizer for soil [1].

Water hyacinth typically contains 1% – 4% of P [5,10–13], which is one of the most important and essential elements for all living organisms [14–17]. P is in high demand, and its main nonrenewable sources (phosphoric rock) are on a decline [18–20]. Therefore, the recovery of P from P-enriched waste has gained significant attention, as it mitigates the scarcity of P-rich fertilizers and also prevents the potential risk of waste disposal [21,22]. However, water hyacinth cannot be directly used as a P source; it must undergo a thermal transformation, which usually involves calcination or pyrolysis [2,23], in both of which water hyacinth ashes are converted into a promising P-recycling source [24]. A considerable reduction in water hyacinth volume ensures satisfactory waste disposal [25]. This waste management initiates a circular design system that transforms wastes into valuable and useful P-rich fertilizers [26].

The use of P-rich biomass ash for recovering and reutilizing of this element is of increasing interest. Regarding resource utilization, meat and bone meal (MBM), incinerated sewage sludge ash (ISSA), agricultural wastes, etc. [22] represent rejects that are widely studied for this proposal. Compared with that in the raw-biomass matrix, the P mass content is enriched during thermal treatments [27]. However, the P remaining after thermal transformation cannot be directly used as a fertilizer, as it is in the inert form, which is not bioavailable to plants [28]. Currently, acid or alkaline leaching and electrodialysis are being reported as satisfactory methodologies that achieve P recovery with high efficiency [27]. However, the solubility of the trace hazardous elements during this pretreatment is problematic [18].

Due to sewage sludge ash (SSA) is the most widely used biomass to recover P after different thermal treatments [21,27,28], several authors have conducted studies to enhance the biocompatibility and bioavailability of P [29]. The most practical method for optimizing the recycling of P is to transform the P present in the ash into a phosphate that is bioavailable to plants, such as hydroxyapatite ($Ca_5(PO_4)_3OH$). Hydroxyapatite is the most abundant and

available phosphate in rocks. It is stable and easy to obtain. Furthermore, it is biocompatible to soils and improves plant growth. In hydroxyapatite, the P is bounded to calcium; therefore, this phosphate can be achieved by adjusting the Ca/P molar ratio. The Ca/P molar ratio ranges from 1.67 to 1.50 [30], thus to biomass with the Ca/P molar ratio of less than 1, and it is necessary to add external sources of Ca.

As shown above and according to the author's knowledge, most of the studies regarding ash transformation to hydroxyapatite are related to sewage sludge [30,31]. There are no studies using ashes produced during the thermal treatment of water hyacinth to produce a valuable resource of P. Water hyacinth ash is a Ca-rich residue; therefore, the Ca that is inherent to ash can be used to produce hydroxyapatite. In this work, the temperatures of calcination for water hyacinth, and the effect during P transformation to hydroxyapatite were worked systematically. The enhancement effect of temperature on P transformation into hydroxyapatite and their fertilizer properties, such as P slow release in aqueous mixtures, was subsequently studied. It is also important to highlight that P recycling from P-enriched wastes is an initiative to close its unidirectional flow, and water hyacinth incineration represents a sustainable strategy for managing this residue.

3.2. Materials and methods

3.2.1. Thermal transformation - Calcination

Water hyacinth rejects were collected at the Ituango Hydroelectric Plant (Hidroituango) located on the Cauca River between the municipalities of Ituango and Briceño, Antioquia, Colombia. It was washed using distilled water to remove impurities, dried an oven at 105 °C for 24 h, ground, and finally passed through a sieve with size < 0.850 mm; subsequently, it was designated as WH. The sample WH was calcined in a horizontal tube furnace at the temperatures of 350 °C, 450 °C, 550 °C, 650 °C, 700 °C, 800 °C, and 900 °C at a heating rate of 10 °C/min, and with isotherm of 2 h in an air atmosphere (100 mL/min). The materials obtained were ground and sieved to a particle size < 0.335 mm and labeled as CWH-X, where X denotes the calcination temperature. Each calcination treatment was performed in duplicate.

3.2.2. Materials characterization

WH was characterized using a thermogravimetric analyzer (TGA Q500, TA Instruments) to determine moisture content, volatile material (VM), fixed carbon (FC), and ash. The contents of metal oxides were determined by X-ray fluorescence, XRF (Thermo Scientific ARL OPTIM'X WDXRF), and elemental composition in C, H, O was determined using the ASTM D-5373-08 method (CHNSO TrueSpec® Micro, LECO). The functional groups present in WH before and after each heat treatment were characterized by Fourier-transformed infrared spectroscopy, FTIR (Spectrum two-PerkinElmer with UATR for a range within 4000–450 cm^{-1}). Moreover, the crystalline phases present in each material were identified by X-ray diffraction (XRD) using a Shimadzu XRD-6100 diffractometer with Cu Kα radiation (λ = 1.5406 Å), at 40 kV in the 2θ angle range of 10° to 80° with a step size of 0.026° and period of 50 s. The yield of CWH in each transformation process was calculated considering the mass ratios before and after calcination. Similar analytical procedures were previously reported by many studies [32,33].

3.2.3. Soluble P of CWH-X

The bioavailability of P was determined by the solubility of P compounds in 2% formic acid following the procedure describe by Shiba et al., 2017 and Zheng et al., 2020 [34,35]. The content of water-soluble phosphorus (WSP) is an indicator of the phosphorus loss when a solid fertilizer is applied to the soil. The WSP was analyzed by following the procedure reported by Liu et al. [36].

3.3. Results and discussion

3.3.1. Materials characterization

- *Raw material - Water Hyacinth*

WH, which has a high content of hemicellulose and lignin [3], can remove metals present in the water, including heavy metals, the presence of these elements in water depends mainly on the origin of the effluent discharge [37]. In our case, hazardous elements were not detected as evidenced in the following characterization (Table 3-1 and 3-2), the water hyacinth used in this study includes Al, Fe, Mg, and Ca, as well as phosphates from aquatic

ecosystems [38]. These elements can be recovered by performing heat treatments [29]. Therefore, WH must be characterized before and after the treatments to identify the type and quantity of phases, such as; carbonates, oxides, and phosphates, which may be present in the treated materials. Accordingly, it would be possible to make decisions regarding the use and final disposal of the material [30,31].

Table 3-1 shows the elemental characterization for WH, which is high in C (49.40%), H (4.80%), and O (44.20%), three of which are the major components of biomass. Other elements, including N and S, are found in smaller quantities (0.30% in both the cases), which may be attributed to the low capacity of water hyacinth to absorb these elements. The proximate analysis shows that WH comprises 76.97% VM, 8.55% FC, and 14.48% ash. The abundant VM has been used to produce biofuels, such as ethanol [39], while FC has been reported to be used in electro-catalysis [40]. Fig. 3-1a depicts the curve of the thermogravimetric analysis. From the curve, it is observed that under a nitrogen atmosphere, the main loss corresponds to the decomposition of cellulose and hemicellulose, both of which are the components of the biomass and have low thermal stability. Upon changing the atmosphere of reaction to air, the oxidation of FC (represented by lignin) occurs followed by ash formation.

Table 3-1. Chemical composition of water hyacinth rejects.

Moisture (wt. %)	Proximate analysis (wt. %)[a]			Elemental analysis (wt. %)				
	VM	FC	Ash	N	C	H	S	O[b]
10.51	76.97	8.55	14.48	0.30	49.40	4.80	0.30	45.2

VM: volatile material; FC: fixed carbon; N: nitrogen; C: carbon; H: hydrogen; S: sulfur; O: oxygen.   [a] dry basis.   [b] obtained by difference.
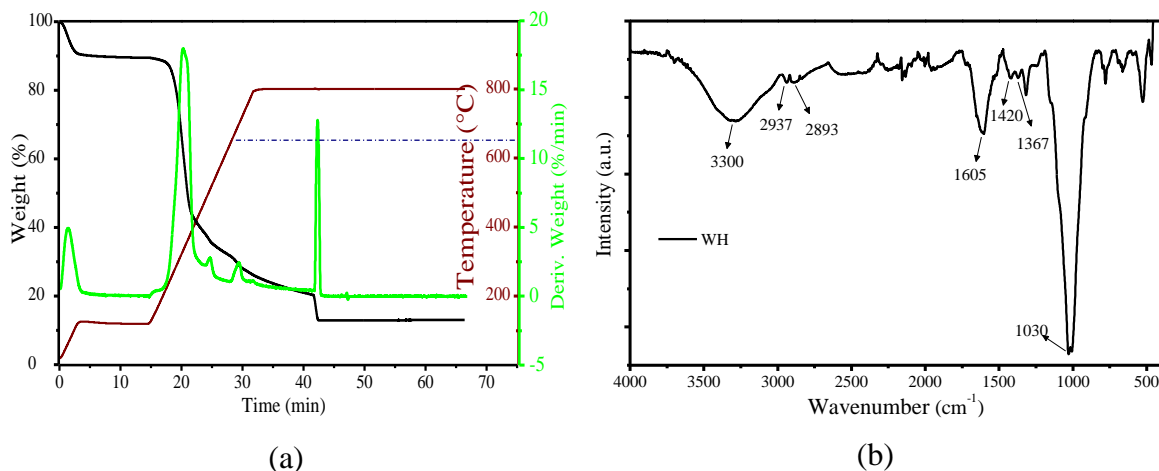
Fig. 3-1. Characterization of water hyacinth (WH). a: proximate analysis; b: FTIR spectrum.

Fig. 3-1b shows the FTIR spectrum for WH. The signal at 3300 cm^{-1} corresponds to the vibration of the –OH groups; the bands at 2893–2937 cm^{-1} correspond to C–H sp^3 stretching vibrations, while those at 1367 and 1420 cm^{-1} may be attributed to –CH$_3$ and –CH$_2$ flexions. The band at 1605 cm^{-1} is attributed to the stretching vibration of –OH deformation, and also to the stretching vibration of the carbonyl C=O of the carboxylic groups of WH [20]. The main band around 1030 cm^{-1} can be attributed to the vibration of the flexion of the C–O bond, or to the out-of-plane bending for carbonates (CO$_3^{2-}$) or O–P–O bonds of the phosphorus present in WH [41,42].

The chemical characterization of the ashes using XRF is shown in Table 3-2, which indicates that the oxides of Ca (32.4%), Si (19.3%), Mg (15.4%), Al (9.2%), and Fe (5.1%) are the main ash components. These oxides have been reported to play a vital role in phosphorus immobilization, as they can react with P to form various phosphates [43,44]. The percentage of P$_2$O$_5$ (8.1%) indicates that water hyacinth naturally removes phosphates from aqueous ecosystems, thereby making it a natural source for the P recovery.

Table 3-2. XRF analysis of the water hyacinth ashes.

X-ray fluorescence											
Oxides	CaO	SiO$_2$	MgO	Al$_2$O$_3$	P$_2$O$_5$	Fe$_2$O$_3$	SO$_3$	K$_2$O	Na$_2$O	TiO$_2$	MnO	LOI[b]
wt. %	4.85	2.88	2.30	1.38	1.21	0.76	0.74	0.53	0.18	0.06	0.06	84.98
wt. % [a]	32.44	19.26	15.38	9.23	8.09	5.08	4.95	3.55	1.20	0.40	0.40	-

[a] composition of the oxides in ash.   [b] Loss on ignition.

29

P can be found in nature in a linked state with other elements in the form of inorganic compounds such as phosphates or organic compounds [45]. These forms of P react with clay, iron, and aluminum compounds present in the soil. Consequently, the solubility of P compounds becomes significantly low such that only a small amount of soil nutrients can be present in solution at any time; i.e., the bioavailability of P for plants is decreased. Therefore, it is necessary to transform the different forms of P into inorganic compounds that can be assimilated by plants, such as hydroxyapatite ($Ca_5(PO_4)_3OH$) [30], which requires a calcium source to maintain the minimum Ca/P molar ratio of 1.67 [31]. From Table 3-2, it can be determined that the Ca/P molar ratio is 5.07 for WH, thereby indicating that to transform P to a value-added and bioavailable mineral such as hydroxyapatite, especially in this case, it is not necessary to add external sources of Ca.

3.3.2. P and Ca-transformation: Effect of calcination temperature

The water hyacinth yields at each calcination temperature, that is, CWH-350, CWH-450, CWH-550, CWH-650, CWH-700, CWH-800, and CWH-900; were 27.7%, 23.1%, 20.7%, 16.7%, 15.8%, 14.7 %, and 14.5% respectively. The decrease in the yield performance with increase in the temperature is in accordance with the literature [3]. This behavior is attributed to the fact that upon increasing the temperature, both the rate of dehydration and decomposition of organic components and the enrichment of minerals in the solid residue increase. Through the calcination process, the Ca^{2+} present in the WH can form different compounds including $CaCO_3$, $Ca(OH)_2$, and CaO [46]. P can mainly form H_3PO_4 at low temperatures irrespective of the calcination conditions, while at higher temperatures oxides including P_4O_{10}, P_2O_5, PO, and PO_2 are formed. However, in the thermal treatment of Ca-containing biomass, the formation of calcium phosphates is expected [18].

- *Low temperatures*

Fig. 3-2 shows the FTIR spectra of WH calcined at three temperatures, i.e., 350 ℃, 450 ℃, and 550 ℃. Generally, for these three temperatures, the signals at 3300 cm^{-1} related to the vibration of –OH groups, the signals between 2893–2937 cm^{-1} related to the stretching of the C–H sp^3 bond, and the signals at 1605 cm^{-1} related to the stretching of the C=O bond considerably decrease in intensity, indicating the decomposition of the main components of WH [47].
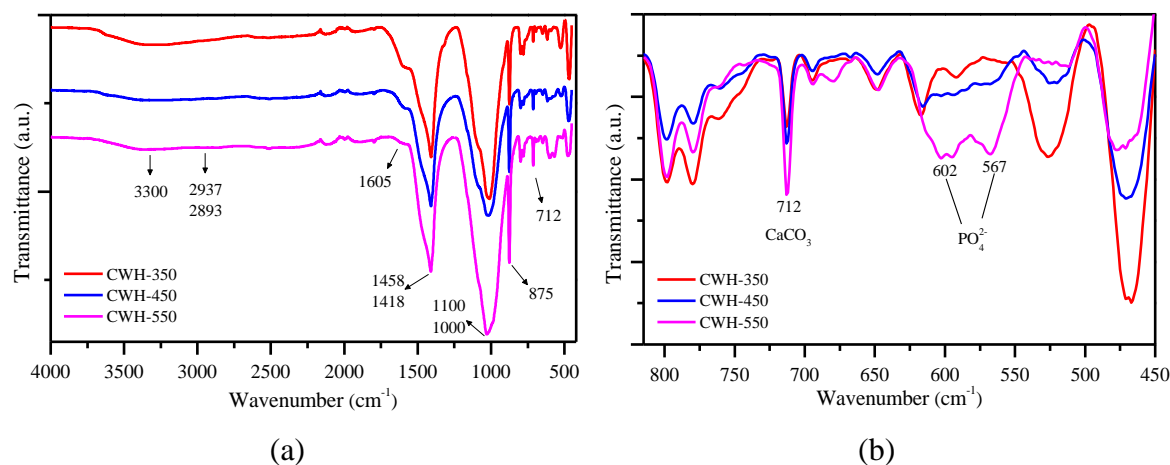
Fig. 3-2. (a) FTIR spectra of water hyacinth (WH). CWH-350: Water hyacinth calcined at 350 °C; CWH-450: Water hyacinth calcined at 450 °C; CWH-550: Water hyacinth calcined at 550 °C. b) Increase in the range: 450–815 cm^{-1}.

For CWH-350, the signals at 712 and 875 cm^{-1} of the -CO$_3^{2-}$ group are observed; these signals are confirmed by the bands of weak intensity, centered at 1418 and 1458 cm^{-1} corresponding to the symmetric and asymmetric stretching modes of the CO$_3^{2-}$ group [48], indicating the presence of CaCO$_3$ [49,50]. Upon increasing the temperature to 450 ºC, the intensity of CaCO$_3$ signals increases and becomes even more at 550 °C. Additionally, CWH-550 shows bands at 567 and 602 cm^{-1} of the PO$_4^{3-}$ group, as verified by the increase in the intensity of the bands around 1000–1100 cm^{-1}, corresponding to the asymmetric and symmetric deformation modes of the [PO$_4$]v_4 group (v_4 O–P–O) [48]. These results indicate that the temperature of 550 ºC initiates the decomposition of inorganic phosphorus.

XRD confirmed CaCO$_3$ formation (see Fig. 3-3). The materials exhibited a peak at $2\theta = 29.4º$, which corresponds to the (104) plane of CaCO$_3$ (ICSD·#: 166364). According to these results, at 550 ºC no intense signals were observed for apatite, indicating that most of the P content was still forming organic structures and that Ca was in the form of CaCO$_3$. Apatite formation, which requires a high temperature, has been reported using Ca(OH)$_2$ as the Ca source [51].

31
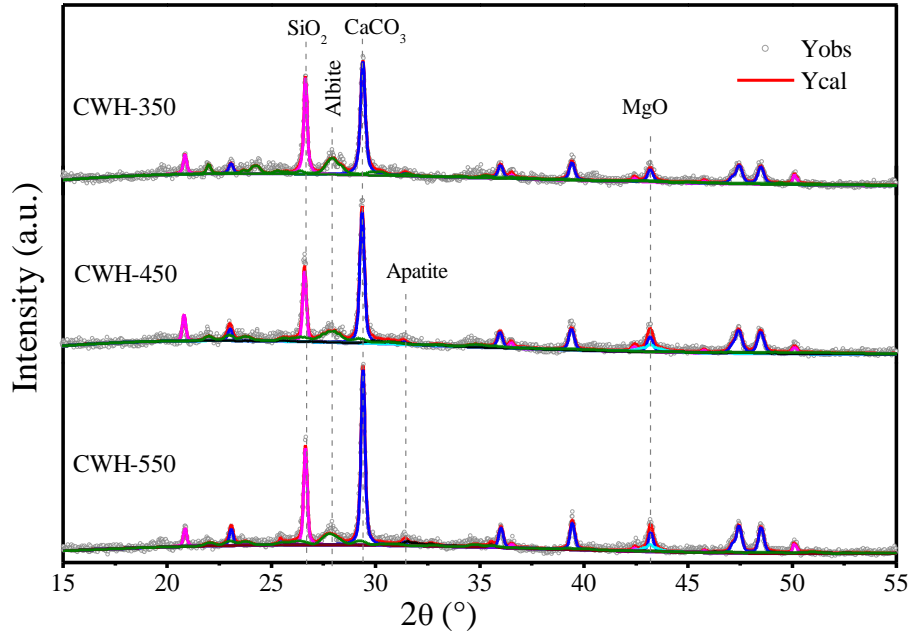
Fig. 3-3. XRD patterns for WH calcined at low temperatures. CWH-350: Water hyacinth calcined at 350 °C; CWH-450: Water hyacinth calcined at 450 °C; CWH-550: Water hyacinth calcined at 550 °C.

- *High temperatures*

Fig. 3-4 shows the FTIR spectra for CHW-650 and CHW-900 samples. New band around 3640 cm^{-1} is observed, while the intensity of the bands at 1418 and 875 cm^{-1} decreases. These observations account for CaCO$_3$ decomposition, which in turn induces the formation of Ca(OH)$_2$ [52]. At 700 ºC the band at 712 cm^{-1} characteristics of CaCO$_3$, considerably decreases, and the decrease in the band at 3640 cm^{-1} at 900 ºC indicates the transformation of Ca(OH)$_2$ to CaO. However, the band at 1030 cm^{-1} of the P–O bond of the [PO$_4$] group and the signals at 567 and 602 cm^{-1} corresponding to the asymmetric and symmetric deformation modes of the [PO$_4$]v_4 (v_4 O–P–O) group increase in intensity. The position of these bands has been reported to be a characteristic of Ca phosphates, especially apatite [48], and becomes increasingly separated or split as crystallinity increases [53].

The v_4 asymmetric bending mode has been used to measure the crystallinity of apatite [54]. To evaluate the effect of heat treatment on the crystallinity of the formed apatite the infrared splitting factor (SF) was calculated as reported by Weiner and Bar-Yosef [53], as the sum of the heights of the 567 and 602 cm^{-1} phosphate peaks divided by the height of

trough between them (Fig. S1). The SF values obtained were 3.67, 4.07, 3.71 and 3.2 for CHW-650, CHW-700, CHW-800, and CHW-900 respectively, showing that crystallinity increases with the calcination temperature until 700 ºC, at higher temperatures, apatite is transformed into other calcium phosphates [55], which may explain the decrease in SF until 3.2 at 900 ºC.

(a)   (b)
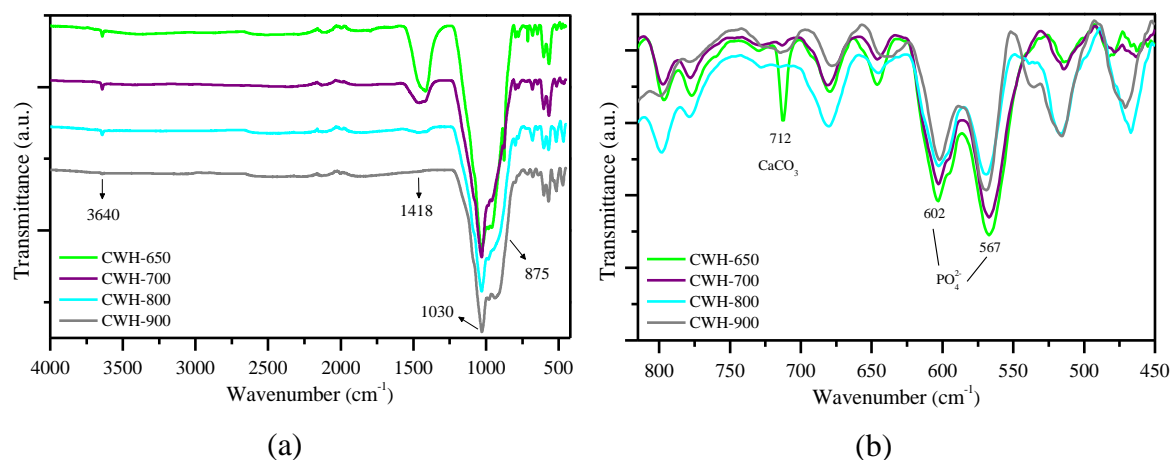
Fig. 3-4. (a) FTIR spectra of water hyacinth (WH). CWH-650: Water hyacinth calcined at 650 °C; CWH-700: Water hyacinth calcined at 700 °C; CWH-800: Water hyacinth calcined at 800 °C; CWH-900: Water hyacinth calcined at 900 °C. b) Increase in range: 450–815 cm^{-1}.

The FTIR results are complemented by the XRD patterns of CWH-650 – CWH-900 (see Fig. 3-5a). It can be seen that CWH-650 presents new peaks at $2\theta = 17.9º$ and $34.0º$ for the (001) and (010) planes, respectively, of $Ca(OH)_2$ (ICSD·#: 202225); additionally, the presence of apatite was confirmed with the peaks at $2\theta = 31.4º$, $32.1º$, and $32.4º$ for the (211), (112), and (030) planes, respectively, of $Ca_5(PO_4)_3(OH)$ (ICSD #: 180315). For CWH-700, the peak at $2\theta = 29.4º$ of the (104) plane of $CaCO_3$ considerably decreased, and diffraction peaks appeared at $2\theta = 32.2º$, $37.3º$, and $53.8º$ for the (111), (002) and (022) planes of CaO (ICSD·#: 60199). For CWH-800, the peak at $2\theta = 29.4º$ $CaCO_3$ disappears completely, and the peaks for $Ca_5(PO_4)_3(OH)$ and CaO show the high intensity for Ca phases. For CWH-900, the peaks corresponding to $Ca_5(PO_4)_3(OH)$ decrease and peaks at $2\theta = 25.9º$ and $31.3º$ corresponding to (200) and (032) planes for $Ca_8(HPO_4)_2(PO_4)_4(H_2O)_5$ appear. These results show WH as a P and Ca source, which, when thermally calcined at high temperatures (> 650 °C), transforms into a value-added product such as hydroxyapatite.

Fig. 3-5b shows the XRD patterns for apatite calculated using Rietveld refinement. The crystallite size are 5.4 nm, 9.4 nm, 10.3 nm, and 11.3 nm for 5.3 for CWH-650, CWH-700, CWH-800, and CWH-900 respectively, this observation is in accordance with the SF determined by FTIR for CWH-650, CWH-700, CWH-800, and CWH-900. Thermal processes have been reported to facilitate the production of various calcium phosphates and improve crystallinity and other physicochemical properties such as bioavailability [56,57].

(a)

34
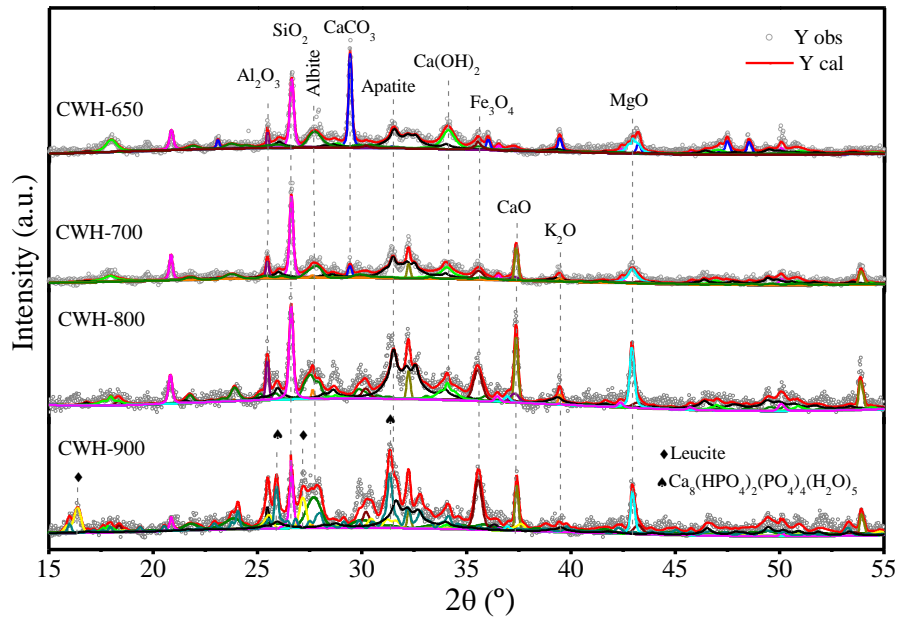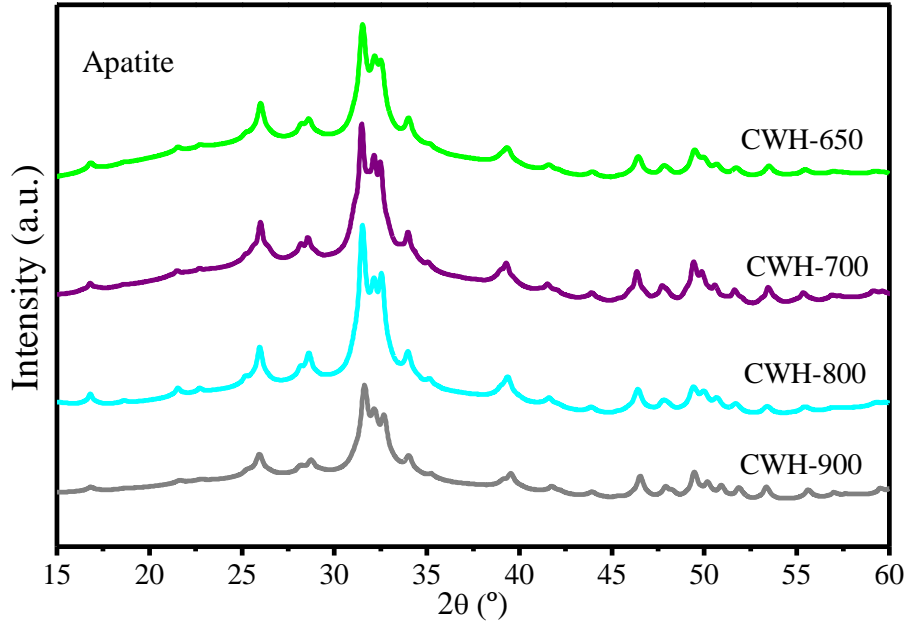
(b)

Fig. 3-5. a) XRD patterns. b) Standard XRD pattern obtained for apatite by Rietveld refinement. CWH-650: Water hyacinth calcined at 650 °C; CWH-700: Water hyacinth calcined at 700 °C; CWH-800: Water hyacinth calcined at 800 °C; CWH-900: Water hyacinth calcined at 900 °C.

3.3.3. Phase quantification by XRD

Rietveld refinement was used to quantify the crystalline Ca phases present as $CaCO_3$, $Ca(OH)_2$, CaO, and $Ca_5(PO_4)_3(OH)$ in the calcined materials (see Fig. 3-6). At temperatures from 350 ℃ to 550 ℃, no significant changes were observed; approximately 50% of the crystalline material corresponded to $CaCO_3$. Upon increasing the temperature to 650 ℃, $CaCO_3$ decomposed into $Ca(OH)_2$ (15.79%) (Reaction 3-4), which is one of the most active phases of Ca in the production of hydroxyapatite and apatite [58,59]. This is reflected from apatite production (26.11%). These results are in accordance with the findings reported for apatite production, thereby establishing that once the apatite nuclei form on the surface, they can spontaneously grow consuming calcium and phosphate [41]. For CWH-700, the amount of apatite increased until 34.04%, while CaO, $CaCO_3$, and $Ca(OH)_2$ were obtained in 6.11%, 3.9%, and 18%, respectively. The hydroxyapatite increases slightly up to 36.64% for CWH-800 and decreases again in CWH-900 as well as Ca and $Ca(OH)_2$, indicating the formation

35

of other phases. These results show that 700 ºC is a suitable temperature for the obtention of a material with high hydroxyapatite content. These results are in agreement with the Ca/P molar ratio present in these materials (5.07). Additionally, it has been reported that for Ca/P molar ratios > 1.67, in addition to obtaining apatite with high crystallinity and thermal stability [56], it is possible to obtain a biphasic mixture with $Ca(OH)_2$ [60]. Apatite has been formed by the thermal treatment of sewage sludge by adding other Ca sources, following which it can be used as a fertilizer [31]. Additionally, CaO and $Ca(OH)_2$ are used for soil neutralization [61], as their appropriate disposition can benefit the crops.
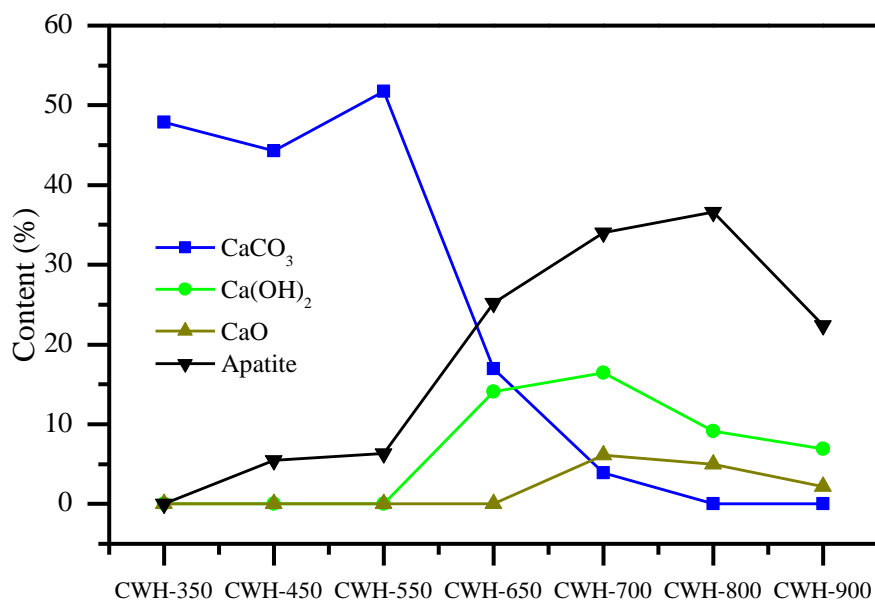
Fig. 3-6. Quantification of the phases of Ca (wt. %) according to the Rietveld refinement of the XRD patterns of calcination treatments at different temperatures for water hyacinth.

Similarly, upon analyzing the metals present in the different materials and their transformation with temperature, the presence of any heavy metal was not observed, which even at low concentrations can negatively affect living beings and thus ultimately destroying the stability of ecosystems [62]. The non-detection of hazardous elements in the different materials obtained in this work can be explained by the origin of the water hyacinth residues, so it can be said that the plant during its growth process did not absorb heavy metals from Cauca River located between the municipalities of Ituango and Briceño, Antioquia, Colombia, at the height of the Ituango hydroelectric plant. The presence of heavy metals in biomass ash is one of the main problems for the disposal and use of the waste [31,36].

36

Additionally, removing heavy atoms increases the cost of transformation, coupled with limited applications in the soil [29,30]. As previously shown, because WHs do not contain hazardous elements, they are appropriate rejects to transform P into hydroxyapatite, which is used as a fertilizer. However, the low solubility of hydroxyapatite is an impediment to producing fertilizers for plants [63,64]. Therefore, the direct use of hydroxyapatite will require an effective yet cheap means of solubilization.

3.3.4. *Proposed reactions during thermal transformations*

It can be concluded that the removal of organic matter, cellulose, hemicellulose, and lignin, occurs mainly at 350 ℃, yielding CO_2 and H_2O as products (Reaction 3-1). Additionally, at low temperatures, the Ca^{2+} of the cell walls can react with O_2 to form CaO, which is known for its ability to capture CO_2; therefore, Reaction 3-2 can also occur [65].

$$C_nH_mO_{(m/2+2n)} \xrightarrow{\text{350 ℃–450 ℃, } O_2} \frac{m}{2} H_2O + n\, CO_2 \tag{3-1}$$

$$CaO + CO_2 \xrightarrow{\text{350 ℃–450 ℃, } O_2} CaCO_3 \tag{3-2}$$
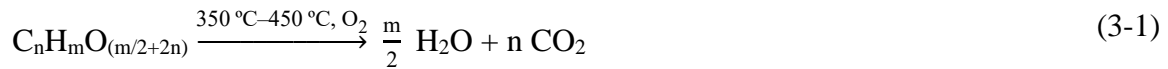
As indicated by the FTIR and XRD results for temperatures up to 550 ℃, the main organic components decompose, and the intensity of the apatite signals is still low. The literature has reported that apatite formation improves with $Ca(OH)_2$ presence; therefore, a high temperature is required to achieve the transformation of $CaCO_3$ [66]. As is showed in Reaction 4 at 650 ℃ $Ca(OH)_2$ formation can occur upon the combination of $CaCO_3$ with the water released in Reaction 3-1.

$$CaCO_3 + H_2O \xrightarrow{\text{650 ℃, } O_2} Ca(OH)_2 + CO_2 \tag{3-4}$$
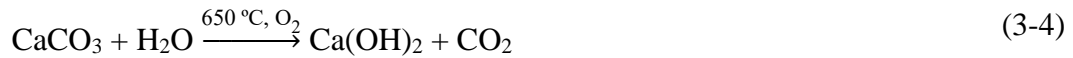
The presence of $Ca(OH)_2$ combined with phosphate facilitates apatite formation (Reaction 3-5) [59]. At temperatures $\geq$ 700 °C, $Ca(OH)_2$ decomposes into CaO (Reaction 3-6), which could disfavor apatite formation.

$$5Ca(OH)_2 + 3PO_4^{3-} \xrightarrow{\text{650 ℃, } O_2} Ca_5(PO_4)_3OH + 9OH^- \tag{3-5}$$

$$Ca(OH)_2 \xrightarrow{700\ ^{\circ}C,\ O_2} CaO + H_2O \qquad\qquad (3\text{-}6)$$
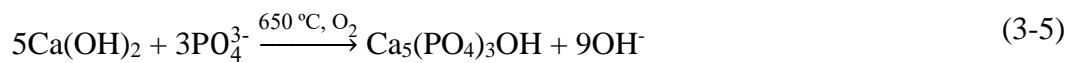
From the XRD and FTIR analyzes, the signals of phosphorus oxides (P_2O_5), or Mg and Al phosphates ($Mg_3(PO_4)_2$ and $AlPO_4$) were not identified, may be because the high amount of Ca present in the material promoted hydroxyapatite formation, which is more effective fertilizer than other sources of P [67]. It was also observed that the total amount of P increased from 0.53% in WH to 3.64% in CWH-900 upon increasing the calcination temperature (see Table 3-S1). This increase in the formation of P is attributed to the breakdown of stable organic matter that produces the phosphorus released from its cell wall [68].

3.3.5. P-bioavailability of CWH-X

Fig. 3-7. shows the solubility of P in a 2% formic acid solution and deionized water for each of the calcination temperatures to which WH was subjected. It can be seen that the solubility of P obtained in deionized water (between; 0.9 and 14.7%) was lower than that obtained in 2% formic acid (between 27.9 and 45.1%).

The content of soluble P in water (WSP) shows that the lower the temperature, the higher the percentage of solubility (14.7% for CWH-350 to 0.9% for CWH-900), which indicates that at high temperatures P can transform into more stable species as hydroxyapatite that in its crystalline forms can be less soluble in water [36]. On the other hand, the high percentage of solubility of P in 2% formic acid indicates that CWH-X can be used as an amendment for acid soils, allowing a release of 45.1% of the P contained in the material in 24 h.
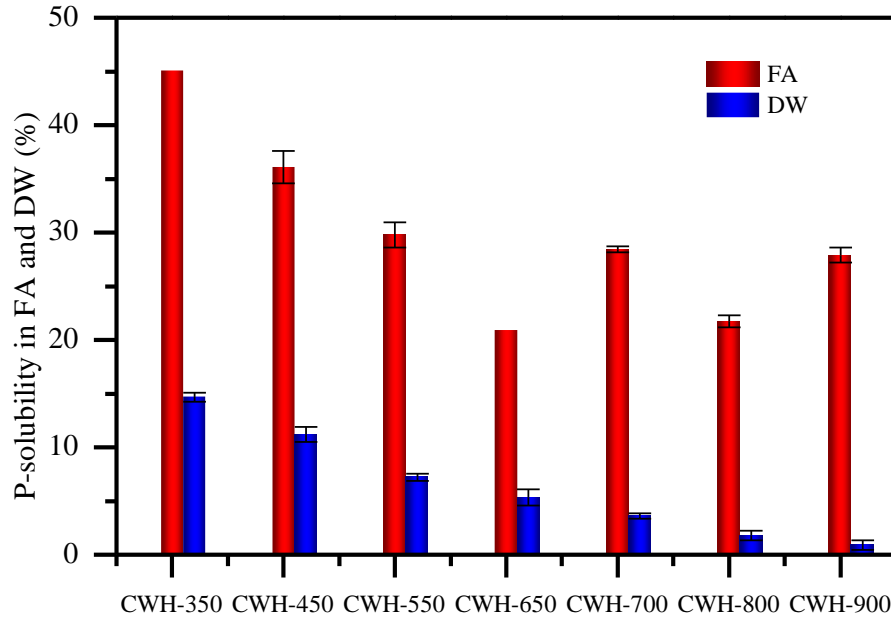
Fig. 3-7. Phosphorus solubility in 2% formic acid (FA), and deionized water (DW).

The results show that although it is possible to reduce the volume of water hyacinth until approximate 14.48% according to proximate analysis (Fig. 3-1) and XRF (ash = 15.02%), the calcination temperature has an important effect to obtain a material rich in hydroxyapatite, as was observed by XRD and FTIR which after its disposal in the soil can release P as fertilizer.

3.4. Conclusions

This research was focused on the phosphorus recovery as hydroxyapatite from water hyacinth and its potential application as fertilizer, to modify the water hyacinth calcination process between 350 ℃ – 900 ℃ and the solids obtained were characterized by FTIR and XRD and the bioavailability of P was determined by the solubility of P compounds in 2% formic acid and deionized water.

- According to characterization, water hyacinth composition has a high Ca content (34.44 % of CaO). The material does not require the addition of extra Ca sources such as $Ca(OH)_2$ or CaO to produce hydroxyapatite.

- The present study shows that the extractable P values of water hyacinth vary with experimental calcination conditions. At low calcination temperatures (350 ℃ – 550

°C), the main crystalline phase is $CaCO_3$, and the P remains in organic form. At high temperatures (650 °C–900 °C), Ca is transformed into $Ca(OH)_2$, and Ca-phosphates such as hydroxyapatite are formed.

- The sample calcine at 700 °C (CWH-700) reached 34.05% hydroxyapatite, which can be used as fertilized with slow P release; the tests carried out showed a P release at 24 h of 28.4% in formic acid and 3.6% in deionized water.

- On the other hand, during the characterization of hyacinth ashes, hazardous elements were not identified, which represents one of the most pressing threats to use this type of biomass as a P-fertilizer.

This work also contributes to the understanding of the transformation into a valuable product, where calcination processes should not only be used to reduce the volume of the removed water hyacinth, but also to obtain a valuable product that can be used as fertilizer. Considering the higher hydroxyapatite content, the behaviors of these compounds in soil and plants require future study.

3.5. References

[1]   F. Zhang, X. Wang, J. Xionghui, Efficient arsenate removal by magnetite-modified water hyacinth biochar, Environ. Pollut. 216 (2016) 575–583. https://doi.org/10.1016/j.envpol.2016.06.013.

[2]   R. Cai, X. Wang, X. Ji, B. Peng, C. Tan, X. Huang, Phosphate reclaim from simulated and real eutrophic water by magnetic biochar derived from water hyacinth, J. Environ. Manage. 187 (2017) 212–219. https://doi.org/10.1016/j.jenvman.2016.11.047.

[3]   R.E. Masto, S. Kumar, T.K. Rout, P. Sarkar, J. George, L.C. Ram, Biochar from water hyacinth (Eichornia crassipes) and its impact on soil biological activity, Catena. 111 (2013) 64–71. https://doi.org/10.1016/j.catena.2013.06.025.

[4]   S. Kumar, S. Deswal, Estimation of Phosphorus Reduction from Wastewater by Artificial Neural Network , Random Forest and M5P Model Tree Approaches, Pollution. 6 (2020) 417–428. https://doi.org/10.22059/poll.2020.293086.717.

[5]   Y. Zhang, H. Liu, S. Yan, X. Wen, H. Qin, Z. Wang, Z. Zhang, Phosphorus removal from the hyper-eutrophic lake caohai (China) with large-scale water hyacinth cultivation, Environ. Sci. Pollut. Res. 26 (2019) 12975–12984. https://doi.org/10.1007/s11356-019-04469-8.

[6]   A. Salas-Ruiz, M.M. Barbero-Barrera, M.I. Sánchez-Rojas, E. Asensio, Water Hyacinth–Cement Composites as Pollutant Element Fixers, Waste and Biomass Valorization. (2019). https://doi.org/10.1007/s12649-019-00674-1.

[7]   G.L. Dotto, J.M. Cunha, C.O. Calgaro, E.H. Tanabe, D.A. Bertuol, Surface modification of chitin using ultrasound-assisted and supercritical CO2 technologies for cobalt adsorption, J. Hazard. Mater. 295 (2015) 29–36. https://doi.org/https://doi.org/10.1016/j.jhazmat.2015.04.009.

[8]   E.C. Peres, J.C. Slaviero, A.M. Cunha, A. Hosseini–Bandegharaei, G.L. Dotto, Microwave synthesis of silica nanoparticles and its application for methylene blue adsorption, J. Environ. Chem. Eng. 6 (2018) 649–659. https://doi.org/https://doi.org/10.1016/j.jece.2017.12.062.

[9]   L. Shi, L. Wang, T. Zhang, J. Li, X. Huang, J. Cai, J. Lü, Y. Wang, Reducing the bioavailability and leaching potential of lead in contaminated water hyacinth biomass by phosphate-assisted pyrolysis, Bioresour. Technol. 241 (2017) 908–914. https://doi.org/10.1016/j.biortech.2017.06.025.

[10]   S. Román, B. Ledesma, A. Álvarez, C. Coronella, S. V. Qaramaleki, Suitability of hydrothermal carbonization to convert water hyacinth to added-value products, Renew. Energy. 146 (2020) 1649–1658. https://doi.org/10.1016/j.renene.2019.07.157.

[11]   E.A. Omondi, P.K. Ndiba, P.G. Njuru, Characterization of water hyacinth (E. crassipes) from Lake Victoria and ruminal slaughterhouse waste as co-substrates in biogas production, SN Appl. Sci. 1 (2019). https://doi.org/10.1007/s42452-019-0871-z.

[12]   K. Blessy, M.L. Prabha, Application of water hyacinth vermicompost on the growth of Capsicum annum, Int. J. Pharma Sci. Res. 5 (2014) 198–203.

[13] P.A. Ogutu, Vermicomposting Water Hyacinth: Turning Fisherman's Nightmare into Farmer's Fortune, Int. J. Res. Innov. Appl. Sci. 4 (2019) 11–14.

[14] N. Acelas, E. Flórez, D. López, Phosphorus recovery through struvite precipitation from wastewater: effect of the competitive ions, Desalin. Water Treat. 54 (2015) 2468–2479. https://doi.org/10.1080/19443994.2014.902337.

[15] N.Y. Acelas, B.D. Martin, D. López, B. Jefferson, Selective removal of phosphate from wastewater using hydrated metal oxides dispersed within anionic exchange media, Chemosphere. 119 (2015). https://doi.org/10.1016/j.chemosphere.2014.02.024.

[16] A. Ramirez, S. Giraldo, J. García-nunez, E. Flórez, N. Acelas, Phosphate removal from water using a hybrid material in a fixed-bed column, J. Water Process Eng. 26 (2018) 131–137. https://doi.org/10.1016/j.jwpe.2018.10.008.

[17] A. Bouzas, N. Martí, S. Grau, R. Barat, D. Mangin, L. Pastor, Implementation of a global P-recovery system in urban wastewater treatment plants, J. Clean. Prod. 227 (2019) 130–140. https://doi.org/10.1016/j.jclepro.2019.04.126.

[18] A. Pettersson, L.E. Åmand, B.M. Steenari, Leaching of ashes from co-combustion of sewage sludge and wood-Part II: The mobility of metals during phosphorus extraction, Biomass and Bioenergy. 32 (2008) 236–244. https://doi.org/10.1016/j.biombioe.2007.09.006.

[19] H.X. XUE Tao, Releasing characteristics of phosphorus and other substances during thermal treatment of excess sludge, J. Environ. Sci. 19 (2007) 1153–1158. https://doi.org/10.1016/S1001-0742(07)60188-0.

[20] X. Li, Y. Xie, F. Jiang, B. Wang, Q. Hu, Y. Tang, T. Luo, T. Wu, Enhanced phosphate removal from aqueous solution using resourceable nano-CaO2/BC composite: Behaviors and mechanisms, Sci. Total Environ. 709 (2020) 136123. https://doi.org/10.1016/j.scitotenv.2019.136123.

[21] N.Y. Acelas, D.P. López, D.W.F. Wim Brilman, S.R.A. Kersten, A.M.J. Kootstra, Supercritical water gasification of sewage sludge: Gas production and phosphorus

recovery, Bioresour. Technol. 174 (2014) 167–175. https://doi.org/10.1016/j.biortech.2014.10.003.

[22] Z. Tan, A. Lagerkvist, Phosphorus recovery from the biomass ash: A review, Renew. Sustain. Energy Rev. 15 (2011) 3588–3602. https://doi.org/10.1016/j.rser.2011.05.016.

[23] Y. Ding, Y. Liu, S. Liu, Z. Li, X. Tan, X. Huang, G. Zeng, Y. Zhou, B. Zheng, X. Cai, Competitive removal of Cd(II) and Pb(II) by biochars produced from water hyacinths: Performance and mechanism, RSC Adv. 6 (2016) 5223–5232. https://doi.org/10.1039/c5ra26248h.

[24] F. Zhang, X. Wang, D. Yin, B. Peng, C. Tan, Y. Liu, X. Tan, S. Wu, Efficiency and mechanisms of Cd removal from aqueous solution by biochar derived from water hyacinth (Eichornia crassipes), J. Environ. Manage. 153 (2015) 68–73. https://doi.org/10.1016/j.jenvman.2015.01.043.

[25] C. Zhang, X. Chen, Y. Tian, Y. Zhou, X. Lu, Conversion of water hyacinth to value-added fuel via hydrothermal carbonization, Energy. 197 (2020) 117193. https://doi.org/10.1016/j.energy.2020.117193.

[26] S. Mignardi, L. Archilletti, L. Medeghini, C. De Vito, Valorization of Eggshell Biowaste for Sustainable Environmental Remediation, Sci. Rep. 10 (2020) 1–10. https://doi.org/10.1038/s41598-020-59324-5.

[27] P. Guedes, N. Couto, L.M. Ottosen, A.B. Ribeiro, Phosphorus recovery from sewage sludge ash through an electrodialytic process, Waste Manag. 34 (2014) 886–892. https://doi.org/10.1016/j.wasman.2014.02.021.

[28] L.M. Ottosen, G.M. Kirkelund, P.E. Jensen, Extracting phosphorous from incinerated sewage sludge ash rich in iron or aluminum, Chemosphere. 91 (2013) 963–969. https://doi.org/10.1016/j.chemosphere.2013.01.101.

[29] L. Fang, F. Yan, J. Chen, X. Shen, Z. Zhang, Novel Recovered Compound Phosphate Fertilizer Produced from Sewage Sludge and Its Incinerated Ash, ACS Sustain. Chem. Eng. (2020). https://doi.org/10.1021/acssuschemeng.9b06861.

43

[30] S. Tang, F. Yan, C. Zheng, Z. Zhang, Novel Calcium Oxide-Enhancement Phosphorus Recycling Technique through Sewage Sludge Pyrolysis, ACS Sustain. Chem. Eng. 6 (2018) 9167–9177. https://doi.org/10.1021/acssuschemeng.8b01492.

[31] J. Chen, S. Tang, F. Yan, Z. Zhang, Efficient recovery of phosphorus in sewage sludge through hydroxylapatite enhancement formation aided by calcium-based additives, Water Res. 171 (2020) 115450. https://doi.org/10.1016/j.watres.2019.115450.

[32] M.L.S. Oliveira, C. Dario, B.F. Tutikian, H.Z. Ehrenbring, C.C.O. Almeida, L.F.O. Silva, Historic building materials from Alhambra: Nanoparticles and global climate change effects, J. Clean. Prod. 232 (2019) 751–758. https://doi.org/https://doi.org/10.1016/j.jclepro.2019.06.019.

[33] M.L.S. Oliveira, B.F. Tutikian, C. Milanes, L.F.O. Silva, Atmospheric contaminations and bad conservation effects in Roman mosaics and mortars of Italica, J. Clean. Prod. 248 (2020) 119250. https://doi.org/https://doi.org/10.1016/j.jclepro.2019.119250.

[34] N.C. Shiba, F. Ntuli, Extraction and precipitation of phosphorus from sewage sludge, Waste Manag. 60 (2017) 191–200. https://doi.org/10.1016/j.wasman.2016.07.031.

[35] X. Zheng, Y. Ye, Z. Jiang, Z. Ying, S. Ji, W. Chen, B. Wang, B. Dou, Enhanced transformation of phosphorus (P) in sewage sludge to hydroxyapatite via hydrothermal carbonization and calcium-based additive, Sci. Total Environ. 738 (2020) 139786. https://doi.org/10.1016/j.scitotenv.2020.139786.

[36] Q. Liu, Z. Fang, Y. Liu, Y. Liu, Y. Xu, X. Ruan, X. Zhang, W. Cao, Phosphorus speciation and bioavailability of sewage sludge derived biochar amended with CaO, Waste Manag. 87 (2019) 71–77. https://doi.org/10.1016/j.wasman.2019.01.045.

[37] R. Yesmeen, H.M. Zakir, M.S. Alam, S. Mallick, Heavy Metal and Major Ionic Contamination Level in Effluents, Surface and Groundwater of an Urban Industrialised City: A Case Study of Rangpur City, Bangladesh, Asian J. Chem. Sci. 5 (2018) 1–16. https://doi.org/10.9734/ajocs/2018/45061.

[38] S.I.A. Sudiarto, A. Renggaman, H.L. Choi, Floating aquatic plants for total nitrogen and phosphorus removal from treated swine wastewater and their biomass

characteristics, J. Environ. Manage. 231 (2019) 763–769. https://doi.org/10.1016/j.jenvman.2018.10.070.

[39] G.R.F. Bronzato, S.M. Ziegler, R.C. Silva, I. Cesarino, A.L. Leão, Characterization of the pre-treated biomass of Eichhornia crassipes (water hyacinth) for the second generation ethanol production, Mol. Cryst. Liq. Cryst. 655 (2017) 224–235. https://doi.org/10.1080/15421406.2017.1360696.

[40] F. Allam, M. Elnouby, K.M. El-Khatib, D.E. El-Badan, S.A. Sabry, Water hyacinth (Eichhornia crassipes) biochar as an alternative cathode electrocatalyst in an air-cathode single chamber microbial fuel cell, Int. J. Hydrogen Energy. 45 (2020) 5911–5927. https://doi.org/10.1016/j.ijhydene.2019.09.164.

[41] C. Ohtsuki, T. Kokubo, T. Yamamuro, Mechanism of apatite formation on CaO–SiO2–P2O5 glasses in a simulated body fluid, J. Non. Cryst. Solids. 143 (1992) 84–92. https://doi.org/10.1016/S0022-3093(05)80556-3.

[42] T.Y. Jiang, J. Jiang, R.K. Xu, Z. Li, Adsorption of Pb(II) on variable charge soils amended with rice-straw derived biochar, Chemosphere. 89 (2012) 249–256. https://doi.org/10.1016/j.chemosphere.2012.04.028.

[43] Lena Johansson Westholm, Substrates for phosphorus removal — Potential benefits for on-site wastewater treatment?, Water Res. 40 (2006) 23–36. https://doi.org/10.1016/j.watres.2005.11.006.

[44] K.W. Jung, M.J. Hwang, K.H. Ahn, Y.S. Ok, Kinetic study on phosphate removal from aqueous solution by biochar derived from peanut shell as renewable adsorptive media, Int. J. Environ. Sci. Technol. 12 (2015) 3363–3372. https://doi.org/10.1007/s13762-015-0766-5.

[45] A.F. Santos, A.L. Arim, D. V. Lopes, L.M. Gando-Ferreira, M.J. Quina, Recovery of phosphate from aqueous solutions using calcined eggshell as an eco-friendly adsorbent, J. Environ. Manage. 238 (2019) 451–459. https://doi.org/10.1016/j.jenvman.2019.03.015.

[46] P.J. White, M.R. Broadley, Calcium in plants, Ann. Bot. 92 (2003) 487–511.

https://doi.org/10.1093/aob/mcg164.

[47]   S. Sukarni, A.E. Widiono, S. Sumarli, R. Wulandari, I.M. Nauri, A.A. Permanasari, Thermal decomposition behavior of water hyacinth (eichhornia crassipes) under an inert atmosphere, MATEC Web Conf. 204 (2018) 00010. https://doi.org/10.1051/matecconf/201820400010.

[48]   L. Berzina-Cimdina, N. Borodajenko, Research of Calcium Phosphates Using Fourier Transform Infrared Spectroscopy, Infrared Spectrosc. - Mater. Sci. Eng. Technol. (2012). https://doi.org/10.5772/36942.

[49]   F.B. Reig, J.V.G. Adelantado, M.C.M.M. Moreno, FTIR quantitative analysis of calcium carbonate (calcite) and silica (quartz) mixtures using the constant ratio method. Application to geological samples, Talanta. 58 (2002) 811–821. https://doi.org/10.1016/S0039-9140(02)00372-7.

[50]   F. Wilson, P. Tremain, B. Moghtaderi, Characterization of Biochars Derived from Pyrolysis of Biomass and Calcium Oxide Mixtures, Energy and Fuels. 32 (2018) 4167–4177. https://doi.org/10.1021/acs.energyfuels.7b03221.

[51]   L. Delgadillo-Velasco, V. Hernández-Montoya, M.A. Montes-Morán, R.T. Gómez, F.J. Cervantes, Recovery of different types of hydroxyapatite by precipitation of phosphates of wastewater from anodizing industry, J. Clean. Prod. 242 (2020). https://doi.org/10.1016/j.jclepro.2019.118564.

[52]   O.B. Ayodele, Y. Uemura, Z. Gholami, W. Mohd, A. Wan, Effect of ethanedioic acid functionalization on Ni/Al2O3 catalytic hydrodeoxygenation and isomerization of octadec-9-enoic acid into biofuel: kinetics and Arrhenius parameters, J. Energy Chem. 25 (2016) 158–168. https://doi.org/10.1016/j.jechem.2015.08.017.

[53]   S. Weiner, O. Bar-Yosef, States of preservation of bones from prehistoric sites in the Near East: A survey, J. Archaeol. Sci. 17 (1990) 187–196. https://doi.org/10.1016/0305-4403(90)90058-D.

[54]   T.A. Surovell, M.C. Stiner, Standardizing infra-red measures of bone mineral crystallinity: An experimental approach, J. Archaeol. Sci. 28 (2001) 633–642.

https://doi.org/10.1006/jasc.2000.0633.

[55] S. Ramesh, Z.Z. Loo, C.Y. Tan, W.J.K. Chew, Y.C. Ching, F. Tarlochan, H. Chandran, S. Krishnasamy, L.T. Bang, A.A.D. Sarhan, Characterization of biogenic hydroxyapatite derived from animal bones for biomedical applications, Ceram. Int. 44 (2018) 10525–10530. https://doi.org/10.1016/j.ceramint.2018.03.072.

[56] K. Tõnsuaadu, K.A. Gross, L. Pluduma, M. Veiderma, A review on the thermal stability of calcium apatites, J. Therm. Anal. Calorim. 110 (2012) 647–659. https://doi.org/10.1007/s10973-011-1877-y.

[57] R. Huang, Y. Tang, Speciation Dynamics of Phosphorus during (Hydro)Thermal Treatments of Sewage Sludge, Environ. Sci. Technol. 49 (2015) 14466–14474. https://doi.org/10.1021/acs.est.5b04140.

[58] S. Türk, Altınsoy, G. ÇelebiEfe, M. Ipek, M. Özacar, C. Bindal, Microwave–assisted biomimetic synthesis of hydroxyapatite using different sources of calcium, Mater. Sci. Eng. C. 76 (2017) 528–535. https://doi.org/10.1016/j.msec.2017.03.116.

[59] W. Kim, F. Saito, Sonochemical synthesis of hydroxyapatite from H3PO4 solution with Ca(OH)2, Ultrason. Sonochem. 8 (2001) 85–88. https://doi.org/10.1016/S1350-4177(00)00034-1.

[60] S. Raynaud, E. Champion, D. Bernache-Assollant, P. Thomas, Calcium phosphate apatites with variable Ca/P atomic ratio I. Synthesis, characterisation and thermal stability of powders, Biomaterials. 23 (2002) 1065–1072. https://doi.org/10.1016/S0142-9612(01)00218-6.

[61] F. Dong, D.W. Kirk, H. Tran, Biomass ash alkalinity reduction for land application via CO2 from treated boiler flue gas, Fuel. 136 (2014) 208–218. https://doi.org/10.1016/j.fuel.2014.07.059.

[62] Y. Zou, X. Wang, A. Khan, P. Wang, Y. Liu, A. Alsaedi, T. Hayat, X. Wang, Environmental Remediation and Application of Nanoscale Zero-Valent Iron and Its Composites for the Removal of Heavy Metal Ions: A Review, Environ. Sci. Technol. 50 (2016) 7290–7304. https://doi.org/10.1021/acs.est.6b01897.

[63] L. Johansson, J.P. Gustafsson, Phosphate removal using blast furnace slags and opoka-mechanisms, Water Res. 34 (2000) 259–265. https://doi.org/10.1016/S0043-1354(99)00135-9.

[64] K. Moriyama, T. Kojima, Y. Minawa, S. Matsumoto, K. Nakamachi, Development of artificial seed crystal for crystallization of calcium phosphate, Environ. Technol. (United Kingdom). 22 (2001) 1245–1252. https://doi.org/10.1080/09593330.2001.9619163.

[65] A.S. Marriott, A.J. Hunt, E. Bergstro, J.H. Clark, R. Brydson, Investigating the structure of biomass-derived non-graphitizing mesoporous carbons by electron energy loss spectroscopy in the transmission electron microscope and X-ray photoelectron spectroscopy, Carbon N. Y. 67 (2014) 514–524. https://doi.org/10.1016/j.carbon.2013.10.024.

[66] P. Ptáček, F. Šoukal, T. Opravil, Kinetics and Mechanism of Thermal Decomposition of Calcite and Aragonite, J. Miner. Met. Mater. Eng. (2017) 71–79.

[67] M.B. Taşkın, Ö. Şahin, H. Taskin, O. Atakol, A. Inal, A. Gunes, Effect of synthetic nano-hydroxyapatite as an alternative phosphorus source on growth and phosphorus nutrition of lettuce (Lactuca sativa L.) plant, J. Plant Nutr. 41 (2018) 1148–1154. https://doi.org/10.1080/01904167.2018.1433836.

[68] R. Kleemann, J. Chenoweth, R. Clift, S. Morse, P. Pearce, D. Saroj, Comparison of phosphorus recovery from incinerated sewage sludge ash (ISSA) and pyrolysed sewage sludge char (PSSC), Waste Manag. 60 (2017) 201–210. https://doi.org/10.1016/j.wasman.2016.10.055.

Capítulo 4

4. Recovering phosphorus from aqueous solutions using water hyacinth (*Eichhornia Crassipes*) toward sustainability through its transformation to apatite

Abstract

This work provides circular leveraging strategies for using water hyacinth *(Eichhornia Crassipes)* (WH) in the removal and recovery of phosphorus (P) from aqueous solutions. This study also assesses the transformation of the adsorbed phosphorus into a high value-added product (apatite) and its potential as a soil amendment. The materials evaluated were recovered from WH calcination at temperatures ranging between 350 °C and 700 °C, which evidenced great amounts of $Ca(OH)_2$, MgO, Al_2O_3, and $Ca_5(PO_4)_3OH$. The material that evidenced highest P removal capabilities was CWH-650, which was produced from calcination at 650 °C; hence, it was used during the P adsorption process. The results showed that chemisorption is the limiting step in the adsorption process, with a maximum adsorption capacity determined by its adaptation to the Langmuir model at 21.21 mg P/g. Likewise, the study determined that the exchange of ligands followed by precipitation in the apatite formation process were the dominant mechanisms during the adsorption process. An additional calcination step conducted on the CWH-650 adsorbent previously used in the removal of P denoted an increase in the amount of apatite (up to 41.0%), as demonstrated through fourier-transform infrared spectroscopy and X-ray diffraction analysis. Subsequently, this study concluded that the Ca- and P-enriched phases exhibited a higher solubility of P in 2% formic acid than in deionized water, which fostered the release of up to 60 mg P/g, indicating its potential use as a phosphate fertilizer and an acid-soil amendment.

4.1. Introduction

Phosphorus (P) is a nonrenewable nutrient essential for the development of plants. It is used in fertilizers generated from phosphoric rock, an almost depleted resource as at least 80%–90% of its world reserves have been exhausted in the last 20 years [1]. Therefore, P is also the main cause of aquatic ecosystem eutrophication, which is generated by P leaching from the soil after its application as a fertilizer and due to the discharge of industrial, livestock, and domestic wastewater with high concentrations of P [2–4]. For this reason, removing and recovering P from aqueous systems, via sustainable and efficient processes, is a topic of high interest.

Adsorption is one of the most widely used technologies not only to remove phosphates from wastewater but also recover and recycle P [5,6]. It has been reported that adsorbents rich in Ca, Al, Mg, Si, Fe, and Zr are selective in the removal of P through the formation of internal sphere complexes, chemical precipitation, and ion exchanges [7–11]. Therefore, biomass rich in these minerals, such as eggshells, Thalia dealbata, peanut shells, sewage sludge, and water hyacinths (WHs), become an alternative for the production of adsorbent materials [11–15]. WH (*Eichhornia Crassipes*) is a weed that reproduces excessively on lake surfaces [15–17]. However, when subjected to heat treatments, Fe, Si, Mg, Ca, or Al minerals commonly found in this biomass [18,19] can be transformed into oxides/hydroxides of these metals, which have been reported as active phases for the selective adsorption of P [20].

Cai et al. [4] studied the adsorption of P using a biochar prepared from the pyrolysis of WHs modified with iron oxide and determined an adsorption capacity of 5.07 mg P/g, wherein the active phases used for the removal of P were Fe_3O_4 and Fe_2O_3, which allowed ligands to be exchanged between the OH^- ions on the surface of the material and a phosphate ion (PO_4^{3-}) solution through the formation of Fe–O–P bonds. On the other hand, Mosa et al. [15] studied the adsorption of P from biochars generated from the pyrolysis of WHs rich in metals (Fe, Mn, Zn, and Cu), obtaining P adsorption capacities from 12.15 mg P/g to 31.55 mg P/g, and reporting the precipitation of P species as the main adsorption mechanism. Among the different metals present in these biomasses, calcium is one of the most attractive for the removal and recovery of P because it favors the formation of apatite ($Ca_5(PO_4)_3OH$)

[12,21]. Apatite is a calcium phosphate biomaterial that constitutes a valuable path for the recovery of P [14,18]. Owing to its biocompatibility with soils, apatite enhances plant growth, which makes it suitable as an alternative amendment acting as a phosphate fertilizer [18,22]. It has also been reported that subjecting apatite to heat treatments below 800 °C increases crystallinity and improves plant bioavailability [23].

In our previous study [18], we determined that WH ashes exhibit a Ca/P molar ratio of 5.07, and as the calcination temperature increases, P and Ca are converted into apatite. In addition, these ashes contain oxides and hydroxides of metals, such as Ca, Al, Mg, and Fe (i.e., $Ca(OH)_2$, Al_2O_3, MgO, and Fe_3O_4), which are active phases in the adsorption of P. To the best of our knowledge to date, there are no known studies in which thermally transformed WH is not only used to adsorb P but also after the adsorption process, wherein, after a simple heat treatment, the adsorbed P may be transformed into a high value-added product, such as apatite, which is also bioavailable for plants.

Therefore, this study seeks to assess the appropriate conditions for obtaining the maximum possible P removal rates from aqueous solutions using WH ash and its subsequent transformation into apatite bioavailable for plants.

4.2. Materials and methods

4.2.1. Material production and characterization

WH waste used for this study was collected at the Ituango Hydroelectric Project (Ituango Dam) located on the Cauca River between the municipalities of Ituango and Briceño in the department of Antioquia, Colombia. The WH-derived adsorbent materials used were prepared by calcination at temperatures of 350 °C, 450 °C, 550 °C, 600 °C, 650 °C, and 700 °C, according to the previously described methodology [18]. The materials obtained were crushed, sieved at a particle size lower than 0.335 mm, and named CWH-X, where X represents the corresponding calcination temperature. Calcination at each temperature was conducted in duplicate to validate the reproducibility of the treatment.

Before and after adsorption, the different materials were characterized by Attenuated Total Reflection-Fourier Transform Infrared (ATR-FTIR) spectroscopy, using a Spectrum two-PerkinElmer with UATR for a range within 4000–450 cm^{-1}, to determine the functional

groups present on the surface and X-ray diffraction (XRD) patterns were obtained using a Shimadzu XRD-6100 diffractometer with Cu Kα radiation (λ = 1.5406 Å), at 40 kV in the 2θ angle range of 10° to 80° with a step size of 0.026° and a period of 50 seconds to identify crystalline phases and their quantification.

4.2.2. Adsorption of P

P adsorption experiments were conducted with the different materials obtained in order to determine the adsorbent with the highest removal capacity and thus perform the adsorption equilibrium and kinetics experiments. Preliminary experiments were conducted by adding 0.05 g from each adsorbent obtained with 50 mL of a synthetic solution at 75 mg/L phosphorus prepared from KH_2PO_4 (Panreac, 99.0%) at a pH level of 5.31 (natural value). The mixture was constantly stirred for 2 h at 200 rpm at 25 °C. The phosphorus concentration remaining in solution throughout the work was determined by the colorimetry method (Hach, PhosVer® 3 Phosphate Reagent), using a DR 3900 spectrophotometer (Hach).

4.2.2.1. Equilibrium and adsorption rate experiments

Based on the previous experiment, the CWH-650 material exhibited the highest percentage of P removal. Hence, the experiments to assess both the kinetics and isotherms of the adsorption process were conducted using this adsorbent. First, KH_2PO_4 was used to prepare a synthetic stock solution at a P concentration of 500 mg/L. And through dilutions, solutions were prepared at different P concentrations (10, 25, 50, 75, 110, and 130 mg/L). The experiments were conducted in a propeller reactor at 200 rpm, adding 500 mL from each solution at their natural pH level (values between 5.13 and 5.98, depending on the concentration) to 0.5 g of adsorbent at 25 °C. Samples were taken at intervals between 2 and 5760 min until equilibrium was reached. During all experiments, we made sure the total volume subtracted did not exceed 5% of the total volume. We also measured the pH level of the solutions periodically, and recorded the changes produced over time.

We considered that we had reached the equilibrium point when we recorded no significant concentration variations (< 2%) in 3 consecutive samples. The P removal percentage and adsorption capacity were calculated according to Equations (4-1) and (4-2) below, respectively.

$$\%R = \frac{C_0 - C_t}{C_0} \times 100 \tag{4-1}$$

$$q_t = \frac{(C_0 - C_t)}{w} \times V, \tag{4-2}$$

where *%R* represents the P removal percentage, C_0 (mg/L) is the initial P concentration in the solution, C_t (mg/L) is the P concentration over time t, q_t (mg/g) is the amount of P adsorbed over time t, V (L) is the volume of the solution, and w (g) is the mass of the adsorbent material.

4.2.2.2. Effect of the initial pH of the solution

Once the equilibrium time was determined in the previous experiments, the effects from the initial pH value of the P solution were assessed by adding 0.05 g of the adsorbent to 50 mL of the different synthetic solutions at a P concentration of 100 mg/L and pH values of 2, 4, 6, 8, 10, and 12 using 1M NaOH or 1M HCl to stabilize the pH levels. The samples were stirred at 200 rpm for 72 h at 25 °C.

4.2.3. P-enrichment and P-solubility

To enrich the CWH-600, CWH-650, and CWH-700 adsorbents with more stable and bioavailable Ca–P phases, once the materials were used to remove P from aqueous solutions following the procedure described in Section 2.2.1, the adsorbents were subjected to an additional calcination process at temperatures of 600 °C, 650 °C, and 700 °C, respectively.

The bioavailability of P in these materials (CWH-600, CWH-650, and CWH-700) was determined by evaluating the solubility of P compounds in formic acid as per the methodology described by Shiba et al. and Zheng et al. [14,24]. The experiments were conducted dissolving 0.05 g from each material in 50 mL of formic acid at 2%. The mixtures were stirred at 200 rpm for 24 h at 25 °C and passed through a 0.45 µm filter to determine the concentration of P. The amount of P bioavailable was standardized based on the mass of the solid sample. On the other hand, the content of water-soluble P (WSP) is an indicator used to evaluate the loss of P when a solid fertilizer is applied to the soil [23]. Hence, our WSP content was assessed following the procedure reported by Liu et al. [23], mixing 0.025 g from each material in 25 mL of deionized water. The mixtures were stirred at 200 rpm for 24 h at 25 °C and passed through a 0.45 µm filter to determine the concentration of P. The

amount of WSP was standardized based on the mass of the solid sample. The bioavailability and WSP experiments were performed before P adsorption, after P adsorption, and after calcining the material with the adsorbed P. All experiments were conducted in duplicate.

4.3. Results and discussion

4.3.1. Adsorption of P

To identify the most efficient material in the removal of P, we analyzed both the WH without transformation and WH calcined at different temperatures. Fig. 4-1 denotes the phosphorus removal percentages from the different adsorbent materials: WH, CWH-350, CWH-450, CWH-550, CWH-600, CWH-650, and CWH-700. Here, we observed that WH without any treatment desorbed P, which is naturally present within the structure of WH (our previous work, [18]). In addition, P removal percentages improved with heat treatments and increased as the calcination temperature increased. However, the removal percentage reported for CWH-700 is very similar to the removal percentage reported for CWH-650 (29.86% and 30.56%, respectively). This is related to the fact that, at 650 °C, the entire WH sample turns into ash, which mostly contains $Ca(OH)_2$ (15.8%, our previous work, [18]), one of the most active calcium phases in the removal of P [12,25]. Previous studies revealed that $Ca(OH)_2$ is produced during the heat conversion of biomass because the Ca present in its structure acts as a precursor in the formation of $CaCO_3$, which is later transformed into $Ca(OH)_2$ [15]. In this study, for CWH-650 and CWH-700, the content of $Ca(OH)_2$ is 15.8% and 16.5%, respectively (our previous work, [18]), which is related to their similar P removal percentages and, in turn, to the presence of this phase of calcium. Fig. 1 evidences that for materials produced at temperatures between 350 °C and 600 °C, the content of $Ca(OH)_2$ is zero. However, P adsorption still occurs, indicating that there are other active phases, such as Al_2O_3, MgO, and Fe_3O_4, that contribute to the adsorption process.

Based on our data, we selected CWH-650 for the removal of P. Consequently, all the P adsorption equilibrium and kinetic experiments were conducted using this adsorbent material.
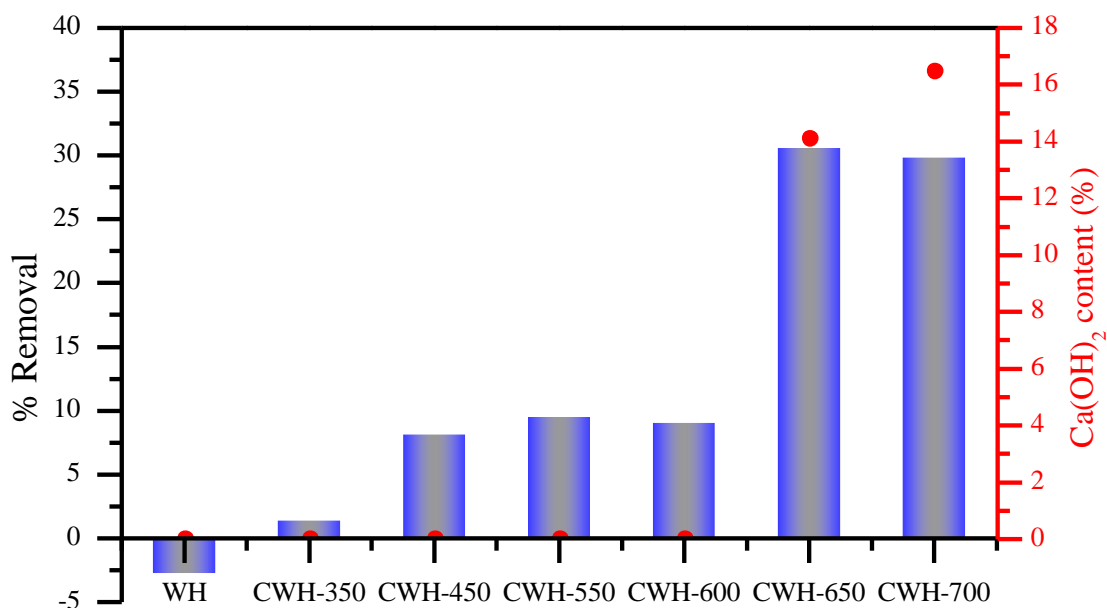
Fig. 4-1. Percentage of phosphorus removal using different water hyacinth transformation and Ca(OH)$_2$ content of each adsorbent [18] (P concentration = 75 mg/L, adsorbent quantity = 0.05 g, pH = 5.31, temperature = 25 °C, stirring speed = 200 rpm, contact time: 2 h).

4.3.1.1. Equilibrium and adsorption rate

The list of the kinetic parameters determined by the good adjustment of the experimental data to pseudo first-order and pseudo second-order kinetic models (Table 4-S1 and Fig. 4-S1) at a correlation coefficient of $R^2 > 0.94$ are shown in Table 4-S2. The adjustment of the experimental data to the pseudo first-order model indicates physisorption between CWH-650 and P; whereas, the good adjustment of the experimental data to the pseudo second-order model indicates chemisorption. These results suggest the existence of different adsorbate–adsorbent interaction energies in the adsorption process. The adsorption capacity values at equilibrium, q_e, determined by the pseudo first-order model are closer to the experimental values, $q_{e\ exp}$, and because k_2 values are less than the k_1 values, chemisorption is the limiting step in the adsorption process of P for CWH-650.

4.3.1.2. Adsorption isotherms

Fig. 4-2 denotes the adsorption isotherms of P for CWH-650 using the Langmuir, Freundlich, Temkin, and Langmuir–Freundlich models (Table 4-S3). Here, we may observe a good adjustment of the experimental data to the four models, which is consistent with the

correlation coefficients listed in Table 4-S4 ($R^2 > 0.99$). In this study, the CHW-650 material exhibits concave isotherms (type L) [26], which indicates that the relationship between the remaining P concentration and P concentration adsorbed decreases as the P concentration value increases. This suggests a progressive saturation of CWH-650.
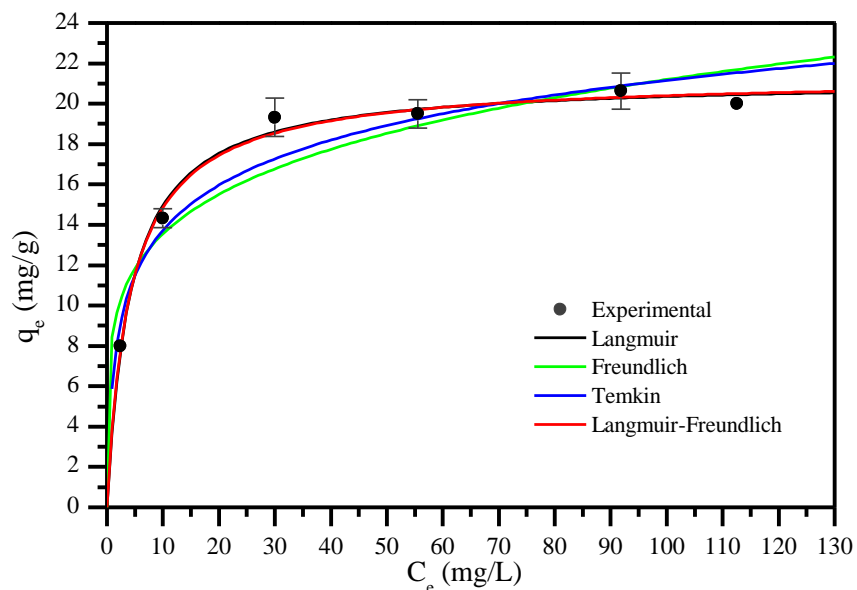
Fig. 4-2. Phosphorus adsorption isotherms in CWH-650 (solution volume = 500 ml, adsorbent amount = 0.5 g, temperature = 25 °C, stirring speed = 200 rpm, contact time = 72 h). CWH-650: water hyacinth calcinated at 650 °C.

The good adjustment of the experimental data to the Langmuir model allowed us to determine the maximum adsorption capacity (21.21 mg/g) and indicate that, at equilibrium, adsorption occurs in a monolayer with a homogeneous surface that presents a fixed number of active sites with the same affinity for P. However, we may also observe a good adjustment of the experimental data to the Freundlich model, which accounts for interactions on multilayered heterogeneous surfaces with different affinities and interaction energies between P and the active sites on the CWH-650 surface. This model predicts that the adsorption process is favorable as $1/n = 0.195$ [27]; whereas, the adjustment to the Temkin model indicates that P adsorption heat decreases linearly within a layer as the surface coverage increases due to the CWH-650–P interactions, wherein adsorption is characterized by a uniform distribution of bond energies [28]. Furthermore, the value of $b = 0.768$ kJ/mol indicates a physical interaction between CWH-650 and P that occurs via Van Der Waals [29].

Finally, the good adjustment to the Langmuir–Freundlich model suggests that the CWH-650 adsorption system has demonstrated Freundlich's behavior at low P concentrations and followed the prediction of the characteristic Langmuir monolayer adsorption capacity at high P concentrations [30]. In addition, the value of n_{LF} = 0.960 indicates that CWH-650 is a heterogeneous material with homogeneous tendencies [31,32].

Hence, we can conclude that there is no single form of interaction between CWH-650 and P and a mixture of adsorption mechanisms is present. This is consistent with the findings reported by other studies on P adsorption using materials rich in Ca-bearing phases. For example, Liu et al. [21] found that a biocarbon rich in CaO could be obtained from eggshells and rice straw. This biocarbon acted as an adsorbent for P, whose process could be described through the Langmuir isotherm model. Mitrogiannis et al. [33] used a natural zeolite pretreated with $Ca(OH)_2$ to recover phosphorus, finding that the Freundlich and Temkin isotherm models better described P adsorption. On the other hand, Markou et al. [34] used bentonite pretreated with $Ca(OH)_2$ for the adsorption of P, and found that the experimental data had a better adjustment to the Freundlich model, which was consistent with the results found by XRD, which revealed that the surface was heterogeneous, so there were different P adsorption models.

4.3.1.3. Effect of the initial pH of the solution

The initial pH of a solution is a parameter that influences the ionization balance of the $H_2PO_4^-$, HPO_4^{2-}, and PO_4^{3-} species, as well as the surface charges of the adsorbent [35], which generates changes in the P adsorption capacity for CWH-650. Fig. 4-3 illustrates the effects from the initial pH of the solution on the ability exhibited by CWH-650 to adsorb P. Here, all solutions increased their initial pH values to produce an increased final pH, thus indicating an increase in the number of OH^- ions present in each solution. During the P adsorption process on metal oxides/hydroxides, the ligand exchange mechanism has been one of the most reported [20,36], in which the PO_4^{3-} anion forms a covalent bond with a metal cation on the adsorbent surface, thus releasing the OH^- ions attached to the metal cation [37], and causing an increase in the final pH value of the solution. This indicates that the ligand exchange is one of the mechanisms by which P is adsorbed onto CWH-650.

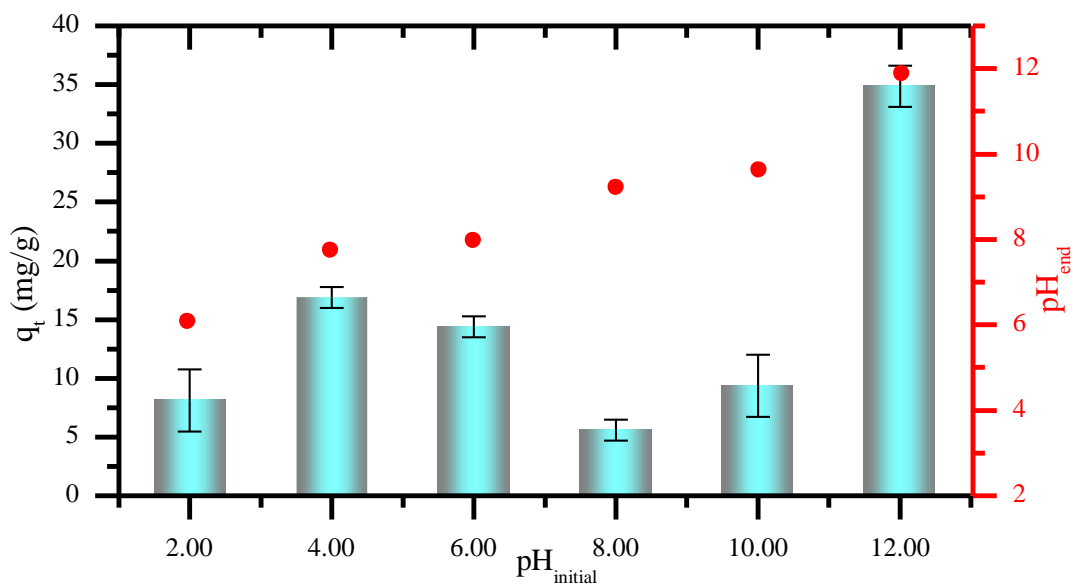**Fig. 4-3.** Effects from the initial pH value on P adsorption (solution volume = 50 ml, adsorbent amount = 0.05 g, temperature = 25 °C, stirring speed = 200 rpm, contact time = 72 h).

Fig. 4-3 evidences that there are no pH adsorption tendencies as the initial pH value of the solution increases. At a pH of 2, adsorption capacity is 8 mg/g. Then, it increases to 17 mg/g when the initial pH value is 4, but it decreases again to 5 mg/g at a pH of 8. However, when the initial pH value of the solution is 12, it exhibits its highest capacity, reaching close to 35 mg/g. This behavior can be explained taking into account that both, the proportion of the H_3PO_4/ $H_2PO_4^-$/ HPO_4^{2-}/ PO_4^{3-} specifies present in the solution and solubility of $Ca(OH)_2$ and $CaCO_3$ phases present in CWH-650, are related to pH levels. As shown in Fig. 4-4, at a pH value of 2, there is high solubility of $Ca(OH)_2$ and $CaCO_3$, forming Ca^{2+} in the solution [38], which additionally favors the H_3PO_4/$H_2PO_4^-$ species [39]. The interaction between Ca^{2+} and $H_2PO_4^-$ may be responsible for the adsorption levels that were determined. However, a large amount of Ca^{2+} still remains in solution (Fig. 4-S2). Increasing the initial pH value (from 4 to 6) favors the formation of HPO_4^{2-}, and the interaction of this species with the Ca^2 from $Ca(OH)_2$ favors the formation of $Ca(H_2PO_4)_2$ and $CaHPO_4$. At these pH values (Fig. S1), the FTIR spectra of the post-adsorption samples exhibit $CaCO_3$-characteristic signs between 1400 and 1500 cm^{-1}, indicating that they do not intervene in the adsorption process. The $Ca(H_2PO_4)_2$ and $Ca(HPO_4)$ compounds formed at pH values of 4 and 6 are known as apatite precursors [40]. Hence, we can produce a complex mixture that involves different

post-adsorption calcium phosphates (Ca–P (Ca(H_2PO_4)$_2$, Ca (HPO_4, $Ca_5(PO_4)_3OH$). This variety of Ca–P species could explain the higher adsorption percentage observed in Fig. 4-3 for initial pH values of 4 – 6. At higher initial pH values (8–10), Ca (OH)$_2$ solubility decreases [38]. Additionally, the presence of HPO_4^{2-} in balance with PO_4^{3-}, increase of PO_4^{3-}, and presence of Ca(OH)$_2$ cause the precipitation of the $Ca_5(PO_4)_3OH$ phase [41], which requires a larger amount of Ca^{2+} for the removal of a P atom (Ca/P = 1.67) than $CaHPO_4$ (Ca/P = 1). Finally, at a pH value of 12, the presence of PO_4^{3-}, which not only interacts with Ca(OH)$_2$, also succeeds in replacing the CO_3^{2-} group from $CaCO_3$ to form $Ca_5(PO_4)_3OH$, which is reflected in an increase in P removal percentages. This is confirmed in the FTIR spectrum (Fig. 4-S2), where the PO_4^{3-} bands in $Ca_5(PO_4)_3OH$ increase considerably after adsorption, while the CO_3^{2-} bands decrease.
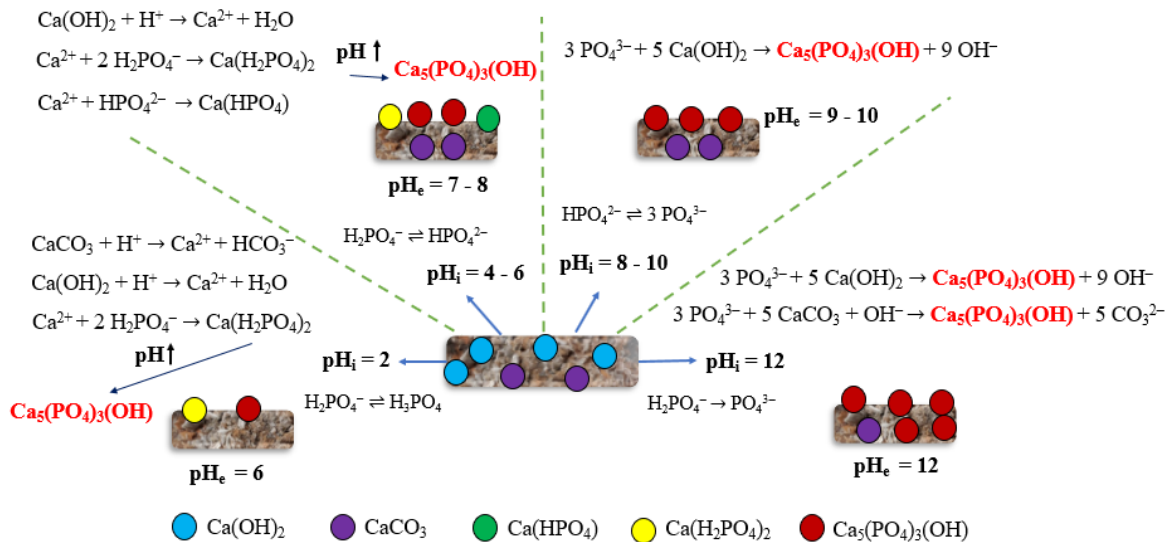
Fig. 4-4. P adsorption at different initial pH.

4.3.2. Characterization of the adsorbed P–Ca species

Fig. 4-5 denotes the FTIR spectra for CWH-650 before and after adsorbing P (CWH-650–P). In addition, the CWH-650–P sample was subjected to a new calcination treatment in order to increase the crystallinity of the phases formed after the P adsorption process (CWH-650–P-650).

CWH-650 features bands at 712 and 875 cm^{-1} for the CO_3^{2-} group. These signals are confirmed by the band centered at 1430 cm^{-1} corresponding to the symmetric and asymmetric

stretching modes of the CO_3^{2-} group [42], and suggesting the presence of $CaCO_3$ [43,44]. The 1030 cm^{-1} band represents the P–O bond from the PO_4^{3-} group, and the signs at 567 and 602 cm^{-1} correspond to the asymmetric and symmetric deformation modes of the PO_4^{3-} (v_4 O–P–O) group, which were initially found in CWH-650 (our previous work, [18]). The position of these bands has been reported as characteristic of calcium phosphates, especially apatite [45]. The stretching and the narrow vibration band observed at 3640 cm^{-1} also indicates the presence of −OH, which corresponds to $Ca(OH)_2$ [46].

After the P adsorption process (CWH-650–P), the bands at 567 and 602 cm^{-1} increase their intensity, suggesting the presence of new phosphate groups on the surface of the material. The $Ca(OH)_2$ band at 3640 cm^{-1} disappears while the bands at 646 and 680 cm^{-1}, corresponding to Al_2O_3 and MgO, respectively, decrease significantly, signaling the intervention of these minerals in the P adsorption process. On the other hand, the bands at 779 and 796 cm^{-1}, assigned to the asymmetric Si–O–Si stretching vibration [43,45] do not show relevant changes, which indicates that SiO_2 does not play a significant role in the adsorption of P.

After calcining the P-adsorbed material, CWH-650–P-650, we observe an increase in the characteristic apatite bands at 567, 602, and 1030 cm^{-1} and a decrease in the $CaCO_3$ bands at 712, 875, and 1430 cm^{-1}. The band at 3640 cm^{-1} corresponding to $Ca(OH)_2$ reappears, indicating that the CWH-650–P calcination process increases the crystallinity of phases, such as apatite, while forming $Ca(OH)_2$ from the decomposition of $CaCO_3$, which still remains in the sample because it did not undergo changes during the P adsorption process. On the other hand, the SiO_2, Al_2O_3, and MgO bands present in CWH-650–P did not experience changes after the second calcination process (CWH-650–P-650).
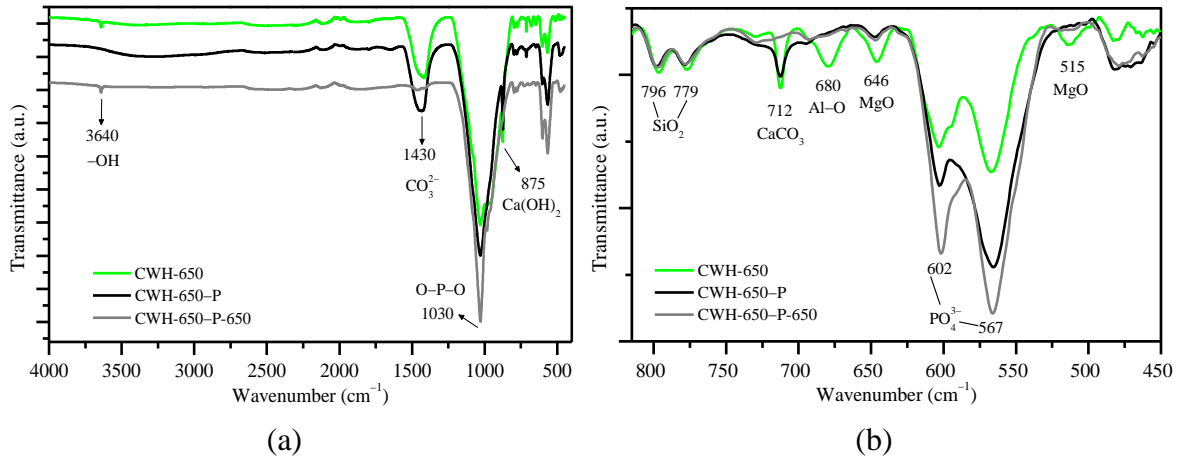
Fig. 4-5. FTIR spectra of the different materials obtained from the water hyacinths.

Next, we obtained XRD patterns in order to supplement the results generated by the FTIR. Fig. 4-6 reveals that CWH-650 presents peaks at $2\theta = 17.9°$ and $34.0°$ for the (001) and (010) planes of $Ca(OH)_2$ (ICSD #: 202225). Furthermore, the presence of $Ca_5(PO_4)_3(OH)$, (ICSD #: 180315) was confirmed by the peaks at $2\theta = 31.4°$, $32.1°$, and $32.4°$ for the (211), (112), and (030) planes, respectively. The peak observed at $2\theta = 26.6°$ corresponds to the (011) plane of SiO_2 (ICSD #: 42498), while the peaks at $2\theta = 42.9°$ and $2\theta = 25.4°$ correspond to the (002) plane of MgO and (012) plane of Al_2O_3, respectively. The presence of aluminum silicate is also observed for the peak at $2\theta = 27.9°$ of the (200) plane of albite ($NaAlSi_3O_8$, $KAlSi_3O_8$). Here, it is evident that after adsorbing P, the CWH-650–P peaks corresponding to the MgO and Al_2O_3 phases decrease in intensity, indicating that they are involved in the P adsorption process. Likewise, the $Ca(OH)_2$ peak decreases while the $Ca_5(PO_4)_3(OH)$ peak increases, thus suggesting that the phosphorus remaining in the solution reacts with $Ca(OH)_2$ present in the material to form more apatite (30.3%). These results are consistent with the FTIR.

61
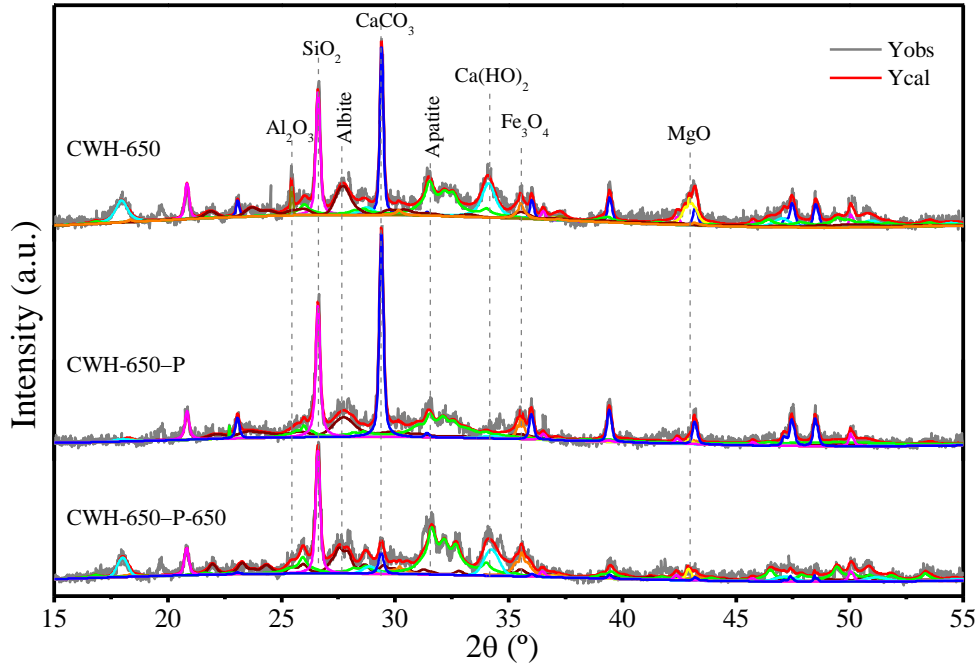
Fig. 4-6. X-ray diffraction patterns for the different materials obtained from water hyacinths.

CWH-650–P-650 denotes a higher level of crystallinity for apatite, with more intense and sharp peaks as shown by phase quantification (Fig. 4-7). After the calcination process, apatite reaches a content of 41.0%, as opposed to the 25% found in CWH-650, while Al_2O_3 and MgO decrease due to their intervention in the P removal process. It has been reported that phosphates are adsorbed on Al or Mg, thus forming Al–O–P and Mg–O–P species [14,35,47], which were detected by XRD possibly due to their smaller amounts. Based on these results, $Ca(OH)_2$ provided the greatest contributions to P adsorption in CWH-650.
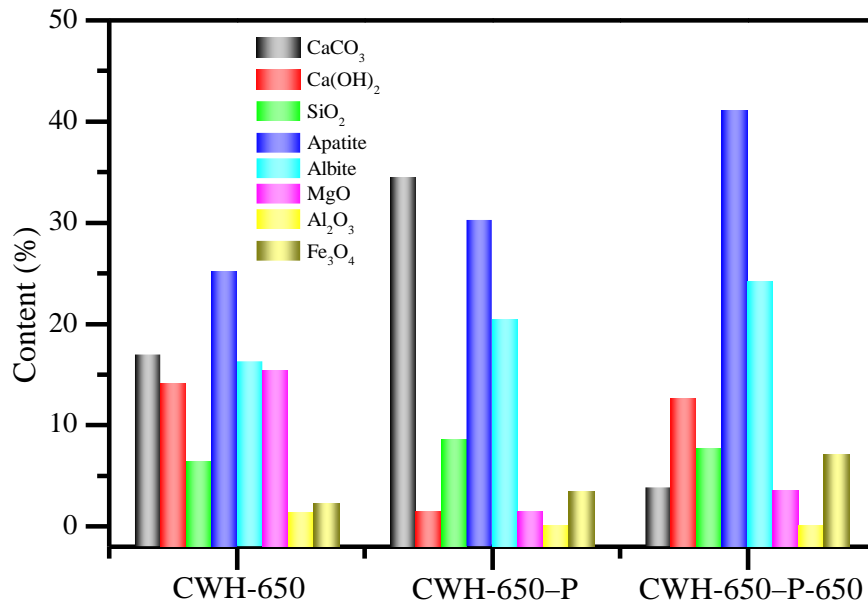
Fig. 4-7. Phase quantification (wt.%) after Rietveld refinement of the XRD patterns for the different materials obtained from water hyacinths.

Therefore, the dominant mechanism in the adsorption of phosphate anions on materials rich in metal oxides/hydroxides, such as CWH-650, is proposed to be the exchange of ligands [6,9]. This may explain why the –OH groups in $Ca(OH)_2$ observed by FTIR and XRD disappear after the P removal process, which then generates apatite precipitation. This process can be represented by the following main reaction:

$$5\ Ca(OH)_{2(s)} + 3\ KH_2PO_{4(aq)} \rightarrow Ca_5(PO_4)_3(OH)_{(s)} + 6\ H_2O_{(l)} + 3\ KOH_{(aq)}$$
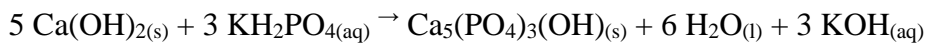
This chemical reaction is general and can involve sub-reactions, which depend on the Ca/P ratio and the pH level, as presented in Fig. 4-4. The reagents can generate precursors such as amorphous calcium phosphate ($Ca_3(HPO_4)_2$, dicalcium phosphate ($CaHPO_4$), tricalcium phosphate ($Ca_3(PO_4)_2$), and octacalcium phosphate ($Ca_8H_2(PO_4)_6$) [48–50].

These results suggest that post P adsorption calcination process fosters the formation of P compounds with higher crystallinity rates, such as the apatite. In this regard, the apatite is more stable and less soluble in water [18,23], which produces a material with higher phosphate content that could act as a slow-releasing phosphate fertilizer.

4.3.3. P-solubility: effect of heat treatment on the adsorbed material

Fig. 4-8 denotes the solubility of P in a 2% formic acid and deionized water solution for the different materials after the P adsorption process (CWH-600–P, CWH-650–P, and CWH-700–P), and after calcining the P-adsorbed material (CWH-600–P-600, CWH-650–P-650, and CWH-700–P-700). The results reveal that the content of water-soluble P decreases for all CWH-XPX materials, which means that after calcining the materials with P adsorbed from aqueous solutions, more stable P phases are formed than those generated after adsorption. These results are consistent with other studies reporting that calcination at high temperatures favors the formation of P phases, such as the apatite, which, due to their high crystallinity level, are more stable and less soluble in water [18,23]. On the other hand, the solubility of P in 2% formic acid is much higher than its solubility in deionized water, and it increases significantly after calcining the material with the adsorbed P. For this reason, these materials are suitable amendments for acid soils. These results are favorable since, to be suitable for soils, the phosphate fertilizer must have low solubility in water to avoid loss of phosphorus by runoff, but, at the same time, it must be able to guarantee a slow release of nutrients to the soil.
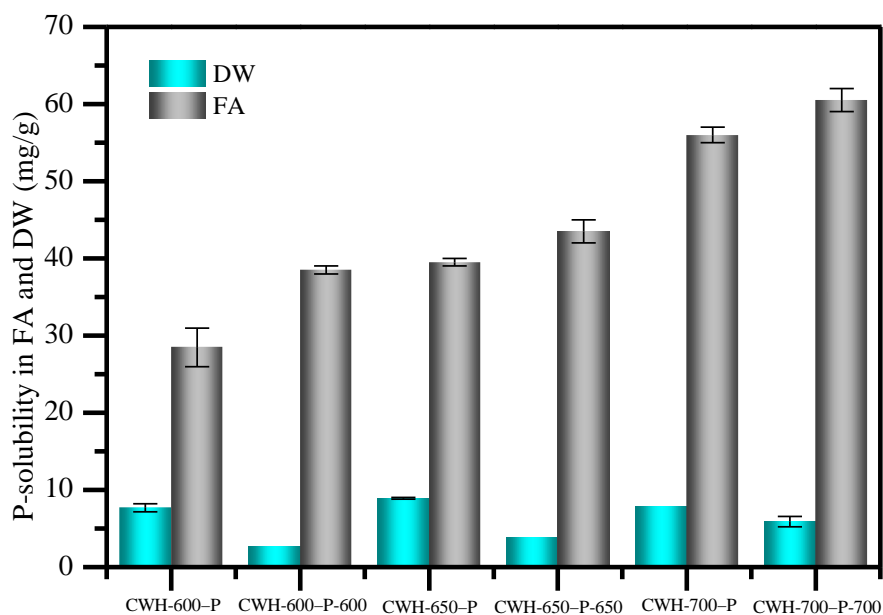

Fig. 4-8. Phosphorus solubility in 2% formic acid (FA) and deionized water (DW).

4.4. Conclusions

WH calcinated at 650 °C evidenced high P removal percentages mainly due to its $Ca(OH)_2$ content and other compounds, such as Al_2O_3 and MgO, acting as active phases in the P adsorption process.

The experimental data validated good adjustments to the pseudo first-order and pseudo second-order kinetic models, suggesting the existence of different adsorbate–adsorbent interaction energies in the adsorption process. However, this study determined that the chemisorption between the P anions and active phases in CWH-650 was the limiting step in the adsorption process. On the other hand, isotherm models, such as Langmuir, Freundlich, Temkin, and Langmuir–Freundlich, proved to be a good adjustment for the experimental data, providing a maximum adsorption capacity of 21.21 mg P/g for the CWH-650 material, and indicating that there is no single form of interaction between CWH-650 and the anions of P. Therefore, a mixture of adsorption mechanisms is presented, wherein ligand exchanges followed by precipitation was the dominant mechanism during the adsorption process.

The pH value of the solution also plays an important role in the P adsorption process due to the variation of P species that interact with the active phases found on the surface of the adsorbent material. Nevertheless, changing the initial pH value of the solution did not exert any significant effect on the P adsorption process; however, an increase in the final pH value of the solution revealed a ligand exchange between the anionic species of P and $Ca(OH)_2$, generating the release of OH^- ions and leading to the precipitation of apatite $[AC_5(PO_4)_3(OH)]$, as validated by FTIR and XRD.

Based on the FTIR and XRD analyses, we were able to determine that subjecting the P-adsorbed material (CWH-650–P) to the calcination process produces a material with a higher apatite content, which increases from 30.3% to 41.0%. This P- and Ca-enriched phase exhibits low solubility in water and is characterized by being biocompatible with the soil as it improves plant growth. Therefore, the bioavailability tests evidenced that the material obtained may be potentially used as a phosphate fertilizer as it presented low solubility in water, which guarantees a slow release of nutrients to the soil, preventing the loss of phosphates due to rainwater runoffs, and, in turn, satisfying the need for the recovery and reuse of phosphorus.

4.5. References

[1]   D. Cordell, J.O. Drangert, S. White, The story of phosphorus: Global food security and food for thought, Glob. Environ. Chang. 19 (2009) 292–305. https://doi.org/10.1016/j.gloenvcha.2008.10.009.

[2]   N. Tran, P. Drogui, J.F. Blais, G. Mercier, Phosphorus removal from spiked municipal wastewater using either electrochemical coagulation or chemical coagulation as tertiary treatment, Sep. Purif. Technol. 95 (2012) 16–25. https://doi.org/10.1016/j.seppur.2012.04.014.

[3]   R. Li, J.J. Wang, B. Zhou, M.K. Awasthi, A. Ali, Z. Zhang, A.H. Lahori, A. Mahar, Recovery of phosphate from aqueous solution by magnesium oxide decorated magnetic biochar and its potential as phosphate-based fertilizer substitute, Bioresour. Technol. 215 (2016) 209–214. https://doi.org/10.1016/j.biortech.2016.02.125.

[4]   R. Cai, X. Wang, X. Ji, B. Peng, C. Tan, X. Huang, Phosphate reclaim from simulated and real eutrophic water by magnetic biochar derived from water hyacinth, J. Environ. Manage. 187 (2017) 212–219. https://doi.org/10.1016/j.jenvman.2016.11.047.

[5]   N.A.A. Salim, M.A. Fulazzaky, M.H. Puteh, M.H. Khamidun, A.R.M. Yusoff, N.H. Abdullah, N. Ahmad, Z.M. Lazim, M. Nuid, Adsorption of phosphate from aqueous solution onto iron-coated waste mussel shell: Physicochemical characteristics, kinetic, and isotherm studies, Biointerface Res. Appl. Chem. 11 (2021) 12831–12842. https://doi.org/10.33263/BRIAC115.1283112842.

[6]   R. Liu, L. Chi, X. Wang, Y. Sui, Y. Wang, H. Arandiyan, Review of metal (hydr)oxide and other adsorptive materials for phosphate removal from water, J. Environ. Chem. Eng. 6 (2018) 5269–5286. https://doi.org/10.1016/j.jece.2018.08.008.

[7]   N.Y. Acelas, B.D. Martin, D. López, B. Jefferson, Selective removal of phosphate from wastewater using hydrated metal oxides dispersed within anionic exchange media, Chemosphere. 119 (2015) 1353–1360. https://doi.org/10.1016/j.chemosphere.2014.02.024.

[8]   N.Y. Acelas, S.M. Mejia, F. Mondragón, E. Flórez, Density functional theory characterization of phosphate and sulfate adsorption on Fe-(hydr)oxide: Reactivity, pH effect, estimation of Gibbs free energies, and topological analysis of hydrogen bonds, Comput. Theor. Chem. 1005 (2013) 16–24.

https://doi.org/10.1016/j.comptc.2012.11.002.

[9] B. Wu, J. Wan, Y. Zhang, B. Pan, I.M.C. Lo, Selective phosphate removal from water and wastewater using sorption: process fundamentals and removal mechanisms, Environ. Sci. Technol. 54 (2020) 50–66. https://doi.org/10.1021/acs.est.9b05569.

[10] Lena Johansson Westholm, Substrates for phosphorus removal — Potential benefits for on-site wastewater treatment?, Water Res. 40 (2006) 23–36. https://doi.org/10.1016/j.watres.2005.11.006.

[11] K.W. Jung, M.J. Hwang, K.H. Ahn, Y.S. Ok, Kinetic study on phosphate removal from aqueous solution by biochar derived from peanut shell as renewable adsorptive media, Int. J. Environ. Sci. Technol. 12 (2015) 3363–3372. https://doi.org/10.1007/s13762-015-0766-5.

[12] S. Pérez, J. Muñoz-Sadaña, N. Acelas, E. Flórez, Phosphate removal from aqueous solutions by heat treatment of eggshell and palm fiber, J. Environ. Chem. Eng. (2020) 104684. https://doi.org/10.1016/j.jece.2020.104684.

[13] Z. Zeng, S. Da Zhang, T.Q. Li, F.L. Zhao, Z.L. He, H.P. Zhao, X.E. Yang, H.L. Wang, J. Zhao, M.T. Rafiq, Sorption of ammonium and phosphate from aqueous solution by biochar derived from phytoremediation plants, J. Zhejiang Univ. Sci. B. 14 (2013) 1152–1161. https://doi.org/10.1631/jzus.B1300102.

[14] X. Zheng, Y. Ye, Z. Jiang, Z. Ying, S. Ji, W. Chen, B. Wang, B. Dou, Enhanced transformation of phosphorus (P) in sewage sludge to hydroxyapatite via hydrothermal carbonization and calcium-based additive, Sci. Total Environ. 738 (2020) 139786. https://doi.org/10.1016/j.scitotenv.2020.139786.

[15] A. Mosa, A. El-ghamry, M. Tolba, Functionalized biochar derived from heavy metal rich feedstock: Phosphate recovery and reusing the exhausted biochar as an enriched soil amendment, Chemosphere. 198 (2018) 351–363. https://doi.org/10.1016/j.chemosphere.2018.01.113.

[16] S.C.H. Barrett, Waterweed invasions, Sci. Am. 261 (1989) 90–97.

[17] R.P. Keller, D.M. Lodge, N. Dame, N. Dame, Invasive Species, in: Pollut. Remediat., Encyclopedia of Inland Waters, Notre Dame, 2009: pp. 92–99. https://doi.org/10.1016/B978-012370626-3.00226-X.

[18] A. Ramirez, S. Pérez, N. Acelas, E. Flórez, Utilization of water hyacinth (Eichhornia

crassipes) rejects as phosphate-rich fertilizer, J. Environ. Chem. Eng. 9 (2021) 104776. https://doi.org/10.1016/j.jece.2020.104776.

[19] L. Bottezini, D.P. Dick, A. Wisniewski, H. Knicker, I.S.C. Carregosa, Phosphorus species and chemical composition of water hyacinth biochars produced at different pyrolysis temperature, Bioresour. Technol. Reports. 14 (2021) 100684. https://doi.org/10.1016/j.biteb.2021.100684.

[20] I.W. Almanassra, G. Mckay, V. Kochkodan, M. Ali Atieh, T. Al-Ansari, A state of the art review on phosphate removal from water by biochars, Chem. Eng. J. 409 (2021) 128211. https://doi.org/10.1016/j.cej.2020.128211.

[21] X. Liu, F. Shen, X. Qi, Adsorption recovery of phosphate from aqueous solution by CaO-biochar composites prepared from eggshell and rice straw, Sci. Total Environ. 666 (2019) 694–702. https://doi.org/10.1016/j.scitotenv.2019.02.227.

[22] A. Fihri, C. Len, R.S. Varma, A. Solhy, Hydroxyapatite: A review of syntheses, structure and applications in heterogeneous catalysis, Coord. Chem. Rev. 347 (2017) 48–76. https://doi.org/10.1016/j.ccr.2017.06.009.

[23] Q. Liu, Z. Fang, Y. Liu, Y. Liu, Y. Xu, X. Ruan, X. Zhang, W. Cao, Phosphorus speciation and bioavailability of sewage sludge derived biochar amended with CaO, Waste Manag. 87 (2019) 71–77. https://doi.org/10.1016/j.wasman.2019.01.045.

[24] N.C. Shiba, F. Ntuli, Extraction and precipitation of phosphorus from sewage sludge, Waste Manag. 60 (2017) 191–200. https://doi.org/10.1016/j.wasman.2016.07.031.

[25] B. Chen, X. Zhang, W. Chen, D. Wang, N. Song, G. Qian, X. Duan, J. Yang, D. Chen, W. Yuan, X. Zhou, Tailoring of Fe/MnK-CNTs composite catalysts for the fischer-tropsch synthesis of lower olefins from syngas, Ind. Eng. Chem. Res. 57 (2018) 11554–11560. https://doi.org/10.1021/acs.iecr.8b01795.

[26] G. Limousin, J.P. Gaudet, L. Charlet, S. Szenknect, V. Barthès, M. Krimissa, Sorption isotherms: A review on physical bases, modeling and measurement, Appl. Geochemistry. 22 (2007) 249–275. https://doi.org/10.1016/j.apgeochem.2006.09.010.

[27] H. Nguyen, S. You, A. Hosseini-bandegharaei, Mistakes and inconsistencies regarding adsorption of contaminants from aqueous solutions : A critical review, Water Res. 120 (2017) 88–116. https://doi.org/10.1016/j.watres.2017.04.014.

[28] A. Ramirez, R. Ocampo, S. Giraldo, E. Padilla, E. Flórez, N. Acelas, Removal of

Cr(VI) from an aqueous solution using an activated carbon obtained from teakwood sawdust: Kinetics, equilibrium, and density functional theory calculations, J. Environ. Chem. Eng. 8 (2020) 103702. https://doi.org/10.1016/j.jece.2020.103702.

[29]   X. Zhang, W. Fu, Y. Yin, Z. Chen, R. Qiu, M.-O. Simonnot, X. Wang, Adsorption-reduction removal of Cr(VI) by tobacco petiole pyrolytic biochar: Batch experiment, kinetic and mechanism studies, Bioresour. Technol. 268 (2018) 149–157. https://doi.org/10.1016/j.biortech.2018.07.125.

[30]   J.A. Marshall, B.J. Morton, R. Muhlack, D. Chittleborough, C.W. Kwong, Recovery of phosphate from calcium-containing aqueous solution resulting from biochar-induced calcium phosphate precipitation, J. Clean. Prod. 165 (2017) 27–35. https://doi.org/10.1016/j.jclepro.2017.07.042.

[31]   E. Turiel, C. Perez-Conde, A. Martin-Esteban, Assessment of the cross-reactivity and binding sites characterisation of a propazine-imprinted polymer using the Langmuir-Freundlich isotherm, Analyst. 128 (2003) 137–141. https://doi.org/10.1039/b210712k.

[32]   R.J. Umpleby, S.C. Baxter, Y. Chen, R.N. Shah, K.D. Shimizu, Characterization of molecularly imprinted polymers with the Langmuir - Freundlich isotherm, Anal. Chem. 73 (2001) 4584–4591. https://doi.org/10.1021/ac0105686.

[33]   D. Mitrogiannis, M. Psychoyou, I. Baziotis, V.J. Inglezakis, N. Koukouzas, N. Tsoukalas, D. Palles, E. Kamitsos, G. Oikonomou, G. Markou, Removal of phosphate from aqueous solutions by adsorption onto Ca(OH) 2 treated natural clinoptilolite, Chem. Eng. J. 320 (2017) 510–522. https://doi.org/10.1016/j.cej.2017.03.063.

[34]   G. Markou, D. Mitrogiannis, V. Inglezakis, K. Muylaert, N. Koukouzas, N. Tsoukalas, E. Kamitsos, D. Palles, I. Baziotis, Ca(OH)2 pre-treated bentonite for phosphorus removal and recovery from synthetic and real wastewater, Clean - Soil, Air, Water. 46 (2018) 1700378. https://doi.org/10.1002/clen.201700378.

[35]   Q. Zheng, L. Yang, D. Song, S. Zhang, H. Wu, S. Li, X. Wang, High adsorption capacity of Mg–Al-modified biochar for phosphate and its potential for phosphate interception in soil, Chemosphere. 259 (2020) 127469. https://doi.org/https://doi.org/10.1016/j.chemosphere.2020.127469.

[36]   I.W. Almanassra, V. Kochkodan, M. Subeh, G. Mckay, M. Atieh, T. Al-Ansari,

Phosphate removal from synthetic and treated sewage effluent by carbide derive carbon, J. Water Process Eng. 36 (2020) 101323. https://doi.org/10.1016/j.jwpe.2020.101323.

[37] P. Loganathan, S. Vigneswaran, J. Kandasamy, N.S. Bolan, Removal and recovery of phosphate from water using sorption, Crit. Rev. Environ. Sci. Technol. 44 (2014) 847–907. https://doi.org/10.1080/10643389.2012.741311.

[38] P.L. Hariani, S. Salni, F. Riyanti, Combination of CaCO3 and Ca(OH)2 as agents for treatment acid mine drainage, MATEC Web Conf. 101 (2017) 2–6. https://doi.org/10.1051/matecconf/201710102004.

[39] H. Bacelo, A.M.A. Pintor, S.C.R. Santos, R.A.R. Boaventura, C.M.S. Botelho, Performance and prospects of different adsorbents for phosphorus uptake and recovery from water, Chem. Eng. J. 381 (2020) 122566. https://doi.org/10.1016/j.cej.2019.122566.

[40] R. Štulajterová, Ľ. Medvecký, Effect of calcium ions on transformation brushite to hydroxyapatite in aqueous solutions, Colloids Surfaces A Physicochem. Eng. Asp. 316 (2008) 104–109. https://doi.org/10.1016/j.colsurfa.2007.08.036.

[41] S. Gu, B. Fu, J.W. Ahn, B. Fang, Mechanism for phosphorus removal from wastewater with fly ash of municipal solid waste incineration, Seoul, Korea, J. Clean. Prod. 280 (2021) 124430. https://doi.org/10.1016/j.jclepro.2020.124430.

[42] L. Berzina-Cimdina, N. Borodajenko, Research of calcium phosphates using fourier transform infrared spectroscopy, Infrared Spectrosc. - Mater. Sci. Eng. Technol. (2012) 123–148. https://doi.org/10.5772/36942.

[43] F.B. Reig, J.V.G. Adelantado, M.C.M.M. Moreno, FTIR quantitative analysis of calcium carbonate (calcite) and silica (quartz) mixtures using the constant ratio method. Application to geological samples, Talanta. 58 (2002) 811–821. https://doi.org/10.1016/S0039-9140(02)00372-7.

[44] F. Wilson, P. Tremain, B. Moghtaderi, Characterization of Biochars Derived from Pyrolysis of Biomass and Calcium Oxide Mixtures, Energy and Fuels. 32 (2018) 4167–4177. https://doi.org/10.1021/acs.energyfuels.7b03221.

[45] A.M. Grumezescu, C.D. Ghitulica, G. Voicu, K.S. Huang, C.H. Yang, A. Ficai, B.S. Vasile, V. Grumezescu, C. Bleotu, M.C. Chifiriuc, New silica nanostructure for the

improved delivery of topical antibiotics used in the treatment of staphylococcal cutaneous infections, Int. J. Pharm. 463 (2014) 170–176. https://doi.org/10.1016/j.ijpharm.2013.07.016.

[46] O.B. Ayodele, K.C. Lethesh, Z. Gholami, Y. Uemura, Effect of ethanedioic acid functionalization on Ni/Al2O3 catalytic hydrodeoxygenation and isomerization of octadec-9-enoic acid into biofuel: Kinetics and Arrhenius parameters, J. Energy Chem. 25 (2016) 158–168. https://doi.org/10.1016/j.jechem.2015.08.017.

[47] D. Jiang, B. Chu, Y. Amano, M. Machida, Removal and recovery of phosphate from water by Mg-laden biochar: Batch and column studies, Colloids Surfaces A. 558 (2018) 429–437. https://doi.org/10.1016/j.colsurfa.2018.09.016.

[48] D. Chen, P. Szostak, Z. Wei, R. Xiao, Reduction of orthophosphates loss in agricultural soil by nano calcium sulfate, Sci. Total Environ. 539 (2016) 381–387. https://doi.org/10.1016/j.scitotenv.2015.09.028.

[49] I. Blanco, P. Molle, L.E. Sáenz de Miera, G. Ansola, Basic Oxygen Furnace steel slag aggregates for phosphorus treatment: Evaluation of its potential use as a substrate in constructed wetlands, Water Res. 89 (2016) 355–365. https://doi.org/10.1016/j.watres.2015.11.064.

[50] H. Yin, X. Yan, X. Gu, Evaluation of thermally-modified calcium-rich attapulgite as a low-cost substrate for rapid phosphorus removal in constructed wetlands, Water Res. 115 (2017) 329–338. https://doi.org/10.1016/j.watres.2017.03.014.

5. The role of inorganic compounds obtained from the calcination treatments of water hyacinth (*Eichhornia Crassipes*) on the Cd^{2+} and Cu^{2+} heavy metals uptake (removal and immobilization) from contaminated water

Abstract

Industrialization activities in Colombia have led to the discharge of heavy metals into water, with an imminent threat to the environment. The use of natural materials as low-cost sorbents for the removal of heavy metals from aqueous solutions has recently received major attention. It is well known that water hyacinth (*Eichhornia crassipes*) is a noxious weed due to its congested growth and rapid spread causing serious environmental problems e.g., in the water quality and its respective fauna. Recently, efforts have been made to utilize in different applications the inorganic materials that are obtained from the weed after heat treatments in a range of temperatures. In this work, the effect of Ca-P-rich minerals formed after a calcination treatment between 350 – 900 ºC of water hyacinth on the removal and immobilization levels of Cd^{2+} and Cu^{2+} from aqueous solutions is reported. It was found that removal efficiency increases with the calcination temperature from 550 ºC (24.9% Cd and 12.7% Cu) to a maximum level at 700 ºC (51.5% Cd^{2+} and 31.8% Cu^{2+}). The reason is that 700 ºC treatments favor the formation of calcium apatite, which is known as an active Ca-P phase for the removal of metallic ions. Compounds produced during the calcination of the water hyacinth promote the Cd^{2+} and Cu^{2+} uptake through the precipitation of $CdCO_3$ - $Cd_2P_2O_7$ and $Cu_{0.05}Mg_{0.95}O$ - $Cu_2P_2O_7$ compounds, among others. These precipitates have

low solubility (0.055% of Cd and 0.003% of Cu) that reduce contaminants mobility and therefore increase removal feasibility.

5.1. Introduction

Contamination associated with industrial wastewater discharges in aqueous systems is nowadays a global concern [1]. Industries mainly dedicated to electroplating, mining, metallurgy, and tanning activities generate wastewater with high content of toxic heavy metals such as cadmium (Cd^{2+}) and copper (Cu^{2+}) [1–3], that can lead to health problems in animals, plants, and humans [4,5]. Among the conventional methods used for the treatment of contaminated wastewater, the adsorption of heavy metals into materials produced during the transformation of biomass has been considered as a viable and efficient method for its removal from aqueous systems [3,6–9]. In particular, it has been found that materials produced during the thermal transformations of water hyacinth (WH) are promising adsorbents to remove heavy metals from contaminated water, [4,10] and using WH in water remediation should represent an efficient option to manage problems related to this invasive species [9]. According to literature reports, the calcination of water hyacinth at different temperatures leads to the formation of inorganic active phases that depending on their stoichiometry show the ability for the adsorption and immobilization of heavy metals [11,12]. After calcination at 350 or 900 °C, the ash content rate from WH varies from 27.7% to 14.5%, respectively. The main phases found in the ashes are $CaCO_3$, $Ca(OH)_2$, $Ca_5(PO_4)_3(OH)$, Fe_3O_4, Al_2O_3, and MgO at low calcination temperatures (350 °C – 550 °C), while at high temperatures (650 ºC – 900 ºC), $Ca(OH)_2$ and Ca-phosphates (Ca-P) such as apatites are formed with the presence of P in WH [13]. It has been demonstrated that these phases are active for the removal/immobilization of heavy metals [1,4,7,10,14–17]. For instance, Flores-Cano et al. [16] used eggshell rich in calcite phase for the adsorption of Cd^{2+}. They found that the sorption was not a reversible process, with low adsorption ability with the value of adsorption capacity of 3.75 mg/g at pH = 6 and, that the main sorption mechanisms were precipitation and ion exchange. On the other hand, Baláž et al. [18] found an increase in the cadmium uptake ability of the eggshell upon milling with an adsorption capacity of 329 mg/g due to the formation of aragonite phase during milling. Additionally, Hu et al. [15] used calcite ($CaCO_3$) to adsorb Cu^{2+} leading to a 99.76% remotion efficiency by copper

precipitation as a basic sulfate like the posnjakite, reducing the residual concentration in the solution to less than 0.5 mg/L.

Different studies have demonstrated that calcium phosphates have a high removal capacity for divalent heavy metal ions in water [19–27]. Liu et al. [28] evaluated Cd^{2+} adsorption onto hydroxyapatite - attapulgite composites for the adsorption of different metals showed that ion exchange also contributed to the Cd^{2+} removal with an adsorption capacity of 131.5 mg/g. Further on, Thanh et al. [29] employed a nanocomposite of magnetic hydroxyapatite as an adsorbent for the removal of Cu^{2+} and Ni^{2+} from aqueous solution obtaining adsorption capacities of 48.78 mg/g and 29.07 mg/g, for Cu^{2+} and Ni^{2+}, respectively.

Even when the adsorption of heavy metals is successfully achieved, the process creates a disposal problem due to the presence of heavy metals in the adsorbent, which potentially leaching out to the environment. Several studies have demonstrated that the adsorption of heavy metals by using calcium phosphates, such as apatite phases generates stable metal-phosphate complexes and reduces their mobility [5,30–32]. For instance, in a related study, Liu et al. [33] demonstrated that during the removal of Cu^{2+} from groundwater by using hydroxyapatite/calcium silicate hydrate 76.3% of the Cu^{2+} adsorbed was immobilized by the material. Li et al. [34] found that phosphate rock combinate with ferric nitrate and ashes produce from biomass immobilize Cd^{2+} with a reduction of Cd^{2+} in the soil of 34.0% and 15.7% by using different extraction tests. The mechanisms for the immobilization of heavy metals that have been proposed are i) adsorption of metallic ion on the calcium phosphate surface followed by cation exchange with calcium, and ii) the dissolution/precipitation of a solid with lower solubility that reduces contaminant mobility and, therefore increased stability [22–27]. Thus, materials based on Ca–P phases are clearly able to immobilize heavy metals. Furthermore, it was reported elsewhere that apatite and other Ca–P phases were obtained after heat treatments of WH materials [13]. Therefore, this paper aims to determine the role of inorganic compounds, which are rich in calcium and phosphate present in WH on the removal and immobilization of Cd^{2+} and Cu^{2+} from aqueous solutions. The adsorbent materials were obtained from the calcination of WH at different temperatures and tested to eliminate Cd^{2+} and Cu^{2+} from aqueous solutions. The Cd^{2+} and

Cu^{2+} immobilization percentage was determined using the Synthetic Precipitation Leaching Procedure (SPLP) from the EPA [35]. Additionally, interactions in the adsorption process were characterized by FTIR, XRD, and XPS.

5.2. Materials and methods

5.2.1. Preparation and characterization of materials

Water hyacinth weed was collected at the Ituango Hydroelectric Plant (Hidroituango) located on the Cauca River between the municipalities of Ituango and Briceño, Antioquia, Colombia. The adsorbent materials derived from water hyacinth used in this study were prepared by calcination at temperatures of 350, 450, 550, 650, 700, 800, and 900 °C according to the methodology described in previous work [13]. The evaluated materials were named CWH-X, where X stands for the calcination temperature.

Materials were characterized by Fourier-transformed infrared spectroscopy, FTIR (Spectrum two-PerkinElmer with UATR for a range within 4000 - 450 cm^{-1}) to determine the functional groups present on the surface of materials. The crystalline phases present in each material were identified by X-ray diffraction (XRD) patterns using a Shimadzu XRD-6100 diffractometer with Cu Kα radiation (λ = 1.5406 Å), at 40 kV in the 2θ angle range of 10° to 80° with a step size of 0.026° and period of 50 s. The chemical environment of the surface of the materials was determined from X-ray photoelectron spectroscopy analysis (XPS) using an XR50 M monochromatic Al Kα1 (hv = 1486.7 eV) X-ray source and a Phoibos 150 spectrometer that has a one-dimensional detector 1D-DLD (SPECS, Berlin, Germany).

5.2.2. Adsorption of Cd^{2+} and Cu^{2+}

Cd^{2+} y Cu^{2+} adsorption experiments were carried out by contacting 0.05 g of each material obtained with 100 mL of synthetic solutions of 200 mg/L of Cd^{2+} and Cu^{2+} prepared from $CdCl_2.2.5H_4O$ (Alfa Aesar, 79.5 – 81.0%) and $Cu(NO_3)_2.3H_2O$ (PanReac, 98 – 100%), with pH values of 6.14 and 5.33, respectively. The mixture was kept under stirring for 24 h at 200 rpm at 25 °C. The concentrations of Cd and Cu were determined by the method of colorimetry (Hach, TNT 852, and TNT 860, respectively) using a DR 3900 spectrophotometer (Hach). All experiments were done in duplicate.

75

5.2.3. Leaching of Cd^{2+} and Cu^{2+}

Batch tests according to a standard SPLP Method 1312 [35] were performed to determine the percentage of immobilization of Cd^{2+} and Cu^{2+} in CWH-based materials after adsorption. CWH-550–Cu, CWH-550–Cd, CWH-700–Cu, or CWH-700–Cd in 0.5 g amounts were mixed in a glass Erlenmeyer flask with 10 mL of an H_2SO_4/HNO_3 solution (relation H_2SO_4/HNO_3 of 60/40 (by weight) diluted with deionized water to pH 4.2). The samples were mixed by shaking at 30 rpm for 18 h at a temperature of 25 °C, then passed through a 0.45 µm filter, acidified with concentrated HNO_3, and the concentrations of Cd and Cu were determined by the colorimetry method (Hach, TNT 852 and TNT 860, respectively) using a DR 3900 spectrophotometer (Hach). All experiments were done in duplicate.

5.3. Results and discussion

5.3.1. Calcination products

Fig. 5-1a shows the characterization by XRD for the WH samples calcine at different temperatures (350 °C to 900 °C). For calcined WH from 350 °C to 650 °C the higher peaks at $2\theta = 26.6º$, and $2\theta = 29.4º$ correspond to the (104) plane of $CaCO_3$ (ICSD·#: 166364) and the (011) plane of SiO_2 (ICSD·#: 42498), with an increase of temperature the peaks corresponding to $CaCO_3$ decrease and the formation of others phases is observed by the presence of new peaks, for example at $2\theta = 17.9º$ and $34.0º$ for the (001) and (010) planes, respectively, of $Ca(OH)_2$ (ICSD·#: 202225); additionally, the presence of calcium apatite (ICSD #: 180315) was confirmed with the peaks at $2\theta = 31.4º$, $32.1º$, and $32.4º$ for the (211), (112), and (030) planes, respectively. Other Ca phase at temperatures higher than 700 °C is CaO (ICSD·#: 60199) which has characteristic peaks at $2\theta = 32.2º$, $37.3º$, and $53.8º$ for the (111), (002) and (022) planes. For CWH-900, the peaks corresponding to $Ca_5(PO_4)_3(OH)$ decrease and peaks at $2\theta = 25.9$ º and $31.3º$ corresponding to (200) and (032) planes for $Ca_8(HPO_4)_2(PO_4)_4(H_2O)_5$ appear. At high temperatures (800 - 900 °C) a peak at $2\theta = 42.9º$ for the (002) plane for MgO (ICSD·#:61325) increases the intensity. Other peaks with lower intensity can be attributed to Fe_3O_4, K_2O, albite ($NaAlSi_3O_8$, $KAlSi_3O_8$), and leucite phases. These results show that the composition change with the temperature obtaining materials with heterogeneous composition.

Fig. 5-1b shows results of phase content according to Rietveld refinement after calcination treatments at different temperatures of the WH samples. The quantification by XRD showed relatively high contents for MgO (11 - 15%), SiO_2 (6.4 - 11.7%), and albite. With increasing temperature, crystalline phases in a lesser extent Fe_3O_4 (3.47%), Al_2O_3 (3.01%), and K_2O (0.73%) are formed, which are commonly found in soils.

Mg phases have been reported to be active in the removal of Cd^{2+} and Cu^{2+} [36,37], through a combined adsorption mechanism together with the Ca phases present as $CaCO_3$, $Ca(OH)_2$, CaO, and $Ca_5(PO_4)_3(OH)$. Transformation of calcium phases with temperature has been previously studied elsewhere [13]. $CaCO_3$ content increases from 350 ℃ to 550 ℃ from 44.27 % to 51.17 %. $CaCO_3$ is also well known to be an active phase in the adsorption of Cd^{2+} and Cu^{2+} through a precipitation mechanism [4,15,38,39]. For CWH-700, the amount of apatite increased to 34.04%, while CaO, $CaCO_3$, and $Ca(OH)_2$ were obtained in 6.11%, 3.9%, and 18%, respectively. The apatite slightly increases up to 36.64% for CWH-800 and decreases again in CWH-900 as well as Ca and $Ca(OH)_2$ indicating the formation of other phases. Calcium apatites are also widely used as efficient adsorbents for toxic metal ion removal from wastewater [40–42]. On the other hand, albite is present in all materials, Chen et al. [43] reported albite-bass porous ceramic for the adsorption of Cd^{2+} and other heavy metals.

Most of the reaction products from the calcination treatment of WH show suitability for the adsorption of heavy metals. For instance, at low temperatures (< 550 ℃) with $CaCO_3$ is the main phase, while at a high temperature (> 650 ℃) calcium apatite is the phase in greater quantity. Both Ca-based phases have been studied in the removal of heavy metals, which makes the materials obtained from WH calcination promising for the adsorption of Cu^{2+} and Cd^{2+}.
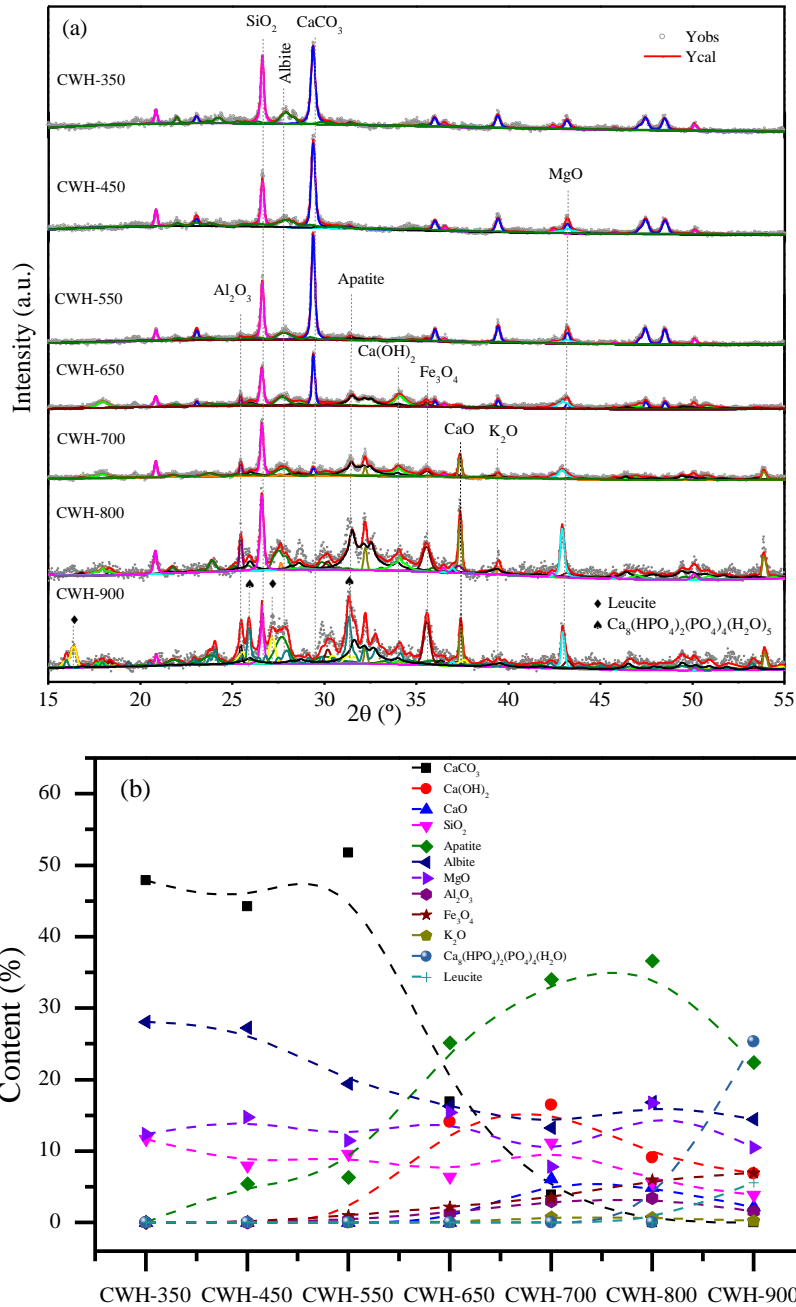
Fig. 5-1. (a) XRD patterns for water hyacinth calcined (CWH) at different temperatures. (b) Quantification of phases (% wt.) according to Rietveld refinement of the XRD patterns of water hyacinth calcined (CWH) at different temperatures.

5.3.2. Adsorption of Cd^{2+} and Cu^{2+}

Fig. 5-2 shows the percentage of removal of Cd^{2+} and Cu^{2+} for WH-material calcinated at different temperatures. From this plot, it can be observed that powder calcined

at temperatures below 650 °C have lower percentages of adsorption of Cd^{2+} (between 17.8 % and 30.2 %) and Cu^{2+} (between 9.6 % and 23.1 %) than those calcined at temperatures between 700 and 900 °C (42.5 – 51.2 % to Cd^{2+} and 22.8 – 31.8 % to Cu^{2+}). Comparing Figures 5-1 and 5-2 a correlation between the percentage of Cd^{2+} and Cu^{2+} removal and composition, e.g., the calcium apatite content can be observed. More specifically, a maximum in the removal percentage seems to be correlated with the material with the highest apatite content (CWH-700, and CWH-800, see Fig. 5-1), at higher temperatures (900 °C) the apatite content decreases and phases such as octacalcium phosphate $(Ca_8(HPO_4)_2(PO_4)_4(H_2O)_5)$ and leucite $(K(Si_2Al)O_6)$ appear, which do not favor the adsorption of Cd^{2+} and Cu^{2+} causing a decrease in the removal percentage. Apart from the relationship between the percentage of adsorption and the composition of the materials one has to take into account specific area, crystallinity, porosity, among other powder properties, which are all affected by calcination conditions, such as temperature and time [42].
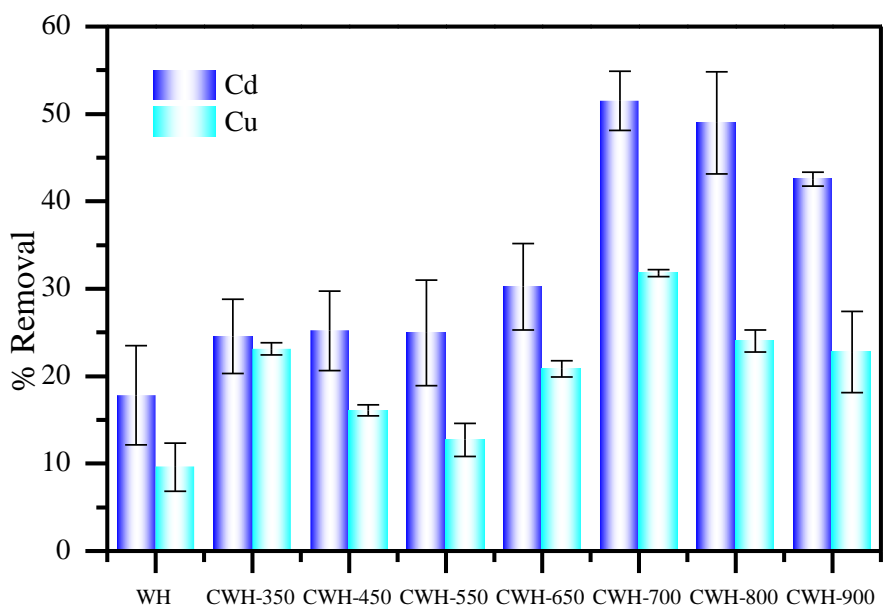

Fig. 5-2. Percentages of removal of Cd^{2+} and Cu^{2+} of water hyacinth calcined (CWH) at different temperatures.

5.3.3. Adsorption mechanisms

Due to the differences in the removal of Cu^{2+} and Cd^{2+} as a function of temperature and to understand the adsorption mechanism and phases responsible for the adsorption of cations WH-samples calcined at 550 and 700 ºC were analyzed before and after adsorption by ATR-FTIR, XRD, and XPS to determine the interaction and formation of new Cu and Cd species.

Fig. 5-3 shows the XRD patterns of CWH-550 and CWH-700 before and after adsorption; the samples were labeled as CWH-500–Cu, CWH-700–Cu in the case of Cu^{2+} removal and CWH-500–Cd and CWH-700–Cd for Cd^{2+} removal. The presence of $CaCO_3$ is confirmed in CWH-550 with the peak at $2\theta = 29.4º$, which corresponds to the (104) plane ($CaCO_3$, ICSD·#: 166364) [45]. The peak observed at $2\theta = 26.6º$ corresponds to the (011) plane of SiO_2 (ICSD·#: 42498), and the peak at $2\theta = 42.9º$ corresponds to the (002) plane for MgO, aluminum is mainly forming an aluminosilicate with a peak at $2\theta = 27.9º$ of the plane (200) for albite ($NaAlSi_3O_8$, $KAlSi_3O_8$). For CWH-700, the peak at $2\theta = 29.4º$ of the (104) plane of $CaCO_3$ is lower. It can be seen that CWH-700 presents peaks at $2\theta = 17.9º$ and $34.0º$, which correspond to the (001) and (010) planes of $Ca(OH)_2$ (ICSD·#: 202225), respectively; additionally, the presence of apatite ($Ca_5(PO_4)_3(OH)$) (ICSD #: 180315) was confirmed with the peaks at $2\theta = 31.4º$ and $32.1º$, for the (211) and (112) planes, respectively, and diffraction peaks at $2\theta = 32.2º$, $37.3º$, and $53.8º$ for the (111), (002) and (022) planes indicating the presence of CaO (ICSD·#: 60199).

The formation of crystalline particles of Cd^{2+} and Cu^{2+} was observed on CWH-550 and CWH-700. XRD patterns of CWH-550–Cd and CWH-700–Cd revealed the formation otavite ($CdCO_3$, ICSD 156740). The diffraction peaks corresponding to MgO decreased significantly whereas those associated to CaO, $Ca(OH)_2$, Al_2O_3, and K_2O vanished, which indicates that these phases were involved in the precipitation of otavite or the formation of other chemical species with Cd. On the other hand, CWH-550–Cu showed intense peaks of Cu-mineral in the form of posnjakite ($Cu_4(OH)_6SO_4.H_2O$, ICSD 100276). In contrast, CWH-700–Cu is a highly amorphous case and does not present peaks for posnjakite making a detailed analysis difficult. However, a peak is observed at $2\theta = 28.4º$ for the (201) plane corresponding to $Cu_2(P_2O_7)$. Otavite and posnjakite have been reported

as a precipitated product in the Cd^{2+} and Cu^{2+}, respectively, using adsorbents containing Ca [4,15].
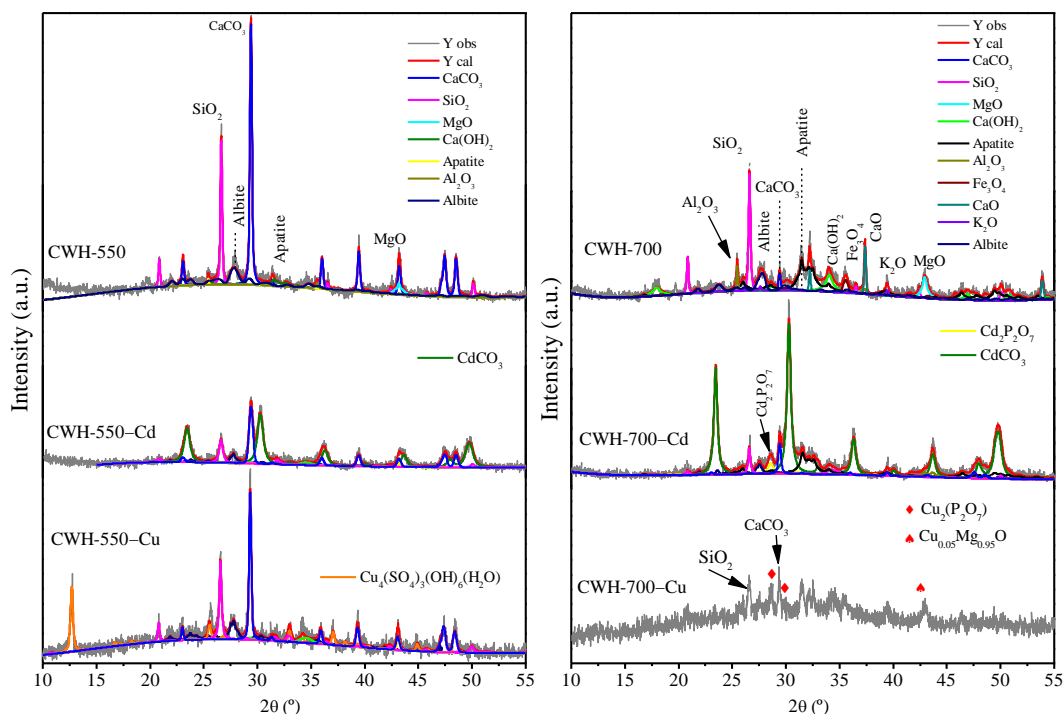

Fig. 5-3. XRD patterns for CWH-550 and CWH-700 before and after adsorption Cd and Cu. CWH-550 and CWH-700: water hyacinth calcined at 550 and 700 °C, respectively; CWH-550-Cu, CWH-550-Cd: water hyacinth calcined at 550 °C after of adsorption Cu and Cd, respectively; CWH-700-Cu and CWH-700-Cd: water hyacinth calcined at 700 °C after of adsorption Cu and Cd, respectively.

Fig. 5-4 shows the FTIR spectra before and after adsorption. Before adsorption for both CWH-550 and CWH-700 bands at 1050 and 960 cm^{-1} are assigned to the Si–O–Si asymmetric stretching vibration and Si–OH asymmetric vibration respectively, while the low intensity band at 779 cm^{-1} is characteristic of the symmetric vibration of the Si–O bond [46,47]. In all cases, the SiO_2 signals are still visible after the adsorption, indicating that SiO_2 does not play a significant role in the adsorption process. On the opposite, the band at 646 cm^{-1} associated to MgO is observed [48] before and after adsorption, which decreases, mainly in the case of Cu^{2+} indicating the formation of a Cu–MgO compound. As previously discussed, a $Cu_XMg_{1-X}O$ solid solution was identified by XRD for CWH-700–Cu.

For CWH-550, the signals at 712 and 875 cm^{-1} corresponding to $–CO_3^{2-}$ group are observed; these signals are confirmed by the bands centered at 1418 and 1458 cm^{-1} corresponding to the symmetric and asymmetric stretching modes of the CO_3^{2-} group [49], indicating the presence of $CaCO_3$ [47,50]. In the case of Cd^{2+} adsorption, new bands were observed at 860 and 840 cm^{-1} for CWH-550–Cd and CWH-700–Cd, respectively.

CWH-550 and CWH-700 also showed bands at 567 and 602 cm^{-1} of the PO_4^{3-} group, as verified by the bands around 1000 and 1100 cm^{-1}, corresponding to the asymmetric and symmetric deformation modes of the $[PO_4]v_4$ group (v_4 O–P–O) [49] corresponding to apatite [13]. The bands at 567 and 602 cm^{-1} change considerably after adsorption indicating that the phosphate group plays a main role in the adsorption of Cd^{2+} and Cu^{2+}. For CWH-550–Cu, the band at 602 cm^{-1} moves to 600 cm^{-1} and also gains intensity, and for CWH-550–Cd, the 567 cm^{-1} band increases its intensity. Again, these changes indicate that calcium phosphates are involved in the adsorption of Cu^{2+} and Cd^{2+}, possibly by a substitution mechanism by cation exchange as it has already been reported elsewhere [40]. However, the XRD pattern of the CWH-700 sample shows an interplay of calcium apatite with amorphous compounds.

The band at 680 cm^{-1} corresponds to Al–O bond, which has a higher intensity for CWH-700 than for CWH-500 and, disappears after adsorption, as does the peak at $2\theta =$ 25.37° in XRD (Fig. 5-3). This fact serves as evidence that Al_2O_3 is also active in the Cd^{2+} and Cu^{2+} removal [51–53].
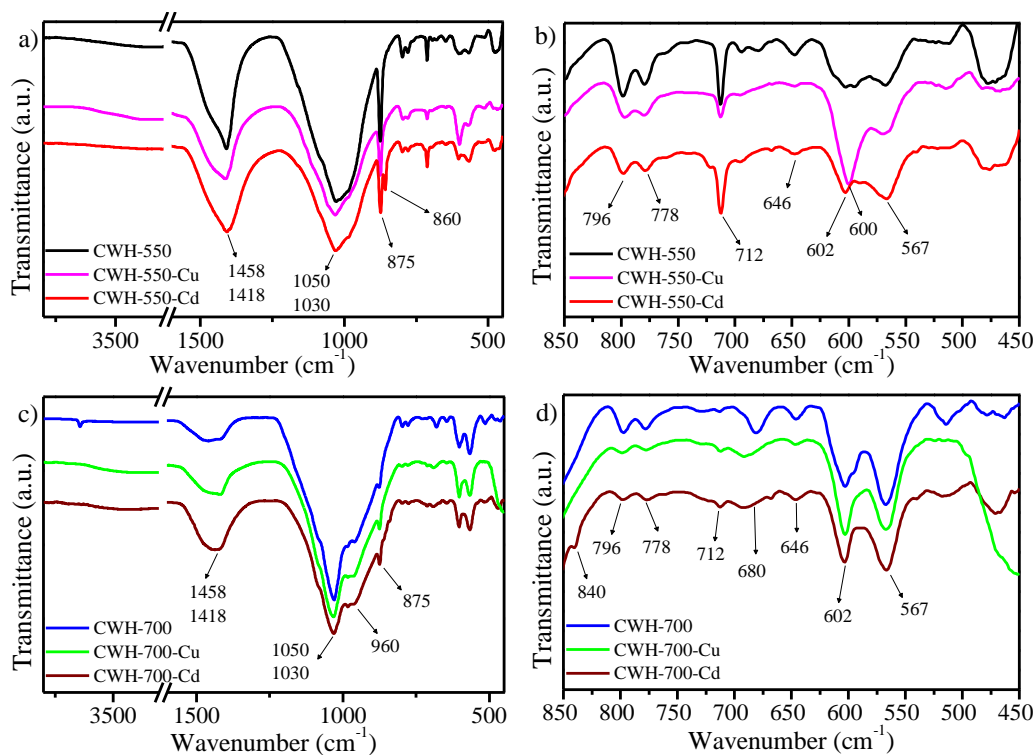
Fig. 5-4. a) and c): FTIR spectra of water hyacinth calcined at 550 °C and 700 ºC; b) and d); Increase in the range: $815 – 450$ cm^{-1}. Before and after Cu^{2+} and Cd^{2+} removal.

Fig. 5-5 and Table 5-1 show the XPS spectra, position, and atomic quantification for CWH-700 before and after Cd^{2+} and Cu^{2+} removal. The XPS survey spectra for CWH-700 (Fig. 5-5a) revealed peaks of C, Al, Mg, P, S, Cl, K, Ca, Na, Si, and O; where O has the highest intensity and atomic composition according to the result in Table 5-1. After removal (Fig. 5-5b and 5-5c) the characteristic peaks for Cd^{2+} and Cu^{2+} were identified. According to the curve-fitting Cd 3p peak consists of two spin-orbit doublets, the higher intensity envelope Cd 3p$_{1/2}$ at 653.9 eV and Cd 3p$_{3/2}$ at 619.5 eV, the second one, with lower intensity envelope Cd 3p$_{1/2}$ at 649.7 eV and Cd 3p$_{3/2}$ at 615.7 eV both doublets in a 1:2 area ratio. The presence of two doublets may be due to the presence of CdCO$_3$ and Cd$_2$P$_2$O$_7$ which agrees with the results observed by XRD (Fig. 5-3). Similar results have been reported for adsorption and precipitation of Cd with phosphate addition in soils [54]. The curve-fitting for Cu 2p shows the doublet for Cu 2p$_{1/2}$ at 955.9 eV and Cu 2p$_{3/2}$ at 936.0 eV for Cu^{2+}, the second doublet corresponds to the shake-up structure for Cu 2p [55]. The value of 936.0 eV is close to the reported for CuSO$_4$ (936.0 eV) and Cu$_3$(PO$_4$)$_2$ (935.85 eV) [56], which complements the results obtained by XRD for CWH-700–Cu.

High-resolution spectra for K, C, Al, Mg, and P, which are possibly involved in the removal of Cd^{2+} and Cu^{2+} are shown in Fig. 5-5d-h. Interactions of these elements with Cd^{2+}as have been reported by Chen et al.[57] that were confirmed with the current results. For instance, C 1s signal at 289.5 eV for CO_3^{2-} increases for CWH-700–Cd indicating the presence of $CdCO_3$. Additionally, the signals for Ca 3p, Mg 1s, Al 2p, and P 2p are all shifted after the adsorption tests indicating the formation of particular compounds or solid solutions associated to Cd^{2+} and Cu^{2+}. In the case of Ca the shifting was from 346.7 eV to 345.7 eV (see Table 5-1), whereas P 2p is shifted from 133.0 eV to 133.3 eV and 133.5 eV after Cd^{2+} and Cu^{2+} removal respectively indicating the formation of phosphates compounds [56]. In the case of adsorption experiments for Cu^{2+} removal, Mg 1s is shifted from 1305.2 to 1304.4 eV which is possibly associated to the $Cu_{0.05}Mg_{0.95}O$ formation observed by XRD. It is worth to note that the signals for Ca and Al decrease in intensity after Cu^{2+} removal, possibly due to a partial dissolution of compounds that contain these elements.
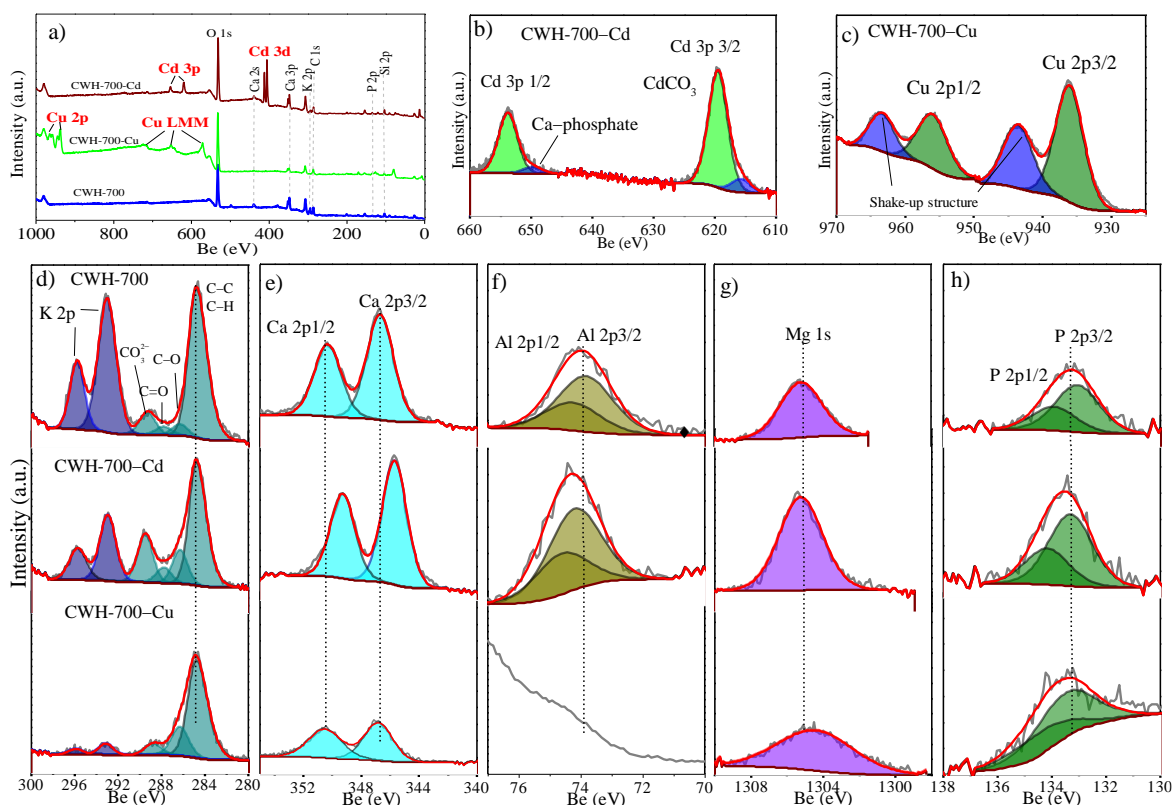

Fig. 5- 5. a) XPS survey for water hyacinth calcined at 700 °C, before and after Cd^{2+} and Cu^{2+} removal, b-h high resolution XPS spectra for Cd, Cu, K+C, Ca, Al, Mg and P.

The surface composition of CWH-700 (Table 5-1) evidenced that the WH ashes do not contain other heavy elements corroborating previous results [13]. After adsorption, the content of Cd^{2+} and Cu^{2+} is 28.0% and 30.3%, while the Ca decreases from 18.0% to 11.6% and 5.4%, respectively. Although other elements were released into the aqueous solution, none present greater risk compared to the removed heavy elements.

Table 5-1. Element quantification and position determined by XPS for CWH-700 before and after Cd^{2+} and Cu^{2+} removal from an aqueous solution.

Element	CWH-700		CWH-700–Cd		CWH-700–Cu	
	Weigh (%)	Position (eV)	Weigh (%)	Position (eV)	Weigh (%)	Position (eV)
Al	5.4	73.80	4.5	74.20	0.0	-
Si	11.2	101.96	8.6	102.17	7.3	102.17
P	3.2	133.03	2.0	133.29	2.7	133.52
S	2.1	168.89	1.7	169.00	3.2	168.44
Cl	3.9	198.74	1.6	198.89	2.2	198.42
C	8.1	284.80	6.1	284.80	6.4	284.80
K	5.6	293.01	1.3	292.95	0.3	293.13
Ca	18.0	346.67	11.6	345.68	5.4	346.79
O	34.2	531.85	29.7	531.63	38.4	531.96
Na	1.3	1073.17	0.0	1073.17	0.0	1073.17
Mg	7.1	1305.21	4.8	1305.23	3.6	1304.41
Cd	0	-	28.0	619.44	0.0	-
Cu	0	-	0.0	-	30.3	936.00

According to the above results, Fig. 5-6 shows a schematic representation of the proposed Cu^{2+} and Cd^{2+} removal mechanism by CWH-550 and CWH-700 from aqueous solutions. The XRD results showed that $CaCO_3$ is the phase in the highest proportion for CWH-550, while $Ca(OH)_2$ and calcium apatites are the main phases in CWH-700. These phases interact promoting the formation of Cu^{2+} and Cd^{2+} precipitates such as $Cu_4(SO_4)_3(OH)_6(H_2O)$ and $Cu_2P_2O_7$ for Cu^{2+}, $CdCO_3$ and $Cd_2P_2O_7$ for Cd^{2+}. Lower proportion phases as MgO and Al_2O_3 present in the adsorbents also intervene, which is evidenced by the change of IR bands corresponding to MgO and Al_2O_3. In the case of Mg, the formation of $Cu_{0.05}Mg_{0.95}O$ was observed, while Al precipitates were not observed, possibly due to its low content in the materials.

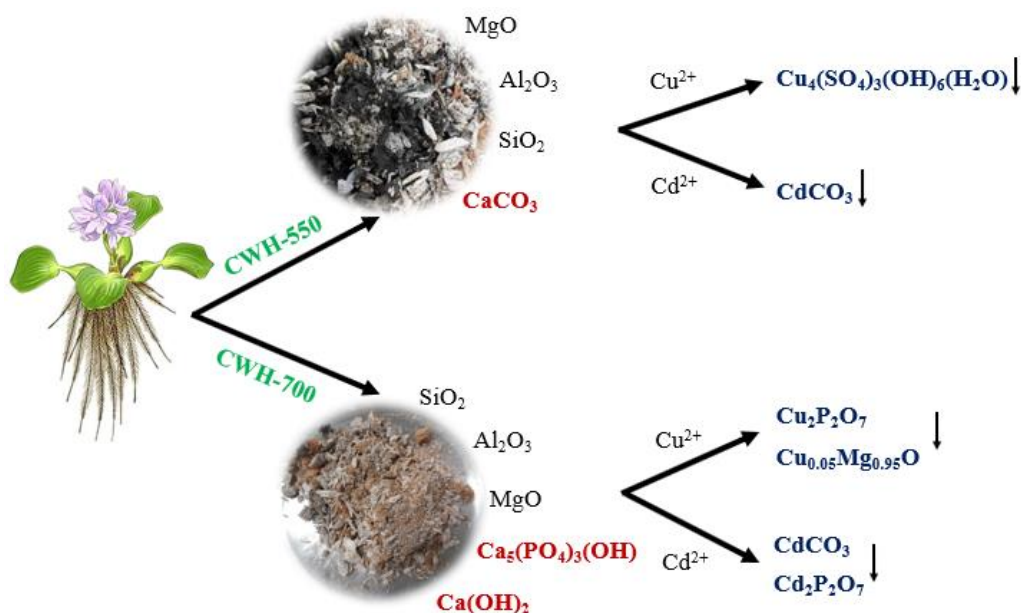**Fig. 5-6**. Scheme of the process of calcination and Cu^{2+} and Cd^{2+} adsorption and the formed precipitated.

5.3.4. Leaching of Cd^{2+} and Cu^{2+}

Fig. 5-7 shows the leaching percentages of Cd^{2+} and Cu^{2+} adsorbed on CWH-550 and CWH-700. It can be seen that the metals adsorbed on CWH-700 present lower leaching percentages (0.003% and 0.055% for Cu^{2+} and Cd^{2+}, respectively) compared to those adsorbed on CWH-550 (0.013% and 0.747% for Cu^{2+} and Cd^{2+}, respectively). However, these leaching percentages are less than 1%, indicating that the materials obtained from the calcination of the water hyacinth immobilize approximately 99% of the adsorbed Cd^{2+} and Cu^{2+} on their surface, which may be related to the presence of phosphate and calcium species (apatite and calcite) that help the formation of species that precipitate during adsorption. In the case of apatite, part of it can dissolve in the aqueous solution under acidic conditions and the dissolved phosphates can react with Cu or Cd to form phosphate-metal compounds such as $Cu_2P_2O_7$ or $Cd_2P_2O_7$. In the case of calcite or other calcium compounds, Cd^{2+} and Cu^{2+} exchange with Ca^{2+} to form stable compounds such as $CdCO_3$. These compounds are highly insoluble and help the immobilization of these metals [33,34]. The potential of phosphate compounds in enhancing the immobilization of heavy metals has been demonstrated in the scientific literature [33,34,41,58]. In general, the presented results indicate that the

immobilization of Cu and Cd by the calcined water hyacinth can substantially reduce the contamination of these metals in the water.
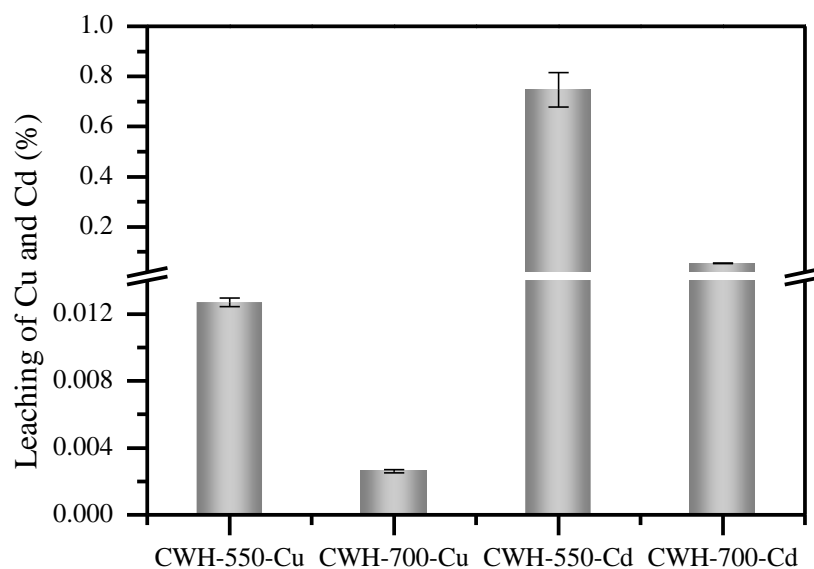

Fig. 5-7. Leaching percentage of Cu^{2+} and Cd^{2+} for adsorbed materials.

5.4. Conclusions

Economic and eco-friendly materials obtained from the calcination of water hyacinth were tested for the successful removal/immobilization of Cu^{2+} and Cd^{2+} from aqueous solutions. The calcination of WH allows mainly the formation of Ca–P phases such as $CaCO_3$, $Ca_5(PO_4)_3(OH)$, and MgO and Al_2O_3 in lower proportion. These phases have a high capacity for adsorption and retention of heavy metals. According to XRD results, Cd^{2+} precipitates as $CdCO_3$ and $Cd_2P_2O_7$ while Cu^{2+} precipitates as $Cu_{0.05}Mg_{0.95}O$ and $Cu_2P_2O_7$ for water hyacinth calcined at 700 °C, (CWH-700). On the other hand, calcium phosphates in materials calcined at temperatures higher than 550 °C play an important role in the removal of Cd^{2+} and Cu^{2+} since the maximum removal percentage matches with the materials with the highest apatite content, possibly by the exchange of Cd^{2+}/Cu^{2+} by Ca^{2+}. The solid precipitates have low solubility in simulated natural precipitation water (< 0.055% of Cd and < 0.003% of Cu) that reduce contaminant mobility and, therefore increased stability in soils preventing new contamination.

5.5. References

[1]   T. Guimarães, L.D. Paquini, B.R. Lyrio Ferraz, L.P. Roberto Profeti, D. Profeti, Efficient removal of Cu(II) and Cr(III) contaminants from aqueous solutions using marble waste powder, J. Environ. Chem. Eng. 8 (2020) 103972. https://doi.org/10.1016/j.jece.2020.103972.

[2]   D. Nagarajan, S. Venkatanarasimhan, Kinetics and mechanism of efficient removal of Cu(II) ions from aqueous solutions using ethylenediamine functionalized cellulose sponge, Int. J. Biol. Macromol. 148 (2020) 988–998. https://doi.org/10.1016/j.ijbiomac.2020.01.177.

[3]   A. Papandreou, C.J. Stournaras, D. Panias, Copper and cadmium adsorption on pellets made from fired coal fly ash, J. Hazard. Mater. 148 (2007) 538–547. https://doi.org/10.1016/j.jhazmat.2007.03.020.

[4]   F. Zhang, X. Wang, D. Yin, B. Peng, C. Tan, Y. Liu, X. Tan, S. Wu, Efficiency and mechanisms of Cd removal from aqueous solution by biochar derived from water hyacinth (Eichornia crassipes), J. Environ. Manage. 153 (2015) 68–73. https://doi.org/10.1016/j.jenvman.2015.01.043.

[5]   I. Mobasherpour, E. Salahi, M. Pazouki, Removal of divalent cadmium cations by means of synthetic nano crystallite hydroxyapatite, Desalination. 266 (2011) 142–148. https://doi.org/10.1016/j.desal.2010.08.016.

[6]   X. hua Zhu, J. Li, J. hong Luo, Y. Jin, D. Zheng, Removal of cadmium (II) from aqueous solution by a new adsorbent of fluor-hydroxyapatite composites, J. Taiwan Inst. Chem. Eng. 70 (2017) 200–208. https://doi.org/10.1016/j.jtice.2016.10.049.

[7]   V.K. Gupta, I. Ali, Utilisation of bagasse fly ash (a sugar industry waste) for the removal of copper and zinc from wastewater, Sep. Purif. Technol. 18 (2000) 131–140. https://doi.org/10.1016/S1383-5866(99)00058-1.

[8]   S.H. Hasan, M. Talat, S. Rai, Sorption of cadmium and zinc from aqueous solutions by water hyacinth (Eichchornia crassipes), Bioresour. Technol. 98 (2007) 918–928. https://doi.org/10.1016/j.biortech.2006.02.042.

[9]   M. Sarkar, A.K.M.L. Rahman, N.C. Bhoumik, Remediation of chromium and copper on water hyacinth (E. crassipes) shoot powder, Water Resour. Ind. 17 (2017) 1–6. https://doi.org/10.1016/j.wri.2016.12.003.

[10]   B.C. Nyamunda, T. Chivhanga, U. Guyo, F. Chigondo, Removal of Zn (II) and Cu (II) ions from industrial wastewaters using magnetic biochar derived from water hyacinth, J. or Eng. 2019 (2019) 1–11.

[11]   N.A. Qambrani, M.M. Rahman, S. Won, S. Shim, C. Ra, Biochar properties and eco-friendly applications for climate change mitigation, waste management, and wastewater treatment: A review, Renew. Sustain. Energy Rev. 79 (2017) 255–273. https://doi.org/10.1016/j.rser.2017.05.057.

[12]   M. Li, Z. Lou, Y. Wang, Q. Liu, Y. Zhang, J. Zhou, G. Qian, Alkali and alkaline earth metallic (AAEM) species leaching and Cu(II) sorption by biochar, Chemosphere. 119 (2015) 778–785. https://doi.org/10.1016/j.chemosphere.2014.08.033.

[13]   A. Ramirez, S. Pérez, N. Acelas, E. Flórez, Utilization of water hyacinth (Eichhornia crassipes) rejects as phosphate-rich fertilizer, J. Environ. Chem. Eng. 9 (2021) 104776. https://doi.org/10.1016/j.jece.2020.104776.

[14]   J.M. Zachara, C.E. Cowan, C.T. Resch, Sorption of divalent metals on calcite, Geochim. Cosmochim. Acta. 55 (1991) 1549–1562. https://doi.org/10.1016/0016-7037(91)90127-Q.

[15]   H. Hu, X. Li, P. Huang, Q. Zhang, W. Yuan, Efficient removal of copper from wastewater by using mechanically activated calcium carbonate, J. Environ. Manage. 203 (2017) 1–7. https://doi.org/10.1016/j.jenvman.2017.07.066.

[16]   J.V. Flores-cano, R. Leyva-ramos, J. Mendoza-barron, G.J. Labrada-delgado, R.M. Guerrero-coronado, A. Aragón-pi, Sorption mechanism of Cd(II) from water solution onto chicken eggshell, Appl. Surf. Sci. 276 (2013) 682–690. https://doi.org/10.1016/j.apsusc.2013.03.153.

[17]   T. Wen, Y. Zhao, T. Zhang, B. Xiong, Effect of anions species on copper removal from wastewater by using mechanically activated calcium carbonate, Chemosphere.

230 (2019) 127–135. https://doi.org/10.1016/j.chemosphere.2019.04.213.

[18]   M. Baláž, Z. Bujňáková, P. Baláž, A. Zorkovská, Z. Danková, J. Briančin, Adsorption of cadmium(II) on waste biomaterial, J. Colloid Interface Sci. 454 (2015) 121–133. https://doi.org/10.1016/j.jcis.2015.03.046.

[19]   M. Ferri, S. Campisi, M. Scavini, C. Evangelisti, P. Carniti, A. Gervasini, In-depth study of the mechanism of heavy metal trapping on the surface of hydroxyapatite, Appl. Surf. Sci. 475 (2019) 397–409. https://doi.org/10.1016/j.apsusc.2018.12.264.

[20]   A. Yasukawa, T. Yokoyama, K. Kandori, T. Ishikawa, Reaction of calcium hydroxyapatite with Cd2+ and Pb2+ ions, Colloids Surfaces A Physicochem. Eng. Asp. 299 (2007) 203–208. https://doi.org/10.1016/j.colsurfa.2006.11.042.

[21]   R.R. Sheha, Sorption behavior of Zn(II) ions on synthesized hydroxyapatites, J. Colloid Interface Sci. 310 (2007) 18–26. https://doi.org/10.1016/j.jcis.2007.01.047.

[22]   S.K. Lower, P.A. Maurice, S.J. Traina, Simultaneous dissolution of hydroxylapatite and precipitation of hydroxypyromorphite: direct evidence of homogeneous nucleation, Geochim. Cosmochim. Acta. 62 (1998) 1773–1780. https://doi.org/10.1016/S0016-7037(98)00098-2.

[23]   Y. Takeuchi, H. Arai, Removal of coexisting Pb2+, Cu2+ and Cd2+ ions from water by addition of hydroxyapatite powder., J. Chem. Eng. JAPAN. 23 (1990) 75–80. https://doi.org/10.1252/jcej.23.75.

[24]   T. Suzuki, T. Hatsushika, M. Miyake, Synthetic hydroxyapatites as inorganic cation exchangers. Part 2, J. Chem. Soc. Faraday Trans. 1 Phys. Chem. Condens. Phases. 78 (1982) 3605–3611. https://doi.org/10.1039/F19827803605.

[25]   S. Bailliez, A. Nzihou, E. Bèche, G. Flamant, Removal of Lead (Pb) by Hydroxyapatite Sorbent, Process Saf. Environ. Prot. 82 (2004) 175–180. https://doi.org/10.1205/095758204322972816.

[26]   Y. Xu, F.W. Schwartz, S.J. Traina, Sorption of Zn2+ and Cd2+ on Hydroxyapatite Surfaces, Environ. Sci. Technol. 28 (1994) 1472–1480. https://doi.org/10.1021/es00057a015.

[27] Y. Xu, F.W. Schwartz, Lead immobilization by hydroxyapatite in aqueous solutions, J. Contam. Hydrol. 15 (1994) 187–206. https://doi.org/10.1016/0169-7722(94)90024-8.

[28] G. Liu, Z. Li, L. Xu, X. Xu, Q. Huang, Y. Zeng, M. Wen, The dynamics and adsorption of Cd (II) onto hydroxyapatite attapulgite composites from aqueous solution, J. Sol-Gel Sci. Technol. 87 (2018) 269–284. https://doi.org/10.1007/s10971-018-4717-8.

[29] D.N. Thanh, P. Novák, J. Vejpravova, H.N. Vu, J. Lederer, T. Munshi, Removal of copper and nickel from water using nanocomposite of magnetic hydroxyapatite nanorods, J. Magn. Magn. Mater. 456 (2018) 451–460. https://doi.org/10.1016/j.jmmm.2017.11.064.

[30] F. Debela, R.W. Thring, J.M. Arocena, Immobilization of heavy metals by co-pyrolysis of contaminated soil with woody biomass, Water. Air. Soil Pollut. 223 (2012) 1161–1170. https://doi.org/10.1007/s11270-011-0934-2.

[31] A. Corami, S. Mignardi, V. Ferrini, Cadmium removal from single- and multi-metal (Cd + Pb + Zn + Cu) solutions by sorption on hydroxyapatite, J. Colloid Interface Sci. 317 (2008) 402–408. https://doi.org/10.1016/j.jcis.2007.09.075.

[32] J. Kumpiene, A. Lagerkvist, C. Maurice, Stabilization of As, Cr, Cu, Pb and Zn in soil using amendments - A review, Waste Manag. 28 (2008) 215–225. https://doi.org/10.1016/j.wasman.2006.12.012.

[33] Y. Liu, R. Zhang, Z. Sun, Q. Shen, Y. Li, Y. Wang, S. Xia, J. Zhao, X. Wang, Remediation of artificially contaminated soil and groundwater with copper using hydroxyapatite/calcium silicate hydrate recovered from phosphorus-rich wastewater, Environ. Pollut. 272 (2021) 115978. https://doi.org/10.1016/j.envpol.2020.115978.

[34] Q. Li, H. Zhong, Y. Cao, Effects of the joint application of phosphate rock, ferric nitrate and plant ash on the immobility of As, Pb and Cd in soils, J. Environ. Manage. 265 (2020) 110576. https://doi.org/10.1016/j.jenvman.2020.110576.

[35] EPA, Method 1312 - Syntetic precipitation leaching procedure, (1994) 1–30. https://www.epa.gov/sites/production/files/2015-12/documents/1312.pdf.

[36] J. Wu, T. Wang, J. Wang, Y. Zhang, W.P. Pan, A novel modified method for the efficient removal of Pb and Cd from wastewater by biochar: Enhanced the ion exchange and precipitation capacity, Sci. Total Environ. 754 (2021). https://doi.org/10.1016/j.scitotenv.2020.142150.

[37] A.Y. Li, H. Deng, Y.H. Jiang, C.H. Ye, B.G. Yu, X.L. Zhou, A.Y. Ma, Superefficient Removal of Heavy Metals from Wastewater by Mg-Loaded Biochars: Adsorption Characteristics and Removal Mechanisms, Langmuir. 36 (2020) 9160–9174. https://doi.org/10.1021/acs.langmuir.0c01454.

[38] J.H. Park, J.H. Eom, S.L. Lee, S.W. Hwang, S.H. Kim, S.W. Kang, J.J. Yun, J.S. Cho, Y.H. Lee, D.C. Seo, Exploration of the potential capacity of fly ash and bottom ash derived from wood pellet-based thermal power plant for heavy metal removal, Sci. Total Environ. 740 (2020). https://doi.org/10.1016/j.scitotenv.2020.140205.

[39] C. Liu, J. Ye, Y. Lin, J. Wu, G.W. Price, D. Burton, Y. Wang, Removal of Cadmium (II) using water hyacinth (Eichhornia crassipes) biochar alginate beads in aqueous solutions, Environ. Pollut. 264 (2020) 114785. https://doi.org/10.1016/j.envpol.2020.114785.

[40] J. Terra, G.B. Gonzalez, A.M. Rossi, J.G. Eon, D.E. Ellis, Theoretical and experimental studies of substitution of cadmium into hydroxyapatite, Phys. Chem. Chem. Phys. 12 (2010) 15490–15500. https://doi.org/10.1039/c0cp01032d.

[41] B. Seshadri, N.S. Bolan, G. Choppala, A. Kunhikrishnan, P. Sanderson, H. Wang, L.D. Currie, D.C.W. Tsang, Y.S. Ok, K. Kim, Potential value of phosphate compounds in enhancing immobilization and reducing bioavailability of mixed heavy metal contaminants in shooting range soil, Chemosphere. 184 (2017) 197–206. https://doi.org/10.1016/j.chemosphere.2017.05.172.

[42] A.I. Ivanets, N. V. Kitikova, I.L. Shashkova, M.Y. Roshchina, V. Srivastava, M. Sillanpää, Adsorption performance of hydroxyapatite with different crystalline and porous structure towards metal ions in multicomponent solution, J. Water Process Eng. 32 (2019) 100963. https://doi.org/10.1016/j.jwpe.2019.100963.

[43] J.H. Chen, P.S. Liu, W. Cheng, PBA-loaded albite-base ceramic foam in application

to adsorb harmful ions of Cd, Cs and As(V) in water, Multidiscip. Model. Mater. Struct. 15 (2019) 659–672. https://doi.org/10.1108/MMMS-07-2018-0140.

[44]   A. Ramirez, S. Giraldo, J. García-nunez, E. Flórez, N. Acelas, Phosphate removal from water using a hybrid material in a fixed-bed column, J. Water Process Eng. 26 (2018) 131–137. https://doi.org/10.1016/j.jwpe.2018.10.008.

[45]   L. Delgadillo-Velasco, V. Hernández-Montoya, M.A. Montes-Morán, R.T. Gómez, F.J. Cervantes, Recovery of different types of hydroxyapatite by precipitation of phosphates of wastewater from anodizing industry, J. Clean. Prod. 242 (2020) 118564. https://doi.org/10.1016/j.jclepro.2019.118564.

[46]   A.M. Grumezescu, C.D. Ghitulica, G. Voicu, K.S. Huang, C.H. Yang, A. Ficai, B.S. Vasile, V. Grumezescu, C. Bleotu, M.C. Chifiriuc, New silica nanostructure for the improved delivery of topical antibiotics used in the treatment of staphylococcal cutaneous infections, Int. J. Pharm. 463 (2014) 170–176. https://doi.org/10.1016/j.ijpharm.2013.07.016.

[47]   F.B. Reig, J.V.G. Adelantado, M.C.M.M. Moreno, FTIR quantitative analysis of calcium carbonate (calcite) and silica (quartz) mixtures using the constant ratio method. Application to geological samples, Talanta. 58 (2002) 811–821. https://doi.org/10.1016/S0039-9140(02)00372-7.

[48]   A. Ansari, A. Ali, M. Asif, Shamsuzzaman, Microwave-assisted MgO NP catalyzed one-pot multicomponent synthesis of polysubstituted steroidal pyridines, New J. Chem. 42 (2018) 184–197. https://doi.org/10.1039/c7nj03742b.

[49]   L. Berzina-Cimdina, N. Borodajenko, Research of calcium phosphates using fourier transform infrared spectroscopy, Infrared Spectrosc. - Mater. Sci. Eng. Technol. (2012) 123–148. https://doi.org/10.5772/36942.

[50]   F. Wilson, P. Tremain, B. Moghtaderi, Characterization of Biochars Derived from Pyrolysis of Biomass and Calcium Oxide Mixtures, Energy and Fuels. 32 (2018) 4167–4177. https://doi.org/10.1021/acs.energyfuels.7b03221.

[51]   T.K. Sen, M.V. Sarzali, Removal of cadmium metal ion (Cd2+) from its aqueous

solution by aluminium oxide (Al2O3): A kinetic and equilibrium study, Chem. Eng. J. 142 (2008) 256–262. https://doi.org/10.1016/j.cej.2007.12.001.

[52]   S. Mahdavi, M. Jalali, A. Afkhami, Heavy metals removal from aqueous solutions by Al2O3 nanoparticles modified with natural and chemical modifiers, Clean Technol. Environ. Policy. 17 (2015) 85–102. https://doi.org/10.1007/s10098-014-0764-1.

[53]   M.H. Stietiya, J.J. Wang, Zinc and Cadmium Adsorption to Aluminum Oxide Nanoparticles Affected by Naturally Occurring Ligands, J. Environ. Qual. 43 (2014) 498–506. https://doi.org/10.2134/jeq2013.07.0263.

[54]   H.H. Lee, V.N. Owens, S. Park, J. Kim, C.O. Hong, Adsorption and precipitation of cadmium affected by chemical form and addition rate of phosphate in soils having different levels of cadmium, Chemosphere. 206 (2018) 369–375. https://doi.org/10.1016/j.chemosphere.2018.04.176.

[55]   M.C. Biesinger, L.W.M. Lau, A.R. Gerson, R.S.C. Smart, Resolving surface chemical states in XPS analysis of first row transition metals, oxides and hydroxides: Sc, Ti, V, Cu and Zn, Appl. Surf. Sci. 257 (2010) 887–898. https://doi.org/10.1016/j.apsusc.2010.07.086.

[56]   M.C. Biesinger, Advanced analysis of copper X-ray photoelectron spectra, Surf. Interface Anal. 49 (2017) 1325–1334. https://doi.org/10.1002/sia.6239.

[57]   Y. Chen, M. Li, Y. Li, Y. Liu, Y. Chen, H. Li, L. Li, F. Xu, H. Jiang, L. Chen, Hydroxyapatite modified sludge-based biochar for the adsorption of Cu2+ and Cd2+: Adsorption behavior and mechanisms, Bioresour. Technol. 321 (2021) 124413. https://doi.org/10.1016/j.biortech.2020.124413.

[58]   O. Ayodele, S.J. Olusegun, O.O. Oluwasina, E.A. Okoronkwo, E.O. Olanipekun, N.D.S. Mohallem, W.G. Guimarães, B.L.F. d. M. Gomes, G. de O. Souza, H.A. Duarte, Experimental and theoretical studies of the adsorption of Cu and Ni ions from wastewater by hydroxyapatite derived from eggshells, Environ. Nanotechnology, Monit. Manag. 15 (2021) 100439. https://doi.org/10.1016/j.enmm.2021.100439.

Capítulo 6

6. Aspectos relevantes y perspectivas

6.1. Conclusión general

Con los resultados obtenidos en este trabajo (Fig. 6-1) se demostró que la transformación térmica (calcinación) del jacinto de agua (*Eichhornia Crassipes*) presenta una vía sostenible para la remoción y recuperación del fósforo presente naturalmente en la biomasa y además en sistemas acuosos. Fue posible obtener un material rico en fosfato de calcio (apatita) con uso potencial de enmienda para suelos ácidos, que actúa como un fertilizante fosfatado de liberación lenta. Además, los materiales obtenidos pueden usarse como materiales adsorbentes del fósforo presente en soluciones acuosas, permitiendo disminuir el problema ambiental de la eutrofización ocasionado por el alto contenido de fósforo. De otro lado, fue posible incrementar el contenido de apatita en los materiales usados en la adsorción de fósforo mediante un tratamiento de calcinación adicional. En esta investigación se demostró que los materiales obtenidos a partir de la calcinación del jacinto de agua no solo actúan adecuadamente para la eliminación y reciclaje del fósforo, sino que también pueden remover e inmovilizar metales pesados como el cadmio y el cobre.
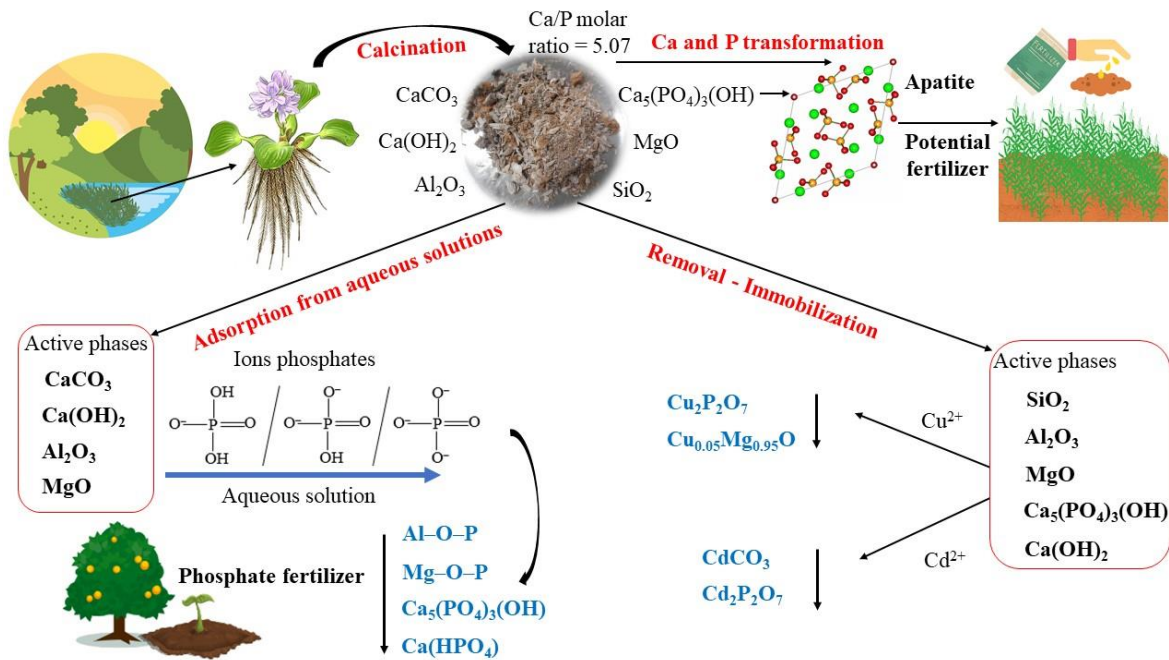
Fig. 6-1. Principales resultados encontrados en este trabajo.

6.2. Conclusiones especificas

o Mediante la caracterización por FRX y XRD del jacinto de agua se evidenció el alto contenido de Ca (34,44% de CaO), lo cual lo convierte en un material que no requiere adición de fuentes externas de Ca para generar la relación adecuada Ca/P (1.67) para producir apatita a diferentes temperaturas de calcinación. Se encontró que a bajas temperaturas de calcinación (350 °C – 550 °C), el CaCO$_3$ es la fase cristalina principal y el P permanece en forma orgánica; mientras que a altas temperaturas (650 °C – 900 °C), el Ca se transforma en Ca(OH)$_2$ promoviendo la formación de fosfatos de Ca como apatita [Ca$_5$(PO$_4$)$_3$(OH)], de la cual se obtiene hasta un 36.64% a 800 °C. Debido al contenido de apatita, los materiales presentan uso potencial como fertilizante con liberación lenta de P; los ensayos realizados mostraron una liberación de P a las 24 h del 28.4% en ácido fórmico y del 3.6% en agua desionizada.

o Al emplear el jacinto de agua calcinado a 650 °C (CWH-650) como un material para la adsorción de fósforo, se encontró alto porcentaje de eliminación de P (29.86%),

generado principalmente por el contenido de $Ca(OH)_2$ y otros compuestos como Al_2O_3 y MgO, que actúan como fases activas en el proceso de adsorción de P. Mediante análisis cinético del proceso de remoción, se determinó que el paso limitante de la velocidad de adsorción es la quimisorción de P sobre CWH-650. Por otro lado, los modelos de isotermas como Langmuir, Freundlich, Temkin y Langmuir-Freundlich ajustaron muy bien los datos experimentales, proporcionando una capacidad máxima de adsorción de 21.21 mg P/g e indicando que no existe una única forma de interacción entre CWH-650 y P. Esto demuestra una mezcla de mecanismos de adsorción, donde el intercambio de ligandos seguido de la precipitación fueron los mecanismos dominantes en el proceso de adsorción. Los análisis de FTIR y XRD permitieron determinar que el proceso de calcinación al material adsorbido con P (CWH-650–P), genera la obtención de un material con mayor contenido apatita, la cual incrementa de 30.3 a 41.0%.

o   El proceso de calcinación del jacinto de agua favoreció la formación de fases de Ca-P como $CaCO_3$ y $Ca_5(PO_4)_3(OH)$, además de MgO y Al_2O_3 en menor proporción. Estas fases tienen una alta capacidad de adsorción y retención de metales pesados. Según los resultados de XRD para el jacinto de agua calcinado a 700 °C (CWH-700) utilizado en la remoción de metales, el Cd^{2+} y el Cu^{2+} precipitaron como $CdCO_3$ y $Cd_2P_2O_7$, y $Cu_{0.05}Mg_{0.95}O$ y $Cu_2P_2O_7$, respectivamente. Se demostró que la apatita y las especies de Ca juegan un papel importante en la eliminación de Cd^{2+} y Cu^{2+} desde soluciones acuosas. El fósforo se puede liberar a la solución y reaccionar con los metales, y el calcio puede presentar intercambio iónico con el Cd^{2+} y el Cu^{2+}. Los precipitados que se formaron durante la adsorción presentaron baja solubilidad (<0.055% de Cd y <0.003% de Cu), reduciendo la movilidad de los contaminantes e incrementando la inmovilización de Cd y Cu en CWH-700.

6.3. Perspectivas de investigación

Este trabajo contribuye al entendimiento de la transformación térmica del jacinto de agua como una metodología económicamente viable para obtener un producto de valor

agregado, con aplicaciones relevantes en la remoción y reutilización de fósforo a partir de medios acuosos, además en la remoción de metales pesados en sistemas acuosos, ambos aspectos relevantes desde un punto de vista ambiental. Mediante el desarrollo de esta investigación se contribuye a ver el proceso de calcinación no solo como un método de disposición el jacinto de agua en la reducción de su volumen, sino también como metodología para obtener un material que pueda usarse como fertilizante y/o adsorbente de contaminantes de medios acuosos.

Los resultados obtenidos en esta investigación, abren las puertas para estudiar las aplicaciones previamente mencionadas a escala real donde:

o Se estudie el comportamiento de estos materiales usando aguas residuales reales mediante experimentos por lote y en continuo, ya que estas suelen brindar información más acorde a los procesos que se dan en plantas de tratamiento de aguas residuales.

o Se evalúe la selectividad hacia el P en presencia se otros aniones competitivos como arseniato, nitrato, sulfato, carbonato, entre otros.

o Se explore el comportamiento de estos compuestos en el suelo y las plantas.

Anexos

Anexo C3: capítulo 3

Table 3-S1. P content for calcined samples

Sample	Yield (wt %)	P_2O_5 (wt %)	P (wt %)
WH	100.00	1.21*	0.53
CWH-350	27.70	4.37	1.91
CWH-450	23.10	5.24	2.29
CWH-550	20.70	5.85	2.55
CWH-650	16.70	7.25	3.16
CWH-700	15.81	7.65	3.34
CWH-800	14.70	8.23	3.59
CWH-900	14.51	8.34	3.64

* Determined by XRF
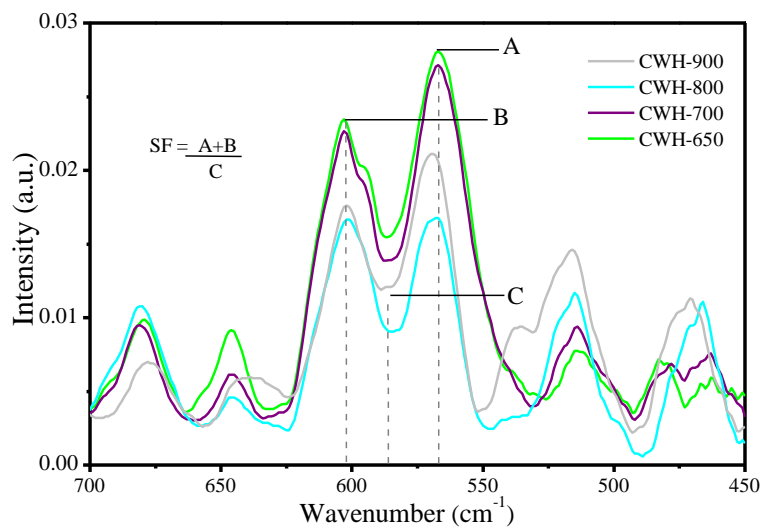
Fig. 3-S1. The splitting factor (SF) of Weiner and Bar-Yosef, (1990). SF is measured as the sum of the heights of the 602 and 567 cm^{-1} phosphate peaks divided by the height of trough between them.
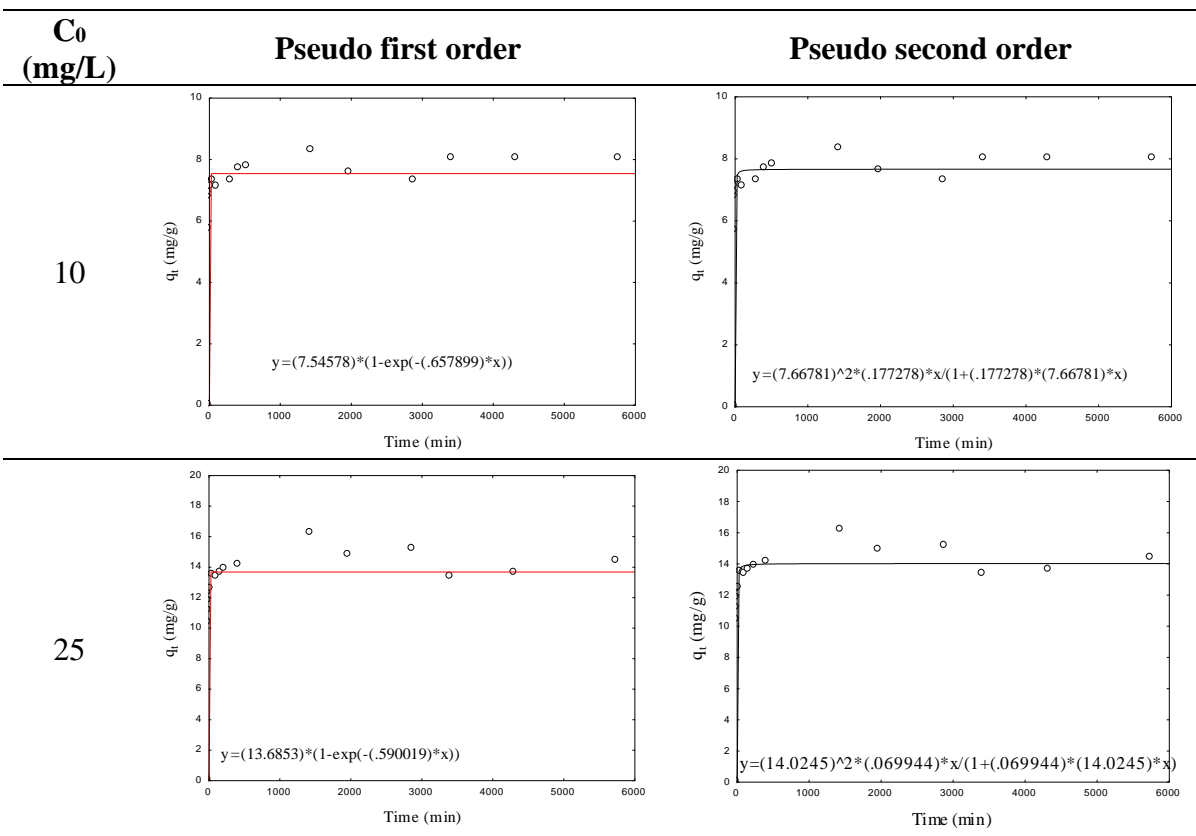
Anexo C4: capítulo 4

      The equations for kinetic models of pseudo first order (equation C4-1) and pseudo second order (equation C4-2) are presented in Table 4-S1.
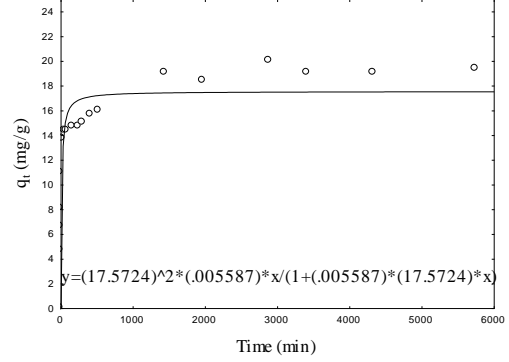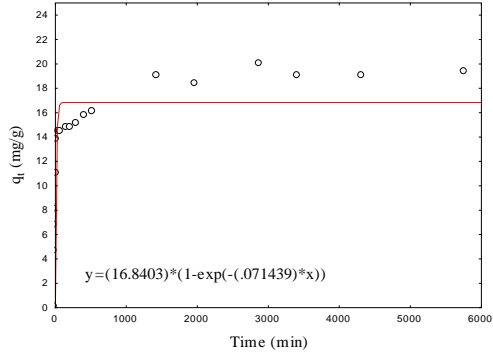
Table 4-S1. Equations for kinetic models.

Models	Equation	
Pseudo first order	$q_t=q_e(1-e^{-k_1 t})$	(C4-1)
Pseudo second order	$q_t=\dfrac{q_e^2 k_2 t}{1+q_e k_2 t}$	(C4-2)

When q_e: is the amount of phosphorus adsorbed at equilibrium (mg/g); q_t: is the amount of phosphorus adsorbed in time (mg/g); t: time (min); k_1: is the pseudo-first-order rate constant (1/min); k_2: is the pseudo second order rate constant (g/mg.min).
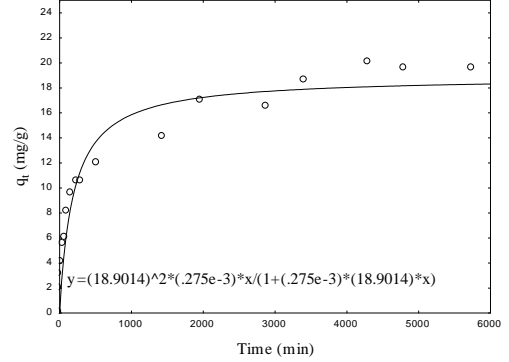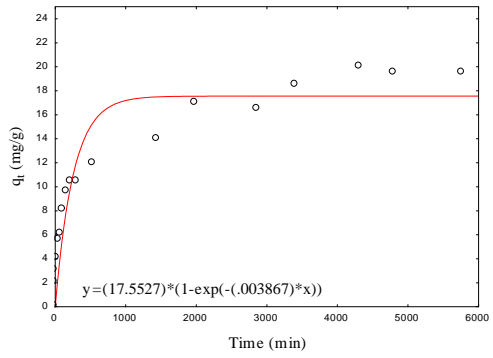
Fig. 4-S1. Fit to pseudo first order and pseudo second order kinetic models.
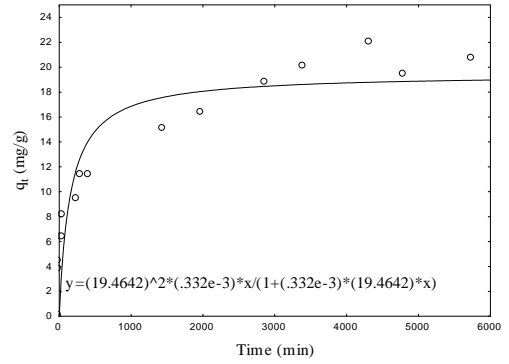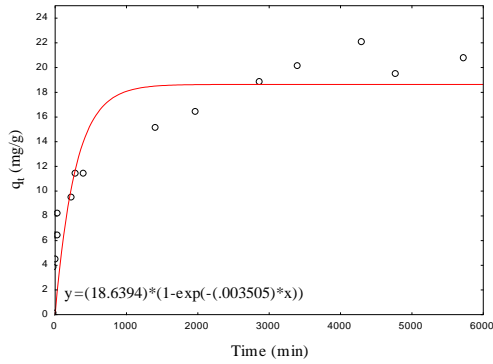
50

$y=(16.8403)*(1-exp(-(.071439)*x))$

$y=(17.5724)^2*(.005587)*x/(1+(.005587)*(17.5724)*x)$

75

$y=(17.5527)*(1-exp(-(.003867)*x))$

$y=(18.9014)^2*(.275e-3)*x/(1+(.275e-3)*(18.9014)*x)$

110

$y=(18.6394)*(1-exp(-(.003505)*x))$

$y=(19.4642)^2*(.332e-3)*x/(1+(.332e-3)*(19.4642)*x)$

130

$y=(16.183)*(1-exp(-(.003253)*x))$

$y=(17.8688)^2*(.214e-3)*x/(1+(.214e-3)*(17.8688)*x)$

101
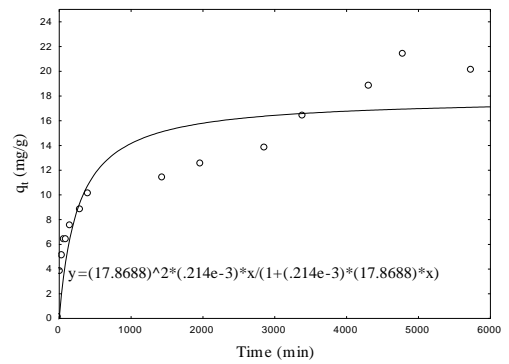
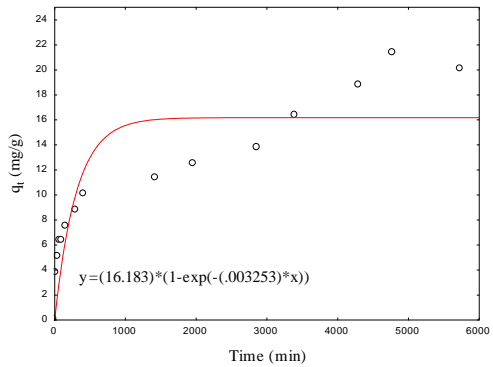**Table 4-S2.** Parameters of pseudo first order and pseudo second order kinetic models.

C_0 (mg/L)	10	25	50	75	110	130
C_e (mg/L)	2.400	10.000	30.000	55.500	91.875	112.500
$q_{e\,exp}$ (mg/g)	8.000	14.333	19.326	19.500	20.625	20.000
Pseudo first order						
k_1 (1/min) x 10	6.579	5.900	0.714	0.039	0.035	0.033
q_e (mg/g)	7.546	13.685	16.840	17.553	18.639	16.183
R^2	0.9888	0.9728	0.9670	0.9764	0.9552	0.9430
Δq_e (%)	6.02	4.74	14.76	11.09	10.65	23.59
Pseudo second order						
k_2 (g/mg.min) x 10	1.773	0.699	0.056	0.003	0.003	0.002
q_e (mg/g)	7.668	14.024	17.572	18.901	19.464	17.869
R^2	0.9934	0.9851	0.9808	0.9873	0.9727	0.9606
Δq_e	4.33	2.20	9.98	3.17	5.96	11.93

The equations for the Langmuir (equation C4-4), Freundlich (equation C4-5), Temkin (equation C4-6) and Langmuir-Freundlich (equation C4-7) isotherm models are shown in Table 4-S3.

Table 4-S3. Isotherm model equations.

Models	Equation	
Langmuir	$q_e = \dfrac{C_e Q_m K_L}{C_e K_L + 1}$	(C4-4)
Freundlich	$q_e = K_F C_e^{\frac{1}{n}}$	(C4-5)
Temkin	$q_e = \dfrac{RT}{b} Ln(K_T C_e)$	(C4-6)
Langmuir-Freundlich	$q_e = \dfrac{Q_m (K_a C_e)^{n_{LF}}}{(K_a C_e)^{n_{LF}} + 1}$	(C4-7)

| | Separation factor | | $R_L = \dfrac{1}{1 + K_L C_0}$ | | (C4-8) |

When q_e: is the amount of pollutant adsorbed at equilibrium (mg/g); Q_m: is the maximum adsorption capacity (mg/g); C_e: is the concentration in equilibrium (mg/L); K_L: is the Langmuir constant (L/g); K_F: is the adsorption capacity in multilayer (mg/g); $\frac{1}{n}$: is a constant linked to the adsorption intensity; K_a: is the adsorption affinity constant (L/mg); n_{LF}: is the index of heterogeneity; R: universal gas constant (kJ/mol.K); T: temperature (K); K_T: Temkin's constant (L/g); b: is a constant related to the heat of adsorption (kJ/mol); C_0: is the initial concentration (mg/L); R_L: is the separation factor (dimensionless).

Table 4-S4. Langmuir, Freundlich, Temkin and Langmuir-Freundlich isotherm parameters.

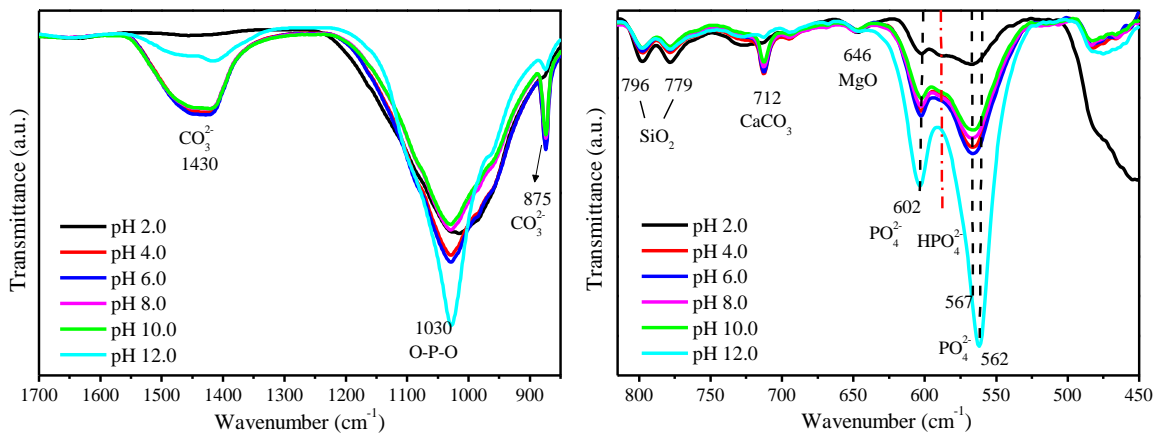|						
Langmuir	Q_m (mg/g)	21.207	Temkin	K_T (L/g)	7.039
	K_L (L/mg)	0.239		b (kJ/mol)	0.768
	R^2	0.9973		R^2	0.9825
R_L		0.031-0.287	Langmuir-Freundlich	Q_m (mg/g)	21.382
Freundlich	K_F (mg/g)	8.656		K_a (L/mg)	0.235
	$1/n$	0.195		n_{LF}	0.96
	R^2	0.9665		R^2	0.9973

Fig. 4-S2. FTIR for CWH-650 after adsorption at different initial pH.